

POLYELECTROLYTE MULTILAYERS CONTAINING
POLYETHYLENE-BASED IONOMERS

A Dissertation

by

HSIU-CHIN HUANG

Submitted to the Office of Graduate and Professional Studies of
Texas A&M University
in partial fulfillment of the requirements for the degree of

DOCTOR OF PHILOSOPHY

Chair of Committee, Nicole Zacharia
Committee Members, Terry Creasy
Donald J Darensbourg
Hung-Jue Sue
Head of Department, Andreas A Polycarpou

August 2014

Major Subject: Mechanical Engineering

Copyright 2014 Hsiu-Chin Huang

ABSTRACT

Layer-by-Layer (LbL) assembly technique is a powerful approach to blend two or more materials to form new materials of thin films on any type of substrate, and the LbL film is called polyelectrolyte multilayers (PEMs). The assemblies are highly influenced by processing conditions and types of incorporated materials, and their morphology and chemical functionality can be controlled and tunable. The advantages allow people to design films with desired properties for a given application. This study uses linear polyethyleneimine (LPEI) and poly(ethylene-co-methacrylic acid) (EMAA) ionomer as main materials. EMAA ionomer is a commercial material known as Surlyn having ethylene as the major component, and dissolved in THF at 65°C but becomes a colloidal dispersion when temperature goes down to room temperature. Water soluble LPEI solution has a large and changeable range of ionization degree by adjusting the solution pH, which also changes chain conformation. Oppositely, the ionomer has a low content of charged carboxylic acid groups, only 1.62 mole %, resulting in energetically favorable aggregation of ionic species.

This study focuses on complexing the polymers having a drastically large difference in terms of ionization degree using LbL technique at a mixed THF-water solvent system. Via electrostatic interactions between LPEI and EMAA ionomers, the blends are successfully fabricated. Thermal, mechanical, and surface properties of the PEMs are investigated. For thermal properties, a new endothermic peak created in PEMs according to results of DSC overlaps with order-disorder transition peak and melting point of ionomer, resulting in an increase of latent energy. The interactions between the materials influence mechanical behavior; the PEMs exhibit higher stiffness and tensile strength, and are still tough. The most interesting and

impressive performance of the blends is surface properties. Micro-sized holes and nano-scale structures (hierarchical morphology) found on the surfaces of LbL assemblies by SEM make the films very hydrophobic and superoleophilic to allow the films to separate water out from an oil-water emulsion. The film surfaces also show rose petal effect to pin water droplet of a high volume even though the surface is turn up side down. The work is the first demonstrator to use EMAA ionomers as a material in the LbL system. Many basic properties of the new complex are investigated and characterized, and these results are believed to benefit the development of novel materials in the future.

ACKNOWLEDGEMENTS

I spent four years and two months at Texas A & M and ten months at the University of Akron for my PhD program. It was such a good opportunity to study in College Station and in Akron because I could experience many things and meet different people in two different places. When I looked back, the time has passed so quickly. I overcame many problems and frustrations. These challenges led me to become a more independent individual. First, I would like to thank my advisor, Dr. Nicole Zacharia. She is a knowledgeable and fine professor with a great heart. She provided me with research space and encouraged me to think independently regarding my own research. From her, I learned a positive attitude toward doing research. She is open-minded toward international students and cultural differences. She was willing to understand my thinking and cared about me personally. I appreciate the time we had together and the relationship that developed. I also want to thank my committee. In my preliminary exam and in the final exam, the questions they asked reminded me of some points I had missed or when I was wrong. My thanks go to colleagues at Texas A & M and at the University of Akron, including Chungyeon, Nina, Sherry, Ryan, Lauren, Kane, MingZhe, Emily, Chi, and Lihua, the undergraduate students who worked in our lab, my friends in other research groups, and the people I met at both universities. They were all important to me during my PhD studies. We helped and encouraged each other, shared information and much happiness. Because of them, my life was enriched. Finally, I would like to thank my husband. His support was the main source of power for me to face difficulties. I was really happy that we could overcome so many troubles together, share every thing, accompany each other and enjoy our life in USA.

TABLE OF CONTENTS

	Page
ABSTRACT	ii
ACKNOWLEDGEMENTS	iv
TABLE OF CONTENTS	v
LIST OF FIGURES	vii
LIST OF TABLES	xii
1. INTRODUCTION	1
2. LITERATURE REVIEW	6
2.1 Layer-by-layer (LbL) technique	6
2.1.1 Ionomers in LbL systems	8
2.1.2 Solvent effect in LbL system	9
2.2 Ionomers	11
2.2.1 Investigation of the existence of ionic aggregations	13
2.2.2 Features of ionic aggregations	14
2.2.3 Ionic clusters in EHM model	16
2.2.4 Poly(ethylene-co-methacrylic acid) (EMAA) ionomers	16
2.2.5 Thermal properties of EMAA ionomers	18
2.2.6 Mechanical properties of EMAA ionomers	21
3. EXPERIMENTAL SECTION: (LPEI/EMAA) LBL FILM FABRICATION	25
3.1 Materials and solution preparation	25
3.2 Layer-by-layer self-assembly and complex of LPEI/EMAA	27
3.3 Elemental analysis and FTIR analysis	31
3.4 Thickness measurement	39
3.5 Surface morphology	43
3.6 Solvent effect	45
4. EXPERIMENTAL SECTION: THERMAL PROPERTIES	49
4.1 Study of glass transition by DSC	51

4.2	DSC thermogram of pure surlyn 8940 and pure LPEI	52
4.3	DSC thermogram of LPEI/EMAA complex and LbL assembly	56
4.4	Water effect on DSC thermogram	62
5.	EXPERIMENTAL SECTION: SURFACE WETTABILITY	67
5.1	Wettability of polyelectrolyte multilayers	69
5.2	Wettability of the ethylene-based ionomers containing LbL films	70
5.2.1	Contact angle and 90° tilting measurements	71
5.2.2	Particles in EMAA THF dispersion	72
5.2.3	Surface morphology of films	73
5.2.4	The effect of surface roughness of hot-pressed films on surface property	76
5.2.5	The surface performance of LbL films	77
5.2.6	LbL films fabricated by water-contained EMAA THF dispersion	80
5.2.7	Water separation from immiscible organic solvents	82
5.2.8	Silica nanoparticles and polystyrene latex in LbL films	85
6.	CONCLUSIONS AND RECOMMENDATIONS	87
6.1	Conclusions	87
6.2	Recommendations	88
6.2.1	Mechanical properties of PEMs	90
6.2.2	Nanoindentation in this study	92
6.2.3	Tensile testing in this study	98
6.2.4	Future work in mechanical properties	104
	REFERENCES	108

LIST OF FIGURES

FIGURE	Page
1.1 The LbL film blended by LPEI and EMAA ionomers contains not only PE crystalline and ionic interactions formed by oppositely charged functional groups of LPEI and EMAA, but also hydrogen-bonds and ionic aggregations in ionomers; they has potential to play the role of sacrificial bonds.	4
3.1 Chemical structure for (a) LPEI; (b) partially Na-neutralized EMAA ionomers.	25
3.2 30 % sodium-neutralized EMAA in different solvents; they were cooled down to RT from 75 °C in cyclohexane, 50 °C in chloroform, 150 °C in DMSO, 150 °C in DMAC, 100 °C in toluene, and 65 °C in THF.	26
3.3 (a)Layer-by-layer process in this study; (b)in the left figure, substrate having a first dip in LPEI pH8.5 was dipped manually at 10 and 30 dipping steps in only EMAA THF solution, and the rinsing solution was THF; in the middle figure, LbL thin films of LPEI(pH8.5)/EMAA were made with 10, 20, and 40 bilayers and the rinsing solutions after LPEI and EMAA solution dipping were DI water and THF, respectively; in the right figure, the rinsing solutions were all DI water.	28
3.4 (a)Free-standing film of (LPEI _{8.5} /EMAA _{0.5wt%}) ₂₅ ; (b)free-standing film made without the first heating procedure.	30
3.5 LbL film of (LPEI/EMAA _{0.25wt%}) ₂₅ and (LPEI/EMAA _{0.5wt%}) ₂₅ at pH values of LPEI solution 4.8, 5.5, 6.5, 7.5, 8.5, and 9.2, measured by elemental analysis presented by LPEI content by weight percent.	32
3.6 LbL film of (FTIR curves of LbL film of (a)(LPEI _{0.1M} /EMAA _{0.5wt%}) ₂₅ and (b)(LPEI _{0.1M} /EMAA _{0.25wt%}) ₂₅ at various pH values; wavenumber range is 3800-1200 cm ⁻¹	34
3.7 LbL film of FTIR spectra of surlyn 8940 pellets and surlyn 8940 dissolved in THF.	35

3.8	FTIR spectra of (a)1 is surlyn 8940 and 2 is LPEI crystalline hydrates; (b)LbL films assembled by 0.5 wt% of EMAA and 0.02M LPEI with various pH, in pH12 sample crystalline hydrates remain in the solution without filtration.	36
3.9	FTIR spectra of (LPEI _{8.5} /EMAA _{0.5wt%}) (1:1) complexes.	37
3.10	FTIR spectra of LbL film, LbL films heated at 120°C for 15 min and 180°C for 15 min, and the corresponding free-standing films of (LPEI _{8.5} /EMAA _{0.5wt%}) ₂₅	38
3.11	Growth curve of (LPEI _{0.02M} /EMAA _{0.5wt%}) LbL films at a range of LPEI pH values and as a function of bilayer number.	40
3.12	(a)Thickness and (b)roughness of (LPEI _{0.01M} /EMAA _{0.25wt%}) ₂₅ and (LPEI _{0.01M} /EMAA _{0.5wt%}) ₂₅ LbL films at various pH values.	41
3.13	Ratio of roughness to thickness of (a)(LPEI _{0.01M} /EMAA _{0.25wt%}) LbL films with 20 and 25 bilayers (b)(LPEI _{0.01M} /EMAA _{0.25wt%}) ₂₀ LbL film and (LPEI _{0.01M} /EMAA _{0.25wt%} adding 0.01 M sebacic acid) ₂₀ LbL film, as a function of LPEI pH value	42
3.14	Surface images of films of (LPEI _{7.5} /EMAA _{0.25wt%}) ₂₅ (a)as deposited (LbL film), (b)heated at 120 °C 15 min, and (c)heated at 100 °C 18 hours, scanned by profilometer	43
3.15	Surface images of films of (LPEI _{7.5} /EMAA _{0.25wt%}) ₂₅ (a)as deposited (LbL film), (b)heated at 120 °C 15 min, and (c)peeled off the substrate (free-standing film), taken by AFM	44
3.16	Stored EMAA dispersion containing water for different time duration. The weight percent of water from left to right vials are 0, 10, 20, 30, 40, 50, 60, 70, 80, and 90 wt%.	46
3.17	The LbL films of (LPEI/EMAA with water) ₁₅ . From left to right, the water weight percent in EMAA dispersion are 0, 10, 20, 30, 50, 60, 70, and 90.	47
3.18	(a)Surface morphology and (b)film thickness and roughness of LbL films of (LPEI/EMAA with water) ₁₅ . In (a), the number on the left top of each microscopic image is the weight percent of water in the EMAA dispersion.	48
4.1	Modulated DSC thermogram of pure LPEI.	52

4.2	Modulated DSC thermogram of pure surlyn 8940.	53
4.3	DSC thermogram of surlyn 8920, surlyn 8940, and nucrel 925.	54
4.4	DSC thermograms of surlyn 8940; after 1 st heating, surlyn was heated at an immediate 2 nd heating, and heated after the storage at RT of 2 hr, 5 hr, 1 day, 5 day, 9 day, 14 day, 20 day, 32 day, 50 day, 70 day, and 95 day.	55
4.5	DSC thermogram of surlyn 8940; before testing, surlyn was stored at 180°C for 0, 1, 3, 5, 6, 20, and 30 hr.	56
4.6	Modulated DSC thermogram of (a)(LPEI _{8.5} /EMAA _{0.5wt%}) (1:1) complexes, (b)(LPEI _{4.8} /EMAA _{0.25wt%}) ₂₅ LbL film.	57
4.7	Total heat flow of MDSC thermogram of (LPEI _{0.01M} /EMAA _{0.25wt%}) ₂₅ LbL films at various pH values.	58
4.8	Non-reversible (Nonrev), reversible (Rev), and total heat flow of MDSC thermogram of isolated (LPEI _{8.5} /EMAA _{0.5wt%}) ₂₅ films.	58
4.9	DSC thermogram of (a)free-standing film of (LPEI _{0.01M} /EMAA _{0.5wt%}) ₂₅ at a function of pH value, (b)surlyn 8940 and LPEI/EMAA complexes after the same post-treatment, (c)LbL film of LPEI _{0.02M} /EMAA _{0.5wt%} at pH12 with crystalline hydrates (dash line) or not (solid line).	60
4.10	MDSC thermogram of surlyn 8940 soaked in water for different duration	63
4.11	MDSC thermogram of free-standing films of (LPEI _{0.01M} /EMAA _{0.5wt%}) ₄₀ soaked in water for different duration; the 40-bilayer LPEI/EMAA LbL film was made using a shorter dipping time.	64
4.12	The increment of conductivity of (LPEI _{0.01M} /EMAA _{0.25wt%}) ₂₅ free-standing film as a function of time.	65
4.13	Modulated DSC thermogram of (LPEI _{0.01M} /EMAA _{0.5wt%}) ₄₀ LbL film (solid line) and free-standing film (dash line) which is soaked in water for 37 hours.	66
4.14	Modulated DSC thermogram of (LPEI _{0.01M} /EMAA _{0.5wt%}) ₄₀ free-standing film that first soaked in water for 20 hours and then soaked in 0.1 M NaOH for different time.	66
5.1	Weight change of EMAA ionomers pellet after THF immersion for different soaking time.	72

5.2	Top-view SEM images of (a)spin-coating of EMAA 0.25 wt% THF solution at room temperature, and (b)dip LbL film of (LPEI _{8.5} /EMAA) ₂₅ . The outmost deposited layer of LbL film is EMAA ionomers.	73
5.3	Top-view SEM images of (a)hot-pressed film of EMAA ionomers, (b)hot-pressed film of LDPE, (c)spin-coated film of EMAA ionomers,(d)spin-coated film of LDPE, (e) and (f) dipped LbL film of (LPEI _{8.5} /EMAA) ₂₅ with different magnifications.	75
5.4	(a)Contact angle and (b)pinning force of hot-pressed LDPE films as a function of surface roughness, (c)contact angle and (d)pinning force of hot-pressed EMAA ionomers films as a function of surface roughness.	77
5.5	(a)Surface roughness, (b)contact angle, and (c)the range of pinning force of dipped LbL films of (LPEI/EMAA) ₂₅ as a function of pH value of LPEI solutions.	78
5.6	(a) and (b) are the SEM images of the LbL films of (LPEI _{8.5} /EMAA) ₂₅ annealed at 100°C for 5 min and 30 min, respectively. (c) to (f) are the film thickness, surface roughness, contact angle, and water pinning force for the same LbL films after annealing with time.	81
5.7	Effective diameters of EMAA particles in water-containing THF solution as a function of different weight percentage of water.	82
5.8	SEM images for EMAA water-containing THF dispersion; (a)90 wt%, (b)70 wt%, (c)50 wt%, (d)30 wt%, and (e)10 wt% of water.	83
5.9	(a)Contact angle and (b)pinning force of the dipped LbL films made by EMAA H ₂ O/THF dispersions and LPEI.	84
5.10	(a)Top-view and (b)side-view of the separated water droplet dyed by methylene blue from decane on the surface LbL films. The inset in (b) is on larger magnification.	84
5.11	(a)Contact angle and (b)pinning force of the LPEI/EMAA LbL film containing silica nanoparticles. (c)Contact angle and (d)pinning force of the LPEI/EMAA LbL films containing PS latex. Blue diamond denotes the samples fabricated by method 1. Red square and cross denote the samples for method 2 that nanoparticles was in LPEI solutions and the films have 15 and 15.5 bilayers, respectively. Green triangle denotes the samples for method 2 that nanoparticles was in EMAA THF dispersion and the films have 15 bilayers.)	86

6.1	Nanoindentation experiment: (a)Force vs. time plot in this study, (b)a typical load-displacement curve.	93
6.2	(a)The young's modulus and (b)hardness of pure surlyn 8940, LbL films and free-standing films of(LPEI _{4.8,5.5,6.5,7.5,8.5,9.2} /EMAA _{0.5wt%}) ₂₅ , heated film of (LPEI _{5.5} /EMAA _{0.5wt%}) ₂₅ at 120°C, free-standing film of (LPEI _{8.5} /EMAA _{0.5wt%}) ₂₅ heated at 180°C before base treatment, and free-standing film of (LPEI _{7.5} /EMAA _{0.5wt%}) ₂₅ soaked in water for 40 hours.	95
6.3	(a)The total energy per volume, (b)the stored energy per volume, (c)the dissipated energy per volume, (d)the fraction of stored energy, (e)the fraction of dissipated energy of pure surlyn 8940, LbL film and free-standing film of(LPEI _{4.8,5.5,6.5,7.5,8.5,9.2} /EMAA _{0.5wt%}) ₂₅ , 120°C-heated film of (LPEI _{5.5} /EMAA _{0.5wt%}) ₂₅ , the 180°C-heated free-standing film of (LPEI _{8.5} /EMAA _{0.5wt%}) ₂₅ , and the free-standing film of (LPEI _{7.5} /EMAA _{0.5wt%}) ₂₅ soaked in water for 40 hours.	97
6.4	The tensile testing results: (a)Young's modulus, (b)yield strength, (c)elongation, and (d)fracture energy of EMAA hot-pressed films, 120°C- and 180°C-heated free-standing films. Red-color square and blue-color diamond denote the results from the first and second experiment conditions, respectively. E, 180, 120, and W denote EMAA hot-pressed films, 180°C-heated free-standing films, 120°C-heated free-standing films, and 120°C-heated free-standing films soaked in water, respectively.	101
6.5	Stress-strain curves of EMAA hot-pressed film and 180°C-heated free-standing film.	102
6.6	Top-view SEM images of surfaces of strained EMAA hot-pressed film (a, b) and 180°C-heated free-standing film (c, d) in the second experiment condition with different magnifications. (f) is SEM image of surface of strained 180°C-heated free-standing film in the first experiment condition.	103
6.7	Temperature dependence of dynamic storage modulus (E'), loss modulus (E''), and $\tan\delta$ at 1Hz for hot-pressed surlyn 8940 films.	106

LIST OF TABLES

TABLE	Page
3.1 Comparison of dielectric constant (k), polarity, and proticity for six different solvents; the solvents include dimethylsulfoxide(DMSO), dimethylacetamide(DMAC), cyclohexane, chloroform, toluene, and tetrahydrofuran(THF).	27
4.1 Comparison of data collected from the thermogram in Figure 4.2 and 4.6-4.8 for different sample types. In type, S8940 means Surlyn8940. The third column (EMAA) indicates the concentration of EMAA ionomer solution and the unit is wt%. T_m and T_c are the peak temperatures of melting point and crystallization during first cooling, respectively, and their units and the unit of T_n are $^{\circ}\text{C}$. ΔH_t , ΔH_n , ΔH_m , and ΔH_c are enthalpy changes of the new peak, melting peak, and crystallization peak during first cooling, respectively, and their units are J/g.	61
4.2 Comparison of the degree of polyethylene (PE) crystallization collected from the thermogram in Figure 4.2 and 4.6-4.8 for different sample types. The degree is the ratio of the enthalpy change of crystallization peak during first cooling (ΔH_c , in Table 4.1) to 290. The unit is %. 290 is the enthalpy change (J/g) of pure PE crystalline. . .	62

1. INTRODUCTION

Investigation and modification of surface properties have been the interest of intense study of the academic community for decades. Fundamental surface science studies the interactions and phenomena at an interface or boundary between solids, liquids, soft matter, and nanostructures. The corresponding surface properties could determine the stability, miscibility, biocompatibility, and functionality of a target in a given environment. Changes in contact angle of water on a hydrophilic or a hydrophobic surface of a substrate typically describes a macro-scale surface effect. In colloidal systems, including solids in liquids (dispersions), liquids in liquids (emulsions), and gases in liquids (foams), the particle size of the dispersed phase in a continuous medium lie from 1 to 1000 nm which is between the sizes of a true solution and a suspension. For particles of this size surface area is a dominant feature compared to bulk material, making interfacial interactions the most important factor in these types of systems. These types of interactions (van der Waals, electrostatics, and so forth) can be controlled by making modifications to colloidal particles at the molecular level. Consequently, a good understanding of the interactions and chemistry of a surface or interface can be crucial in terms of creating desired properties and industrial design; typical applications are in foods, detergents, paints and coatings, ceramics and composites, medicines and biocides.

Synthesizing functional molecules on a target surface is one of popular methods of manipulating the surface properties, especially in colloidal systems. This might involve the absorption of surfactant molecules in aqueous solutions at a surface in the form of a monolayer and the deposition of multilayer thin film on solid materials or colloidal particles to exhibit remarkable electrical, optical, chemical, or mechan-

ical properties. The layer-by-layer (LbL) technique is a novel approach to build versatile and nano-scale thin films known as polyelectrolyte multilayers (PEMs) on the surface of nearly any type of substrate, and it can also be adapted to colloidal systems [157]. This technique is usually used in an aqueous environment. A great diversity of nanomaterials and polymers, such as polyelectrolytes, clay, biological molecules, nanoparticles, conducting polymers etc. have already been used in this thin film technique. Polyelectrolytes, or polymer taking on charges in water, are the most commonly used material in this fabrication technique. This simple but very powerful method of directing the self-assembly of multivalent molecules for material design was published by Decher and coworkers in 1997 and rapidly became well-established [32]. Before the discovery of the LbL technique, in the early twentieth century, Langmuir and Blodgett demonstrated a Langmuir-Blodgett (LB) monolayer deposition technique in which an organic monolayer is formed by spreading a drop of solution containing amphiphilic molecules on the water's surface and then isolating it into a solid surface [97, 9, 10]. Using the LB technique, it is possible to get a single molecular layer and ultra-thin film with high degree of structural order that is homogeneously deposited over a substrate surface. However, assembling molecules in this method requires water solubility, and at least two opposite characteristics such as polar head and apolar tail. This requirement for surfactant like properties results in a limited amount of suitable materials. Besides this, the assembly is necessary to be executed under a specific range of solution concentration and pressure condition. Because of these disadvantages, the LB method is not very feasible in some applications and limits the types of thin films that can be made.

In this study, LbL assembly method is used to make a new material on the surfaces of glass slides and silicon wafers. One of the materials used is linear polyethyleneimine (LPEI) as polycation. It is a commonly used weak polyelectrolyte

which has a large range of possibly ionization degree that is tunable by varying solution pH. The other material used, the anionic component, is a polyethylene based ionomer, poly(ethylene-co-methacrylic acid) (EMAA). EMAA is made by Dupont company with the commercial brand name of Surlyn and Nucrel. The critical characteristic of ionomers is that they contain up to 15 mole % ion containing repeat units which leads to a bulk morphology containing nano-scaled ionic aggregations. These ionic aggregations and surrounding mobility-restricted regions act as chemical and physical cross-links in the material, which leads to a significant influence on ionomer properties, especially in terms of mechanical behaviour. The assemblies of LPEI and EMAA ionomers are accomplished under a solvent-mixed system followed by water rinsing; LPEI is used in an aqueous solution and EMAA is dispersed as colloids in THF. Presented here is one more case of PEMs successfully fabricated in nonaqueous media and also adds ionomers into the list of LbL materials. These LbL films can also be modified after assembly with a range of treatments such as exposure to acid/base or heat treatment.

The goal of this study is to combine the advantages of LbL technique and the superior mechanical properties of EMAA ionomers to develop a damage-resistant surface. First of all, the protective coating can be as part of devices to resist external damage in a harmful environment, allowing to diminish the deformation and fracture of the main body, or can serve as a damper by sandwiched between two objects. This kind of functional surface against abrasion and mechanical vibration is significant for many sophisticated equipment or supplies in medical, electrical, or aerospace applications. Using LbL technique, the functional film can well-integrate with the dimension of the protected target, avoid interface problem occurring in many reinforced composites, and can be highly tunable by material choices, adjusting sample preparation, as well as applying post-treatment. Many biomimetic structures

demonstrate brick-and-mortar architectures, porous or honeycombed structures, or sacrificial bonds and hidden length to act as mechanical shock-absorbers and to benefit the fracture toughness so as to withstand damage and extend lifetime of main bonds [44, 45, 99, 158, 186, 103, 179]. The concept from nature that plenty of mechanical energy dissipated through breaking sacrificial bonds and subsequently opening hidden length [44, 45] inspires this study to employ ionic aggregations and clusters, the respectively ionic and physical crosslinking inside EMAA ionomers, and the created secondary interactions between polymers in LbL self-assemblies as desirably sacrificial bonds to achieve the goal of dissipating energy, and Figure 1.1 is the schematic drawing.

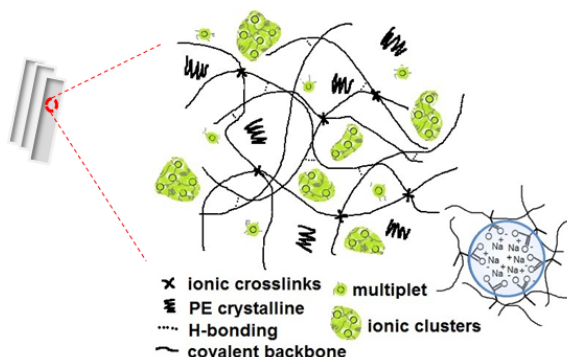


Figure 1.1: The LbL film blended by LPEI and EMAA ionomers contains not only PE crystalline and ionic interactions formed by oppositely charged functional groups of LPEI and EMAA, but also hydrogen-bonds and ionic aggregations in ionomers; they has potential to play the role of sacrificial bonds.

This study characterizes the physical, thermal, surface, and mechanical properties of the LbL assemblies containing EMAA ionomers mainly by differential scanning calorimetry (DSC), dynamic mechanical analysis (DMA), tensile testing, nanoindentation, fourier transform infrared spectroscopy (FTIR), atomic force microscopy

(AFM), scanning electron microscope (SEM), contact angle, dynamic light scattering (DLS) et al., and the characterizations are reported in the following sections.

2. LITERATURE REVIEW

2.1 Layer-by-layer (LbL) technique

The layer-by-layer method was first demonstrated by Decher and coworkers in 1997 [32]. The fabricated assembly of polyelectrolyte chains, called a polyelectrolyte multilayer (PEM), is usually formed from aqueous solutions. The versatile method reduces the difficulty of fabricating multifunctional thin films and allows the control of film thickness by layer number and also the control of many other properties, such as wettability, permeability, and antifouling ability. The LbL process simply put is to expose a clean substrate alternately into a positively-charged polymer (polycation) solution and a negatively-charged polymer (polyanion) solution. The substrate can be of nearly any type of geometry and material even colloidal particles or nanoscale channels. Every dipping step is followed by a water rinsing step in order to remove any excess of the dipping component, yielding a fairly reproducible deposition technique. The polymer components in LbL technique are usually polyelectrolytes although some neutral polymers can be used for hydrogen bonding driven assembly. During deposition the polymer chains generally interpenetrate with one another, leading to "fuzzy" layers that bleed into one another.

For most polyelectrolyte complexes, which are formed by direct mixing of oppositely charged polyelectrolytes, and for PEMs as well, the two oppositely charged polymers associate with a 1:1 stoichiometry of charged repeat units [49, 32, 17]. The self-assembly force between the charged materials relies not only on electrostatic force but on entropic gain since the small molecular counterions associated with the polyelectrolyte chains are released upon polyelectrolyte complexation and leave from close association with the polyelectrolytes to go into solution [17, 37]. There is hardly

any enthalpic gain or loss when complexing two polyelectrolytes [8]. Hydrophobic interaction is another important contribution to the formation of stable multilayers, which belongs to van der Waals force existing between hydrophobic portions of the incorporated polyelectrolytes and occurs when the structured water molecules are released from these hydrophobic regions [87]. Literature reports about using hydrogen bonding [156, 81, 82] and charge transfer [147, 148] as interaction force between molecules to form PEMs were also published considerably in the past 20 years.

Polyelectrolytes are categorized into strong and weak polyelectrolytes. The functional groups for strong polyelectrolytes, like strong acid and bases, are always fully charged in water; consequently, the high repulsion between charged groups stretches the polymer backbones into an extended conformation. This kind of extended chain conformation depositing onto a surface results in a very thin LbL film. Examples of strong polyelectrolytes commonly used in LbL systems are poly(sodium styrene-sulfonate) (SPS, polyanion) and poly(diallyldimethylammonium chloride) (PDAC, polycation). Changing the solution coil conformation strong polyelectrolytes relies on adding salts to solutions as salt ions are able to shield the charged groups reducing intramolecular forces and causing the polymer chains to become more coiled. The phenomenon is called charge screening. Through charge screening or changing ionic strength in polyelectrolyte solutions, thickness and mechanical properties of the fabricated assemblies can be controlled [37, 155, 66, 67]. In contrast to strong polyelectrolytes, the charge density of weak polyelectrolytes is highly dependent on the pH of their environment and based on the pKa of the specific polyelectrolyte the charge density and correlative chain conformation in solution can roughly be determined. Although the pKa of weak polyelectrolytes may change or drop when incorporated into a LbL system, the pH of the polyelectrolyte dipping solutions will lead to dramatic changes in degree of chain interpenetration between layers and film

thickness [149, 33]. Commonly used weak polyelectrolytes include poly(acrylic acid) (PAA), poly(ethyleneimine) (PEI), and poly(allylamine hydrochloride) (PAH).

2.1.1 Ionomers in LbL systems

There are numerous investigations focusing on the applications of polyelectrolytes in LbL self-assembly systems, including both strong and weak polyelectrolytes. However, most ionomers are hydrophobic, unlike polyelectrolytes which are generally water soluble, and as a consequence, there are only a small number of reports incorporating ionomers into LbL assemblies. There are many types of ionomers beside the ethylene-based ionomer which is the main material in this study, such as styrene containing ionomers, polytetrafluoroethylene (PTFE) ionomers, poly(methyl methacrylate) ionomers, polyurethane ionomers, and polyphosphate ionomers. Nafion, perfluorosulfonate ionomers developed by the DuPont company in the 1960s is the most commonly reported ionomer in used in LbL system. Nafion is a good ion conductor with reasonable mechanical properties and is one of the most popular electrolyte materials used for polymer electrolyte membrane fuel cell (PEMFC) and direct methanol fuel cell applications. Researchers have used the LbL technique to fabricate membrane electrode assembly (MEA) using Nafion solution [123, 104] and coat polyelectrolyte multilayers on the Nafion membrane to improve the efficiency of fuel cells [46, 202, 201, 2, 203, 72]. It is worth mention that in 2003 Hammond's group in MIT carried out the polymer electrolyte containing LPEI and Nafion using LbL method for power storage device [35]. Different from the LPEI/EMAA system in this study, LPEI/Nafion system was considered as a strong polyacid system due to the sulfonate groups of Nafion, and hence the effect of ionic strength of the dipping solutions is much stronger than that of solution pH for this case.

Other ionomers in the LbL system shown in the literatures include that Chen

and Hara used polystyrene ionomers and poly(methyl methacrylate) ionomers as weak polyions to build up ionomers LbL film in both tetrahydrofuran (THF) dipping and rinsing solvents, and studied the fracture mechanism by TEM [23]. Ohta et al. synthesized and deposited ionomers, polystyrene phosphazanium cation (SP-C) and polystyrene diborateimidazolidide (SP-A), on silica nanoparticles; the decreased QCM (quartz crystal microbalance) frequency supported the built-up of LbL films containing ionomers in a less-polar media [128]. There are also some investigation about liquid crystalline ionomers in a mixture of THF or highly polar solvents reported [28, 132, 126, 27]. Evidently, ionomers have been in the list of the materials for LbL technique although not yet widely. The fact that in contrast with common polyelectrolytes, most ionomers are soluble in organic solvents; therefore, the ionomers PEMs fabricated in nonaqueous media also points out the high flexibility of LbL assembly method. However, in these reports about ionomers LbL system the influence of LbL assembly method on the morphology of ionomers especially on ion-rich domain did not be subsumed into discussion and examination.

2.1.2 Solvent effect in LbL system

Deposition of LbL thin films in low-dielectric or non-polar solvents and the investigation of solvent effect remain rare as well because polyelectrolytes are charged in water. For industrial applications, the development of nonaqueous working is necessary and would be the future topic. The nonaqueous working solvents for LbL fabrication have been published include formamide [79], ethanol [210, 37, 136], methonal [209], N, N-dimethylformamide (DMF) [210, 178, 168, 211], dichloromethane (DCM) [13], acetone [128], THF [23, 24, 132, 28], as well as dimethyl sulfoxide (DMSO) [61, 132, 28]. The growth of these assemblies under the organic solvents are proved based on the detection of UV-vis, ellipsometry, QCM et al. Kamineni et al. took

formamide, an organic solvent with high polarity, to dissolve poly(sodium styrene sulfonate) (SPS) and poly(allylamine hydrochloride) (PAH) that are usually solved in water in order to figure out the problem of water-sensitive substrate [79]. The SPS/PAH PEMs are still formed by charge compensation driving-force even though under nonaqueous environment; on the other hand, LbL films based on hydrogen-bonding can also be fabricated in organic solvents [210, 209].

It is known that solution pH and ionic strength are two primary parameters to modulate the properties of LbL films compared to the less important variables, such as molecular weight, solution concentration, and deposition time. In 1999 and 2004, Schlenoff's and Caruso's groups respectively carried out that altering solvent quality is another efficient way to tune the relative strength of interactions between inter- and intra-molecules [37, 136]. Schlenoff et al. changed the solvent composition of water/ethanol in SPS/poly(diallyldimethylammonium chloride) (PDAC) spin coating system, and found when the fraction of ethanol increases, the film thickness increases. Caruso's group got the consistent PEMs thickness result by dipping substrates in SPS and PAH water/ethanol solutions. Both groups all attributed the thickness change to the solvent effect of adding ethanol. According to these literatures, it is able to summarize that solvents with low dielectric constant or dipole moment would leads to unfavorable polymer segments-solvent interactions when the polymers are the charged and hydrophilic polyelectrolytes. As a result, the tendency for solvent molecules to diffuse into or swell the polymer becomes weak and the solvation process would be not thermodynamically favored. Ethanol causes the amount of solvated polyelectrolytes ions decreases; consequently, the ion pairs between charged functional groups of polymer chains and counterions are relatively stable. Ethanol screens the intra-molecular charge repulsion of main chains, and on the other side, the hydrophobic interactions between the polyelectrolytes chains are

enhanced. The solvent effect, therefore, results in a similar influence of ionic strength on the adsorption solution; meanwhile, the polyelectrolytes chains in ethanol, a poor solvent, become more coiled and flexible. Although while the fraction of ethanol is approaching Θ condition of the system, the precipitation of polymers occurs, the more coiled or globular conformation allows polyelectrolytes to gain more available surface area and absorb more tightly to sharply increase the thickness and roughness of multilayers [178].

Another example of solvent effect is that Zhang et al. in 2008 made LbL self-assemblies of poly(dimethyldiallylammonium chloride) (PDDA) in an aqueous solution and sulfonated poly(sulphone) sodium salts (SPSF) in N,N-dimethyl formamide (DMF)/water mixed solvent [211]. The study indicated the mixed solvent with various DMF contents affected the intrinsic viscosity and conductivity of SPSF, and further they were used to characterize the polymer chain conformation or dimension and charge density of sulfonic groups, respectively. Since SPSF is not water soluble, theoretically water would decrease the intrinsic viscosity of SPSF but increase its conductivity because of the increase of polarity; however, the hydrogen bonding between water and DMF affects the congeries of water molecules which complicate both the solvating degree and ionization degree of SPSF chains and make SPSF behave like weak polyelectrolytes. Identical to the investigation of Schlenoff's and Caruso's groups mentioned above, the solvent composition decided how thick and rough the PDDA/SPSF films are. In addition, the solvent quality in Zhang's work also tuned the surface hydrophobicity based on contact angle examination.

2.2 Ionomers

Ionomers are a class of copolymers with both neutral and charged repeat units. They can be either random or block copolymers. One of repeat units of the copoly-

mers is of low dielectric constant, such as ethylene or styrene, and the other repeat unit has a functional group that is charged like carboxylate, phosphate, or sulfonate. The charged group is the minority component, usually less than 15 mol% of the polymer chain. As the neutral repeat unit is the majority of the polymer, ionomers are low dielectric materials and are soluble in organic solvents with low dielectric constant. For instance, poly(ethylene-co-methacrylic acid) (EMAA), trade name surlyn 8940 from Dupont company, is a copolymer having 94.6 mole % of polyethylene and 5.4 mole % of methacrylic acid (MA) groups in which only 30 % of MA groups is neutralized by sodium. The low ion content, usually less than 15 mole %, is the crucial characteristics of ionomers and lets ionomers not be categorized with polyelectrolytes [43]. This feature also profoundly influences the bulk properties of the copolymers. For example, compared to nonionic polymers, ionomers typically have higher viscosity and longer terminal relaxation time since ionic interactions affect the melt flow behaviour of ionomers [58]. Another example is that incorporating some ionic groups into polyurethane backbones could make water-dispersible products, and the presence of ions potentially disrupt the urethane hydrogen bonds and microphase-separated structures resulting from the incompatibility between hard and soft segments of polyurethane chains [25, 191].

Because of the apolar and hydrophobic hydrocarbon backbones and strong electrostatic force between an ion and its counterion, energetically favourable and discrete aggregations of ions and counterions, called multiplets or ionic aggregations, are formed. This does not mean isolated ion pairs (a charged functional group and its counterion) are absent. The ion-rich domains are present no matter if the ionomers are in the bulk state, the melt state, or dissolved in organic solvents. It is known that the aggregations can persist at above 300 °C, the decomposition temperature of ionomers [192]. Moreover, an ion pair in the aggregation can diffuse with its associ-

ated backbone to another multiplet by ion-hopping mechanism [169]. The formation of multiplets are influenced by ion concentration, type of functional group and counterion, spatial hindrance, intensity of electrostatic force, and the nature of chains. These factors may also decide the size and shape of multiplets.

2.2.1 Investigation of the existence of ionic aggregations

In 1968, Wilson et al. and Longworth and Vaughan found a new small angle X-ray scattering (SAXS) peak at low angle for ethylene-based ionomers material [110, 192]. This peak is referred to as "ionomer peak" and assigned as the presence of multiplets, generally observed at scattering vector (q) $1\text{-}5\text{ nm}^{-1}$ [200, 92, 5]. Since the ionic aggregations disperse in the amorphous phase and efficiently interfere the inserted X-ray light, the SAXS feature has been considered as interaggregate scattering. Subsequently, many theoretical models about spatial arrangements of ionic aggregations were developed in order to interpret the experimental result. These models include multiplet-cluster concept proposed by Eisenberg in 1970 [41], hard-sphere model developed in 1969 [34] and subsequently modified in 1973, 1983, and 1985 [118, 199, 200], core-shell model developed by MacKnight in 1974 [116] et al. Widely used models are Yarusso-Cooper model and its modified version, Kinning Thomas models. They assumed the shape of ionic aggregations is hard spheres which distribute in the polymer matrix of low electron density and attempted to define the aggregate composition [200, 83]. Another famous model is Eisenberg-Hird-Moore (EHM) model which was published in 1990 by Eisenberg et al.. EHM model modified multiplet-cluster concept in 1970 and provided a physical picture of ionomers morphology, and successfully explained both the SAXS ionic peak and the mechanical behaviours of the ionomers [42].

In EHM model, a multiplet is a spherical-drop like and only contains ionic species,

and surrounded by a restricted mobility layer that is formed by the apolar hydrocarbon backbones anchored by the aggregated charged groups. The thickness of limited-mobility layer might correlates with the ionomers chemical structures, degree of neutralization, acid content, and cation radii [215, 20]. There are two mechanisms involving the spontaneous accumulation of polymer chains around the multiplets; one is the released electrostatic energy during the formation process of multiplets raises surface energy, and the other mechanism is polymer chains gather in created extra space by chain extension. The accumulation of polymer chains, therefore, causes the increase of effective molecular weight nearby the multiplets and weak mobility of these anchored chains [43]. But, on the other hand, ion-hopping between multiplets can release the stress of these anchored hydrocarbon backbones with a characteristic time and ultimately permit the relaxation of the entire chains.

2.2.2 Features of ionic aggregations

The example in the literature of EHM model showed the size of a multiplet in polystyrene ionomers was around 0.6 nm in diameter and the whole region including the mobility-restricted layer was 2.6 nm [42]. Instead of scattering and spectroscopy methods which are model-dependent, in 1989, Register et al. attempted to use high voltage electron microscopy (HVEM) to detect ionic aggregations directly [107]. In 1981 Macknight et al. used amplitude contrast of transmission electron microscopy (TEM) in order to look for ionic aggregates by image method [55]; however, the chemical stains still could not provide sufficient image selectivity. Start from 1998, Dr. Karen Winey's group put plenty of efforts on directly detecting and determining the presence, size, shape, size distribution, shape variation, and spatial distribution of the ion-rich entity by scanning TEM (STEM). She also synthesized well-controlled ionomers with precisely spaced functional groups to investi-

gate the effect of counterions, acid content, neutralization level, sample preparation method, thermal treatment, and chemical nature of copolymers on ionic aggregations [100, 193, 86, 85, 163, 6, 191, 184, 144]. Then in 2003, she introduced deconvolution STEM into the investigation of ionic aggregations to quantitatively improve STEM images [84].

Different from amplitude contrast of TEM, STEM provides the advantages of absence of chemical stains and reduced effect of phase contrast because image contrast in STEM relies on atomic number. Metal cations with high atomic number, such as Zn and Cs, therefore, benefit to label the locations of ionic aggregations and get relevant information. For counterions with low or close to atomic numbers of C and H, like sodium, another tool, energy dispersive X-ray spectroscopy (EDS), was used to determine the local elemental composition of ionic aggregations to distinguish the Na-rich domain and Na-poor polymer matrix [163, 191]. For STEM, way of sample preparation is important, such as specimen thickness, because it might affect the determination of aggregation size [4].

A series of STEM images featured a variety of amorphous and semicrystalline ionomers with different acid copolymers, like EMAA, SPS, polydimethylsiloxane, polyurethane et al., and couple types of shapes (solid spheres, metastable vesicles, and rod-like aggregate) were demonstrated. The ion-rich aggregates in poly(ethylene-co-methacrylic acid) (EMAA) ionomers are spherical and for Zn-neutralized EMAA (Zn-EMAA), the diameters of monodispersed ionic aggregations was approximately 2-3 nm.[100, 163]. Different from EHM model that the interface between multiplets and mobility-restricted layer should be fairly sharp, the ionic aggregations detected from STEM include polyethylene chains and unneutralized acid groups to form acid salts. The concentration of associated acid groups in the aggregates is as function of the neutralization degree and counterion types [177]. Moreover, the fact that three

phases/multi-dispersions of ionic aggregations in EMAA ionomers neutralized by Na after post-treatments (hot-pressing) and featureless of as-extruded Na-EMAA used as received increased the complexity of the morphology of Na-EMAA [163]. Thermal history and pressure might influence the microstructure of EMAA ionomers, and thus correct interpretation of Na-EMAA behaviours from bulk measurements would be more difficult. In 2000, the spherical shape for ionic aggregations in EMAA was also found by Sauer and McLean using atomic force microscopy (AFM) [140].

2.2.3 Ionic clusters in EHM model

Not only morphology but also the physical properties of copolymers would make drastic alterations when increasing ion content in ionomers. The increment of ion content potentially shortens the distance between ionic aggregations and induces sufficient interference between the discrete multiplets. Above a critical point, EHM model predicted that the raised interference leads to the overlapping of mobility-restricted regions surrounding multiplets [42]. As a result, a new phase appears in the morphology of ionomeric materials and the phase is so-called ionic clusters. The cluster concept in EHM model was corrected by Eisenberg so it is different from the theoretical point of cluster formation in multiplet-cluster concept in 1970. Each cluster is irregular and according to EHM model, it apparently consists of the ionic aggregations at low volume fraction and large contiguity of polymer backbones with low dielectric constant. The microphase-separated structure is of importance in EHM model since it is the key point of interpreting the ionic peak of SAXS results and a series of mechanical studies for ionomers.

2.2.4 Poly(ethylene-co-methacrylic acid) (EMAA) ionomers

Ethylene-based ionomers are thermoplastics and have been commercially available for dozens of years. The applications involve adhesives, high strength, and

abrasion-resistant products, such as packaging, ski boots, and coatings. Famous examples of ethylene-based ionomers are Surlyn and Nurel ionomers which are random copolymers and fabricated from Dupont company, and their monomer carrying functional groups is methacrylic acid (MAA). Classical high-pressure free radical polymerization is commonly employed to synthesize methacrylic acid, a polar comonomer, into polyethylene to form EMAA copolymer, same process to produce low-density polyethylene (LDPE) [134]. Another reason of highlighting surlyn products is because the EMAA ionomers can self-heal following a high-energy puncture without adding any healing agents [77, 78, 76, 171, 195, 170]. The ability of self-repairing mainly relies on two steps; first step is related to high melt strength which is provided by ionic clusters phase and allows the damaged part to close the puncture hole automatically, and second step is to re-order ionic domains to recover strength even though chain diffusion takes a long relaxation time. In the morphology, beside ionic clusters polyethylene (PE) crystallinity and amorphous phase are also included, and the presence of PE crystallinity are by two types of chain-folded lamellae and bundle-like crystal. In the most of investigations, EMAA are partially or fully neutralized by different types of metal cations, such as alkali metal, alkaline earth metal, transition metal ions, and even rare earth ions [54, 1, 131, 137, 58]. The unneutralized acid groups prefer to form acid dimers by hydrogen bonds instead of aggregations or being free acid group, but these acid dimers still can raise the viscosity of ionomers [40, 177]. When unneutralized acid chooses to associate with a metal salt or when it incorporates into the ionic aggregations, the charged hydrogen ion would leave by bonding with another carboxylate anion. The process is analogous to ion-hopping mechanism so that the process can facilitate chain relaxation and stress release.

2.2.5 Thermal properties of EMAA ionomers

EMAA ionomers are crystallizable copolymers, which raise the structural complexity and cause complicated thermal and thermomechanical behaviour. There are two endothermic peaks (energetic barrier) shown in differential scanning calorimetry (DSC) thermogram for EMAA ionomers in the first heating, and the result was first noticed by Marx and Cooper in 1974 [120]. The high-temperature peak, 94 °C, is assigned to the melting point (T_m) of PE crystallinity (lamellar thickening), and the PE crystallinity behaves similar to intermediate and high density polyethylene [51, 59]. Since polyethylene re-crystallizes during the first cooling, this peak is still present in the second heating process. However, the low-temperature peak, 50 °C, is depressed when the second heating process is run right away while the peak appears again and becomes stronger after storage at room temperature with time [161]. There are two major explanations for the origin of the low-temperature peak except another interpretation that Cooper et al. demonstrated the latent energy of the low-temperature peak contains the contribution from water vaporization from ionic aggregations in 1994 [51]. But, there is no definitive evidence able to support these explanations due to the colloidal size of ionic aggregations.

First explanation assumes the origin is from the PE crystalline. Marx and Cooper in 1974 thought this endothermic peak derived from the melting of short imperfect PE chains since based on the correlation between annealing temperature and peak temperature, the behaviour was similar to lamellar thickening normally found in intermediate and high density polyethylene [119, 120]. Tsujita et al. in 1987 suggested that beside chain-folded PE lamellae EMAA ionomers also contain bundle-like PE crystals which result in the low-temperature endotherm and affected by annealing [167]. In 2002, Kuwabara and Horii compared the measurements of DSC and solid-

state NMR spectroscopy for as-received and quenched samples and concluded the melting of small crystallites produces the endothermic peak [93]. In 2005, Register et al. aged EMAA ionomers and combined DSC, variable-temperature SAXS, and wide-angle X-ray diffraction (WAXD) techniques to determine the origin [111]. They believed that the melting of secondary PE crystals results in this endothermic peak and the thin crystalline are interlamellar formed between the primary PE crystalline. Some literatures also used this model to interpret the mechanical behaviour of EMAA ionomers [175, 174, 153].

Second explanation assumes the origin is related to the ionic aggregations. In 1989, Tadano et al. conducted the study about the thermal transition by DSC and believed the peak was attributed to the change of magnitude of the association between ion pairs in the ion-rich domain, i.e. ionic crystallite melting, instead of the melting of PE quasi-crystallites [161]. They annealed the EMMA ionomers, detected the change of specific volume with time and temperature, and measured the dynamic behaviour as well as dielectric constant to support their model. In their model, this endothermic peak is called "order-disorder transition peak" and below the transition temperature (T_i) the association between ion pairs is strong since charged functional groups arrange in an ordered state, while above T_i the arrangement are in a disorder state and the association becomes weak. The order-disorder thermal transition model were then used to well explain many physical properties of EMAA ionomers such as yield strength, hardness, and bending modulus [161, 57, 89, 58]. In 1992, Yano et al. assumed that ionic aggregations included not only ordered ion pairs also a small portion of ordered PE chains because they found the T_i peak still exists even when the ionic aggregations are fully hydrated [90, 198]. Meanwhile, because the incorporated water molecules (3 water molecules per Na^+) can completely destroy the ordered ion pairs in general, they supposed an orderness should still remain

inside ionic aggregations and the orderness perhaps originates from the arrangement of short segments of PE backbones adjacent to ionic groups. In 1995, Yano et al. showed again that the degree of water plasticizing ionic aggregations for Na-neutralized EMAA is much larger than for Zn-neutralized EMAA; in other words, Zn-neutralized EMAA is insensitive to humidity [160]. Changes of DSC and stiffness of Na- and Zn-neutralized EMAA ionomers immersed in water were examined, and both of them decrease and increase with immersion time for Na- and Zn-neutralized EMAA, respectively. Consequently, they believed that ordered ionic aggregations is the origin of the low-temperature endtherm instead of melting of secondary PE crystals. In 2000, Yano et al. carried out noncrystallinity EMAA ionomers containing 13.3 mole % of methacrylic acid also exhibits the T_i peak in DSC thermogram and ionic aggregations contain unneutralized COOH [91]. Changes in enthalpy, peak temperature, and relaxation phenomenon of this noncrystallinity EMAA ionomers with ageing are similar to that of partly crystalline EMAA ionomers. Besides, the effect of water sorption was discussed; EMAA ionomers stored in high humidity environment does not always promise to increase T_i and enthalpy gain; and even for "dry" EMAA ionomers, the T_i peak is still present. The literature emphasized again that in addition to T_i and T_m , one more endothermic peak appears when the ionomers are annealed at a temperature between T_i and T_m , and the new peak temperature is always higher than the annealing temperature and probably originate the melting of PE quasi-crystalline [161, 91]. All results were used to support the the low-temperature peak is referred to a thermal transition of ion pairs in ionic aggregations from ordered arrangement to disorderd state at heating.

Poly(ethylene-co-methacrylic acid) ionomers have quite high thermal stability. FTIR and thermal gravimetric analysis were used for the study of thermal degradation and found that the threshold of decomposition and the temperature at maximum

rate was closed to those of polyethylene [121, 88]. Degradation initially takes place from the neutralized groups. During the decomposition process, except degradation from chain ends, chain scission, side group scission, and transfer reactions all occur. The volatile components mainly include ethylene, carbon dioxide, propylene, dimethylketene and so on. At the high temperature, sodium carbonate and zinc oxide are the residues of Na-neutralized and Zn-neutralized EMAA ionomers (Na-EMAA and Zn-EMAA), respectively.

2.2.6 Mechanical properties of EMAA ionomers

It is well-known that mechanical properties of ionomers have dramatic changes when ion pairs aggregate. In general, neutralization is helpful for the formation of ionic clusters and depresses PE crystallization depending on the ion size and valence; therefore, the strength of ionic interactions and micro-structure of the aggregates are as function of degree of neutralization (DN) and metal type. Investigating the changes in DN and different compositions are commonly suggested by using Fourier transform infrared (FTIR) spectroscopy [54, 29, 177, 15]. For instance, the intensity of absorption peak and its corresponding wave number of COOH dimers and COO⁻ of EMAA ionomers can provide information about DN and force constant of the ionic bonds [54].

DN and counterions, including alkali, alkaline and transition metal salts, not only affect thermal properties of ethylene ionomers but also improve tensile performance and dynamic mechanical behaviour based on plenty of comparable curves [58, 153, 143]. For EMAA ionomers neutralized by alkali and alkaline metal ions, the yield stress (σ) and young's modulus (E) reaches a maximum at a certain neutralization degree, while for transition metal-neutralized EMAA both mechanical properties keep increasing with DN. According to the DN (33 %) at the maximum of E and

σ , the space formed by three carboxylate groups per Na or K ion is optimal [153, 58, 12, 138, 192]. The improvement of mechanical strength is explained by the contributions of PE crystal slide/plasticity, the separated relaxation processes in amorphous phase involving mobility-restricted regions of ionic clusters and formed secondary PE crystals. The thin secondary PE crystals, formed especially after ageing, act as a bridge between primary PE line and the regions of restricted mobility so that higher force is required to deform neutralized EMAA ionomers [143].

Besides, by comparing the DSC thermogram of un-stretched and 300 % elongated samples, Hirasawa et al. in 1991 was found the low-temperature peak and peak temperature of the latter sample depresses drastically, and they assumed that the ordered ionic pairs in aggregates are destroyed after the large-stain deformation [58]. Akimoto et al. found that high neutralization (>40 %) leads to the decrease of elongation at failure when Na-EMAA and Zn-EMAA are deformed by a high-speed strain [1]. The disappearance of DSC low-temperature peak was also detected for stretched EMAA ionomers neutralized by Na [1].

Water sorption also involves mechanical performance of EMAA ionomers since it basically works as a plasticizer which benefits ion hopping. Water affects ionic clusters on the surface first; as the amount of water achieves a level, it starts to enter the ion domains, stronger for Na-salts than for Zn-salts, resulting in screening of the interactions between counterions and carboxylate anions [90]. This phenomenon is also evidenced by Yano et al. in 1995 who showed the metal cation affects the response of EMAA ionomers to humidity [160]; high humidity causes the drop of stiffness with ageing time for Na-EMAA not for zn-EMAA. The moisture result from Akimoto et al. in 2001 was consistent; they took moisture absorption and ageing time into the parameters of low-speed and high-speed deformation testing for Na- and Zn-EMAA ionomers and showed water reduces the electrostatic forces more for

Na-EMAA since ion-hopping and chain relaxation happen in Na-EMAA at higher frequency than in Zn-EMAA [1].

Study of dynamic mechanical behavior of ethylene-methacrylic acid ionomers attract many attentions [159, 43, 114, 57, 115, 175]. EMAA ionomers are the copolymer of ethylene and small fraction of methacrylic acid (MA) so basically their dynamic mechanical properties resemble that of low-density or branched polyethylene. The incorporation of methacrylic acid can cause degree of PE crystallinity decreases, PE crystals become thinner, and glass transition temperature (T_g) increases drastically. Register et al. showed that in EMAA copolymer, PE primary and thin secondary crystals are $\approx 6\text{nm}$ and $\approx 3\text{nm}$, respectively [142]. When content of thin crystals or MAA content increases over a limitation, the overlapped α and β relaxation of low-density polyethylene (LDPE) in dynamic mechanical analysis [80] will merge into a single peak (β relaxation). The β peak of EMAA copolymers is regarded as the glass-rubber transition in amorphous phase where carboxylic acid dimers work as cross-links to limit the chain mobility and shift to higher temperature [115, 58]. The shift of T_g and strain rate let methacrylic acid-based PE copolymers differ from other PE copolymers, such as ethylene copolymers with styrene and α -olefins comonomers. When the content of these comonomers increases, PE crystalline decreases, which resulting in lower young's modulus. But for EMAA copolymers, a marked increment of yield stress and young's modulus even though at low PE crystalline occurs. The peculiar fact is because not only crystal slide/plasticity but vitrification of amorphous phase and incomplete relaxation process, their relative contribution highly affect the mechanical properties [173, 142].

Furthermore, once carboxylic acid groups are neutralized by metal cations, the rheology changes. Register et al. discussed the difference of yield stress of EMAA copolymers with zero-degree neutralization and Na-EMAA ionomers [142, 143]. Al-

though ageing and type of metal ions affect the dynamic modulus, the most significant factor of determining the viscoelastic response is how many carboxylic acid groups are neutralized. Degree of neutralization governs the formation of ionic cluster phase and change degree of polyethylene crystallinity. The mobility-restricted regions surrounding ionic aggregations in ionic clusters will prohibit the motion of polymer chains, resulting in the increase in chain relaxation time in amorphous phase compared to acid copolymer and allowing strain rate to play an important role in yield strength of EMAA ionomers [143]. Register et al. in 2006 assumed thin secondary PE crystals exist between PE primary crystalline and the mobility-restricted region [175] so that the secondary crystals also contribute to the relaxation time and the melting temperature of these crystals is affected by annealing temperature. Due to the mobility-restricted regions in ionic clusters and secondary PE crystals, the β relaxation peak of EMAA copolymers splits into two peak, so-called α and β relaxation. β peak is still attributed to glass transition of ion-depleted matrix; the new α relaxation is assigned to the motion of PE chains anchored by ionic aggregations and the thin PE crystals, concluded by Register et al. [143]. There is another assumption for α relaxation peak. They thought the origination was from the glass-rubber transition of the ion-rich domains [135, 58, 159]. Additionally, one more relaxation peak, α' , shown before the temperature of α peak, is independent of frequency, and its peak temperature agreed with that of low-temperature peak (Ti) in DSC thermogram; as a result, they believed the presence of α' confirmed the order-disorder transition of ionic aggregations [159].

3. EXPERIMENTAL SECTION: (LPEI/EMAA) LBL FILM FABRICATION

3.1 Materials and solution preparation

The two main polymers used in this study are linear polyethyleneimine (LPEI) as polycation and poly(ethylene-co-methacrylic acid) (EMAA) ionomers as polyanion. Their chemical structures are shown in Figure 3.1. The nominal molecule weight

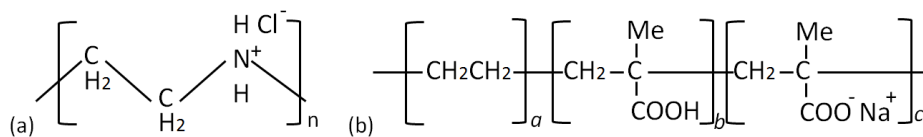


Figure 3.1: Chemical structure for (a) LPEI; (b) partially Na-neutralized EMAA ionomers.

of LPEI is 40,000 g/mol bought from Polysciences, Inc. and was used as received. LPEI is weak polyelectrolyte; its PK_a is 5-6 [113, 18], and in this study, pH of LPEI solutions are in the range of 4-10. EMAA ionomers used in this study was a commercial product which is provided from Dupont company, and its brand name is surlyn 8940 in which 5.4 mol% (15 wt%) of methacrylic acid (MAA) is contained and 30 % of MAA groups have been neutralized by sodium.

LPEI is water-soluble; so the concentration 0.01 and 0.02 M of aqueous LPEI solutions were prepared by directly adding LPEI as received into deionized (DI) water, and either diluted NaOH or HCl were used to adjust the pH value. Na-neutralized EMAA ionomers (Na-EMAA) does not dissolve in water. In this study, we tried many organic solvents to attempt to dissolve Na-EMAA. The solvents included n-Butyl alcohol, ethyl alcohol, ethylene glycol, methyl alcohol, toluene, cyclohexane,

chloroform, dimethylacetamide (DMAC), dimethylsulfoxide (DMSO), and tetrahydrofuran (THF). These solvents were chosen based on the data of chemical resistance of surlyn resin from Dupont company website; surlyn resin shows poor resistance in these solvents at room temperature or 60 °C. In the latter six solvents, soaked surlyn 8940 had more obvious changes in volume (swelling), and it can be found in Figure 3.2 that surlyn 8940 disperses much better in THF than in other solvents after heating.

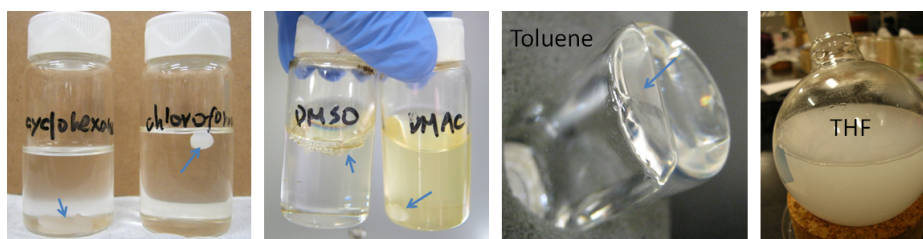


Figure 3.2: 30 % sodium-neutralized EMAA in different solvents; they were cooled down to RT from 75 °C in cyclohexane, 50 °C in chloroform, 150 °C in DMSO, 150 °C in DMAC, 100 °C in toluene, and 65 °C in THF.

Table 3.1 compares the solvents in terms of dielectric constant, polarity, and with or without hydroxyl (OH)/amine (NH) group. The EMAA ionomers are stirred and dissolved at 65 °C overnight; at this temperature, solution is transparent. After cooling down to room temperature (RT), EMAA ionomers uniformly disperse in THF, resulting in an opaque colloidal dispersion, and the particle size measured by dynamic light scattering (Brookhaven Zeta-85 Plus/PALS analyser) is ~750 nm. So, in this study THF was used as solvent for EMAA ionomers, and pH value of the solution was not in concern. The concentration of EMAA THF solution is ~0.5 wt%; lower concentration (0.25 wt%) of the solution was made by adding THF into 0.5

wt% solution directly. Non-ionized surlyn 8940 (EMAA copolymer with 5.4 mol% of MAA, brand name is nucrel 925) solution can be produced by the same process in THF, and it also belongs to colloidal dispersion although shorter heating time was required to get an uniform solution.

Table 3.1: Comparison of dielectric constant (k), polarity, and proticity for six different solvents; the solvents include dimethylsulfoxide(DMSO), dimethylacetamide(DMAC), cyclohexane, chloroform, toluene, and tetrahydrofuran(THF).

	DMSO	DMAC	cyclohexane	chloroform	toluene	THF
k	47	37.8	2.02	4.81	2.38	7.5
Polarity	Polar	Polar	Non-polar	Non-polar	Non-polar	Polar
Proticity	Aprotic	Aprotic	Aprotic	Aprotic	Aprotic	Aprotic

3.2 Layer-by-layer self-assembly and complex of LPEI/EMAA

Since LPEI is in an aqueous solution and EMMA ionomers disperse in THF, the LbL assembly of LPEI/EMAA was fabricated in a mixed solvent system. The process is shown in Figure 3.3(a); in the most of cases, the rinsing solution is DI water. The thin films were formed either manually or using Zeiss HMS serious programmable slide stainer, and in this study the substrates, which were cleaned before use by pirahana solution, 7:3 volume ratio of H_2SO_3 to H_2O_2 , at RT around 40 min, included glass slide, silicon wafer, and Teflon sheet. When using programmable slide stainer, clean substrates were first dipped into positive-charged LPEI solution for 10 min and subsequently rinsed by DI water for total 2.5 min so that the substrates were coated by one layer and the surface charge becomes positive. Formation of second layer to make one bi-layer was to expose the substrate right away into negative-charged EMMA THF solution for 10 min followed by total 2.5 min of DI water or

THF rinsing. When cycling the procedures, the polyelectrolyte multilayers (PEMs) containing EMAA ionomers were formed through electrostatic force and entropic gain [17, 37] and the number of bilayer and film thickness can be under a control. But, for manual LbL film, the dipping time was 3 min and film was rinsed for 1 min total. The LPEI/EMAA assemblies were dried in ambient environment for around one week before characterization.

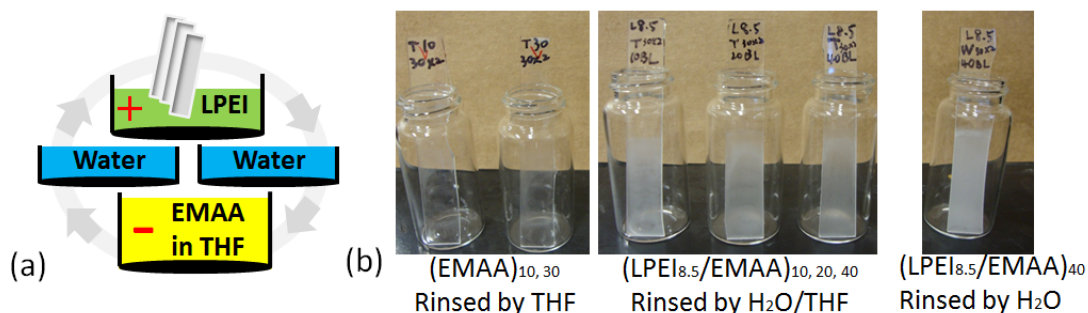


Figure 3.3: (a) Layer-by-layer process in this study; (b) in the left figure, substrate having a first dip in LPEI pH8.5 was dipped manually at 10 and 30 dipping steps in only EMAA THF solution, and the rinsing solution was THF; in the middle figure, LbL thin films of LPEI(pH8.5)/EMAA were made with 10, 20, and 40 bilayers and the rinsing solutions after LPEI and EMAA solution dipping were DI water and THF, respectively; in the right figure, the rinsing solutions were all DI water.

In order to confirm LPEI/EMAA thin films were really built up by LbL assembly method, not just coating of EMAA, we dipped glass slides in EMAA only as a control (Figure 3.3(b)). The control sample only dipped in EMAA THF solution was followed by THF rinsing; it showed that even increasing the number of bilayer, without LPEI dipping, EMAA cannot build up a thick film on its own way. However, when LPEI was deposited to become the outmost surface of the substrate before every EMAA dipping, the film can grow up and it was confirmed by thickness measurement. Also in

Figure 3.3(b), the film looks more opaque and thicker when water rinsed the substrate after EMAA dipping. The reason probably is because water is a bad solvent for EMAA ionomers, the EMAA which only physically bound on the substrate surface are rinsed away incompletely, or the chain conformation of EMAA becomes more coiled in water so that more EMAA leave on the substrate and the color becomes dark.

Complexes of LPEI and EMAA were made by directly mixing pH8.5 LPEI solution and EMAA THF solution. The concentration of both solutions were 0.5 wt%, and the ratio of solution volume was 1:1. LPEI solution was slowly poured into EMAA solution; after waiting for 5 minutes, opaque LPEI/EMAA complexes were rinsed by DI water thoroughly, and then dried at 50 °C overnight.

In this study, We needed to prepare free-standing film for some characterization, such as dynamic mechanical analysis (DMA). Free-standing film is the film peeled off from the substrate; since the thickness of polyelectrolyte multilayers is usually on nano-scale, it is difficult or necessary to grow hundreds bilayers to get a free-standing film. There are some literature showing different methods to isolate polyelectrolyte multilayers; for example, exposing the film into solvents [16, 214], making a sacrificial layer [52], and using low surface energy substrate, such as Teflon [112, 146]. In this study, Teflon substrate has been tried but the result was bad. Assembly of LPEI/EMAA not only can not be peeled off but also had a powder-like surface; the film did not grow well on Teflon substrate. Therefore, a post-treatment for de-attachment of LbL LPEI/EMAA film was introduced and included three procedures. First procedure was to heat LbL film at 120 °C for 15 min; second procedure was to soak the heated film in 1 M NaOH and shake it by a vortexer for 3 min, and final one was to rinse the film by seven-times separated DI water for 11 min total. After the post-treatment, it was very easy to peel the film off substrate, and the transparent

stand-alone film, shown in Figure 3.4(a), was dried and stored in a desiccator until testing.



Figure 3.4: (a) Free-standing film of $(\text{LPEI}_{8.5}/\text{EMAA}_{0.5\text{wt}\%})_{25}$; (b) free-standing film made without the first heating procedure.

The reason of why NaOH is the medium to isolate film is that the base bath deprotonates the secondary amine groups of LPEI (decrease of charge density) so that the electrostatic attraction between LPEI and negative-charge surface of the substrate are broken. But concurrently, the carboxylic acid groups are deprotonated, which may create more ionic bonding between LPEI and EMAA ionomers. In some cases, strong base and addition of salts can swell and decompose LbL film by decreasing intrinsic compensation of polymer/polymer interactions [26, 38]. In LPEI/EMAA system, we used 1 M NaOH with pH value ~ 13.5 ; although the base is very strong, no destruction of film was observed and it was proved by a constant LPEI content.

The heating temperature, 120°C , is above the melting point of the (LPEI/EMAA) LbL film (the detail about the melting point will be in section 4). So, the heating process improves the polymer chain diffusion and decreases the free volume to make the film more compact. Figure 3.4(b) is the free-standing film which was made without going through heating process, and obviously, the film is still opaque and very

brittle.

3.3 Elemental analysis and FTIR analysis

The literatures involving incorporation of ionomers into LbL system are few since most materials for LbL system are polyelectrolytes. LPEI/Na-EMAA LbL system made its debut in this study. So, it is necessary to confirm the build-up of LbL film and investigate its basic characteristics before doing further complicated characterization. Here, elemental analysis and fourier transform infrared spectroscopy (FTIR) characterizing the physical properties of LPEI/EMAA multilayers are discussed first. Analysis of FTIR spectra were taken with a Bruker Optics ALPHA-P 10098-4 in ATR mode.

In order to understand the content of each component inside the assembly, LPEI and EMMA containing films fabricated by LbL technique and scratched from substrates were sent to Atlantic Microlab, Inc. for elemental analysis. With the help of elemental analysis, percent by weight of important elements inside the sample (C, H, and N) was determined, and based on the data, the weight % of LPEI or EMMA was calculated and shown in Figure 3.5(a). Error range is ± 0.3 %, provided by the company.

Figure 3.5(a) demonstrates the content of LPEI in 25-bilayer of LPEI/EMAA LbL films at different deposition pH and concentration of EMMA THF solution. The LPEI content in the pH 4-9 range all are less than 10 wt%. It is relative low compared to common polyelectrolyte multilayers, and according to our experiments, when pH of LPEI solution was smaller than 4.8, the LbL film was hardly fabricated. But since surlyn 8940 only has 4.5 wt% of MAA groups neutralized by sodium, in order to balance 1:1 stoichiometry of charged repeat units, it is reasonable to get a low LPEI content. For example, suppose that 100 gram of LPEI/EMAA film consists

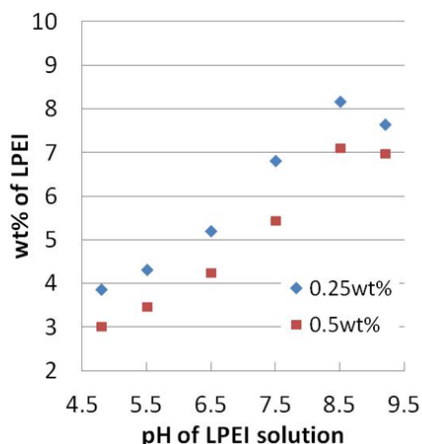


Figure 3.5: LbL film of $(\text{LPEI}/\text{EMAA}_{0.25\text{wt}\%})_{25}$ and $(\text{LPEI}/\text{EMAA}_{0.5\text{wt}\%})_{25}$ at pH values of LPEI solution 4.8, 5.5, 6.5, 7.5, 8.5, and 9.2, measured by elemental analysis presented by LPEI content by weight percent.

of χ gram of LPEI and $100-\chi$ gram of EMAA, here LPEI is fully charged (solution pH is ~ 2.6) and EMAA has $0.045 \times (100-\chi)$ gram of charged MAA groups. If all COO^- in EMAA interact with charged 2^{nd} amine groups of LPEI, a formula " $\chi \div 46189.5 \times 581 = 0.045 \times (100-\chi) \div 108$ (unit: mole)" should be agreed. In this formula, 108 is the MW of a charged MAA group, and 46189.5 is the real MW of LPEI in which one chain contains ~ 581 repeat units announced on Polysciences, Inc. website (MW of one repeat unit is 79.5 and MW 40,000 g/mol is just a nominal value). By this formula, we can get χ is 3.2; in other words, only 3.2 wt% of fully charged LPEI at 2.6 is needed to compensate the all negative-charged carboxylic acid groups in EMAA. So, low LPEI content is expected.

However, 3.2 wt% is very close to elemental data of 3.87 and 3.03 wt% at pH 4.8; at pH 4.8, charge density of LPEI should be between 50-100% since pKa of LPEI solution is 5-6 [113, 18]. Theoretically, more LPEI at pH 4.8 are needed to compensate the COO^- groups on the condition of 30 % of MAA groups neutralized by sodium.

As a result, there are some $\text{COO}^- \text{Na}^+$ still existing in LbL films of LPEI/EMAA. Another evidence to prove the existence of $\text{COO}^- \text{Na}^+$ is that at pH5.5, LPEI content in $(\text{LPEI}/\text{EMAA}_{0.25\text{wt}\%})_{25}$ and $(\text{LPEI}/\text{EMAA}_{0.5\text{wt}\%})_{25}$ are 4.33 and 3.77 wt%, respectively, both of them are smaller than 2 times of 3.2 wt%, calculated based on 50% ionization degree of LPEI.

The assumption that at various pH, neutralization degree of MAA groups does not change and keep 30% by sodium actually is wrong. Figure 3.6 is FTIR analysis for LbL films of LPEI/EMAA and min-max normalization method was used to normalizaed all spectra. The figure demonstrates the peak at wavenumber 1698 cm^{-1} depresses and a broad peak at $1500\text{-}1590 \text{ cm}^{-1}$ increases with the increase in solution pH. The peaks of 1698 cm^{-1} peak and $1500\text{-}1590 \text{ cm}^{-1}$ peak are assigned to COOH dimers and COO^- asymmetric stretches, respectively. The broadness of carboxylate peak originates from ionic bonds with different force constants [54] and a peak at 1541 cm^{-1} is attributed to some sort of local structure found in multiplets and clusters.

Compare to the intensity of COOH and COO^- peak of surlyn 8940, it can be found that at pH4.8-7.5, neutralization degree is lower, but at pH8.5-9.2 the degree is higher, although the neutralization degree (ND) of EMAA in THF solution drops a little bit in Figure 3.7. In other words, at low pH incorporation of LPEI acids EMAA ionomers in LbL assemblies while at high pH EMAA ionomers neutralizes LPEI. It is necessary to know that there is no pKa for EMAA THF solution and the solution pH did not be changed. So, ND of EMAA is not dependent on pH value of its solution, unlike weak polyelectrolyte aqueous solution [149, 33], but it is possible that the charged density of absorbed LPEI chains affects ND of EMAA. About the origin of protons that acid the EMAA ionomer at pH4.8-7.5, perhaps it can be explained by the migration of protons from LPEI to EMAA.

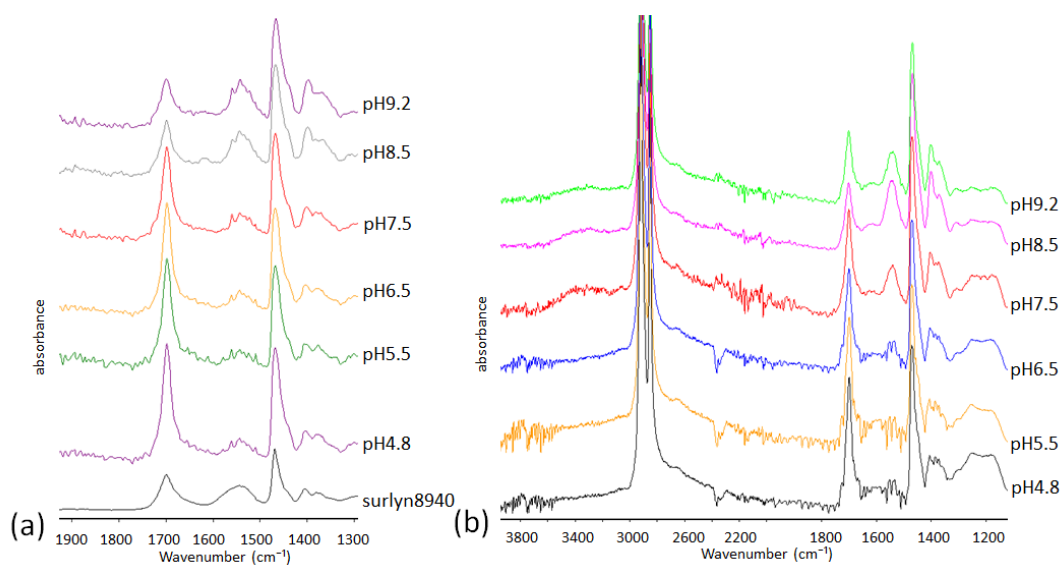


Figure 3.6: LbL film of (FTIR curves of LbL film of (a)(LPEI_{0.1M}/EMAA_{0.5wt%})₂₅ and (b)(LPEI_{0.1M}/EMAA_{0.25wt%})₂₅ at various pH values; wavenumber range is 3800-1200 cm⁻¹).

According to lower LPEI content than calculated value, a small portion of COO⁻ does not form electrostatic interactions with charged 2nd amine groups. For other portion of COO⁻, when their amount decreases, they do not need so many charged amine groups to achieve charge balance any more. Under the requirement of not decreasing LPEI content, the charged density of LPEI chains has to diminish. As a result, donating protons from LPEI to EMAA can not only decrease ionization degree of LPEI but also raise the intensity of COOH in EMAA ionomers resulting in additional hydrogen bonding. The same explanation adapts to pH8.5 and pH9.2 cases. At pH8.5, LPEI is partially charged; at pH9.2, LPEI is almost completely deprotonated and maybe few precipitation occurs [190]. The migration of protons from EMAA causes the increment of charge density of LPEI to compensate negative charges of COO⁻. Since the release of hydrogen ions, ND of EMAA increases shown in Figure 3.6. The migration of protons occurs on both LbL thin films dipping in

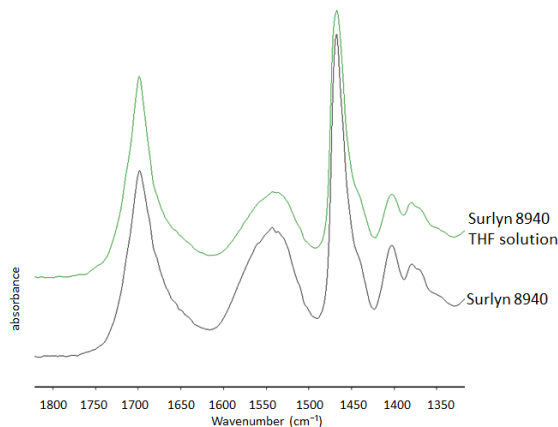


Figure 3.7: LbL film of FTIR spectra of surlyn 8940 pellets and surlyn 8940 dissolved in THF.

EMAA THF solutions of different concentration, but it does not affect the remaining of $\text{COO}^- \text{Na}^+$ ionic bonds in EMAA ionomers.

The migration of protons has an influence on pKa of LPEI in LbL assemblies. It is because at pH 4.8-7.5, compared to ionization degree of initial LPEI solutions, that of absorbed LPEI onto EMAA layer becomes larger so that effective pKa of LPEI is pushed to a lower value after incorporating into polyelectrolyte multilayers containing EMAA. There is a similar case about pKa change of polyelectrolytes in LbL PAA/PAH assemblies been investigated by Rubner et al. in 2000 [149, 33].

From Figure 3.5, it also can be found that the LPEI content at all pH values in LbL of $(\text{LPEI}/\text{EMAA}_{0.25\text{wt}\%})_{25}$ is higher than that in $(\text{LPEI}/\text{EMAA}_{0.5\text{wt}\%})_{25}$. In both cases, ionic bonds between COO^- and metal ions do not all destroyed by the incorporation of LPEI. But, lower concentration can lead to lower viscosity of EMAA THF solution. It benefits the penetration of LPEI into ionic aggregations in EMAA ionomers [150] to increase the opportunity of bonding with carboxylate groups. Consequently, LPEI content increases for the sample of low EMAA concentration and

the migration of protons does not affect the result. Moreover, in this study, we also tried to quench EMAA by liquid nitrogen to increase LPEI content. We used liquid nitrogen to quench melt EMAA pellets which were heated at 130 °C right away, and then dissolved the EMAA in THF at 65 °C overnight. We found LPEI content of the LbL films assembled by LPEI at pH7.5 and the specific EMAA THF dispersion is higher than the regular one; LPEI content, 7.09 wt%, is 1.3 times larger than that of (LPEI_{7.5}/EMAA_{0.5wt%}) LbL film.

LPEI crystalline hydrates in Figure 3.8 is the precipitation of LPEI in aqueous solution at high pH, usually at pH ≥ 9.4 [190]. Since highly deprotonated LPEI chains precipitate and form the crystalline hydrate, the free 2nd amine groups are the characteristics of the two strong peaks of ~ 3260 and ~ 1115 cm⁻¹ in Figure 3.8(a). The two peaks also emerge obviously on the sample of LbL (LPEI₁₂/EMAA_{0.5wt%})

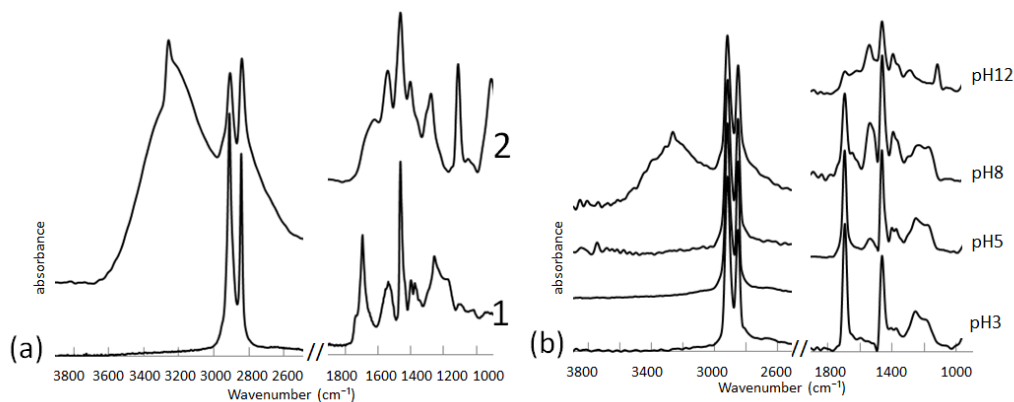


Figure 3.8: FTIR spectra of (a)1 is surlyn 8940 and 2 is LPEI crystalline hydrates; (b)LbL films assembled by 0.5 wt% of EMAA and 0.02M LPEI with various pH, in pH12 sample crystalline hydrates remain in the solution without filtration.

film in which LPEI crystalline hydrates were contained since LPEI was at a very high pH value.

In Figure 3.6(b), as pH increases, a peak at high wavenumbers also emerges but shifts to 3300 cm^{-1} a little bit; this peak is attributed to both of free secondary amine groups and water hydroxyl groups (O-H) [152]. Charged 2^{nd} amine groups, on the other hand, are present by a weak peak at $\sim 1615\text{ cm}^{-1}$ in Figure 3.6. The peak intensity also becomes stronger when pH of LPEI solution is above 7.5. The appearance and increase in intensity of peak 1615 cm^{-1} are consistent with the raise of carboxylate groups; besides, the emerge of this peak also verified the existence of LPEI in the PEMs containing EMAA ionomers. The IR spectra of complexes of

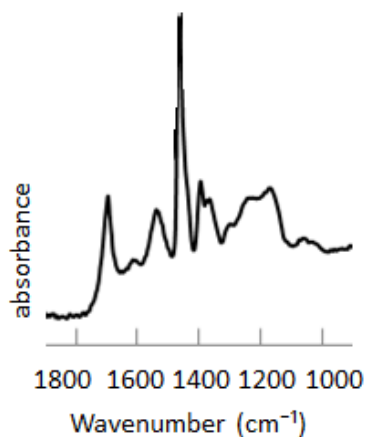


Figure 3.9: FTIR spectra of $(\text{LPEI}_{8.5}/\text{EMAA}_{0.5\text{wt}\%})$ (1:1) complexes.

LPEI/EMAA were also measured by FTIR, seen in Figure 3.9. Like LbL films, a peak at $\sim 1615\text{ cm}^{-1}$ representing charged 2^{nd} amine groups was also detected.

In order to know the alternation in ionization degree of these functional groups during the post-treatment for making free-standing film, $(\text{LPEI}_{8.5}/\text{EMAA}_{0.5\text{wt}\%})_{25}$ LbL film was taken as representative for FTIR measurement. The LbL film was heated at two different temperatures, 120 and 180 °C, and then using base treatment the heated films were peeled off to get free-standing films. Both temperatures are above

melting point (T_m) of EMAA ionomers (~ 94 °C) and there is no T_m for pure LPEI. The FTIR spectra is present in Figure 3.10. When the heating temperature is 120

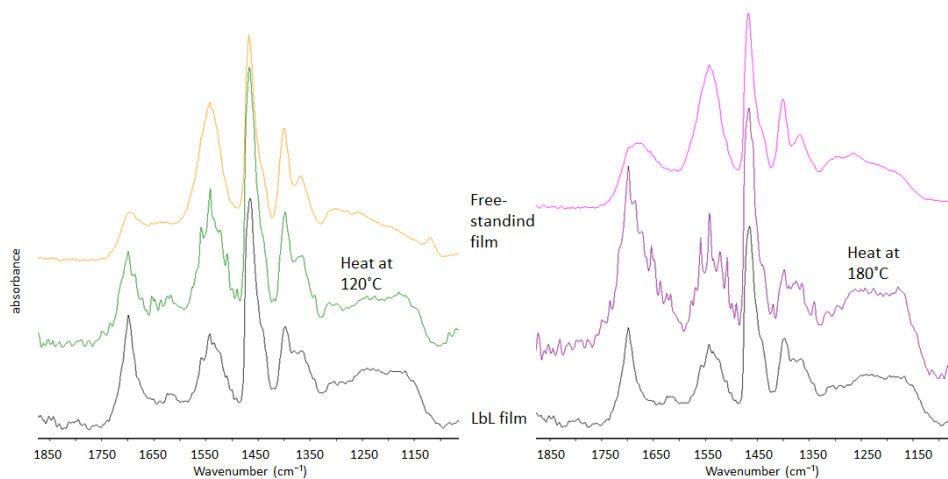


Figure 3.10: FTIR spectra of LbL film, LbL films heated at 120°C for 15 min and 180°C for 15 min, and the corresponding free-standing films of $(\text{LPEI}_{8.5}/\text{EMAA}_{0.5\text{wt}\%})_{25}$.

°C, we found that the neutralization degree of heated film increases, which results in the improved transparency. The increment of ND by thermal energy was also found in some literatures [141]. High temperature induces the flow of polymer chains that the PE crystalline in EMAA are melt but ionic aggregations still persist. So, the slow-reformation of crystalline allows to reduce internal haze and the high melting strength provided by ionic aggregations makes EMAA ionomers a good adhesives and no obvious flow of materials occur during the heating process, even at 180 °C. After NaOH immersion, no matter heated at 120 or 180 °C the corresponding free-standing films have a dramatic increase in the degree of neutralization, characterized by the strong intensity of wavenumber ~ 1540 cm^{-1} . It is because sodium hydroxide highly deprotonates EMAA ionomers; concurrently, plenty of free amine groups generate

that causes clear peaks at wavenumber 3260 and 1115 cm^{-1} emerge (only show 1115 cm^{-1} in Figure 3.10). The NaOH immersion may also cause the swelling of films. So, compared to LbL films, more ionic bonds of $\text{COO}^{-}\text{Na}^{+}$ form in the free-standing film and may affect the film properties.

When the heating temperature is 180 $^{\circ}\text{C}$, the film becomes yellow, which indicates the existence of amide groups and covalent bonding, and the ND does not increase as the case at 120 $^{\circ}\text{C}$. However, a new peak at $\sim 1675 \text{ cm}^{-1}$ appears; the peak originate from the tertiary amide and the creation of thermal cross-linking should be formed by the charged amine groups and carboxylate groups. The amide peak is more easily seen in the free-standing film. It overlaps with the COOH dimers peak. Its existence confirm the successful incorporation of LPEI into LbL system with EMAA ionomers again.

3.4 Thickness measurement

The thickness and surface roughness of films are measured by profilometer (KLA Tencor Instruments P-6). The growth at every step in Figure 3.11 verifies the assembly is truly a multilayers blended by the two materials using LbL technique. From Figure 3.11, it can be found that the films are thick and presents an exponential growth. Usually, LbL films assembled by polyelectrolytes are thin; they have nano-scale thickness. The thick LPEI/EMAA film results in part from EMAA and solvent effect because EMAA in THF solution is colloidal dispersion and water is a bad solvent for EMAA ionomers, which is able to cause the cluster of EMAA in THE/water mixture.

Figure 3.12 shows the concentration effect of EMAA THF solution on the LbL film thickness and roughness. It is found that the film mad by low concentration of EMAA is thinner and some of thickness change with pH values follow the trend of

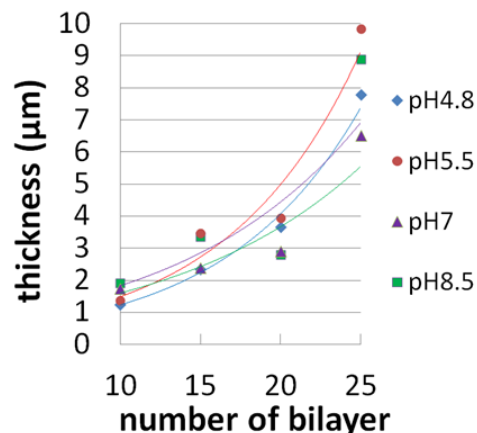


Figure 3.11: Growth curve of (LPEI_{0.02M}/EMAA_{0.5wt%}) LbL films at a range of LPEI pH values and as a function of bilayer number.

LPEI content in Figure 3.5. We believe EMAA solution is a dispersion and particles are on a colloidal size so that EMAA content in the film will have a momentous influence on the thickness. So, the lower EMAA content in the LbL films made by dilute EMAA solution causes a thinner absorbed layers than the layers made by 0.5 wt% of EMAA solution. However, on the other hand, at the same concentration the film at pH8.5 shows the largest thickness while based on Figure 3.5, the EMAA content at this condition is lowest. Therefore, the explanation that more EMAA has thicker films does not work in this case. It is known that thickness of LbL film is highly affected by chain conformation and the conformation is highly dependent on ionic strength and pH of solutions [149, 204, 37, 39, 38]. For strong polyelectrolytes, the fabricated film without controlling or increasing ionic strength will be very thin and even disassembled. It is because the intramolecular repulsive force on the fully charged polymer chains lets chains stretched and solid into a flat conformation. In contrast, when chains become coiled by adding salts into solution or changing solution pH value to decrease charge density on each chain due to charge screening,

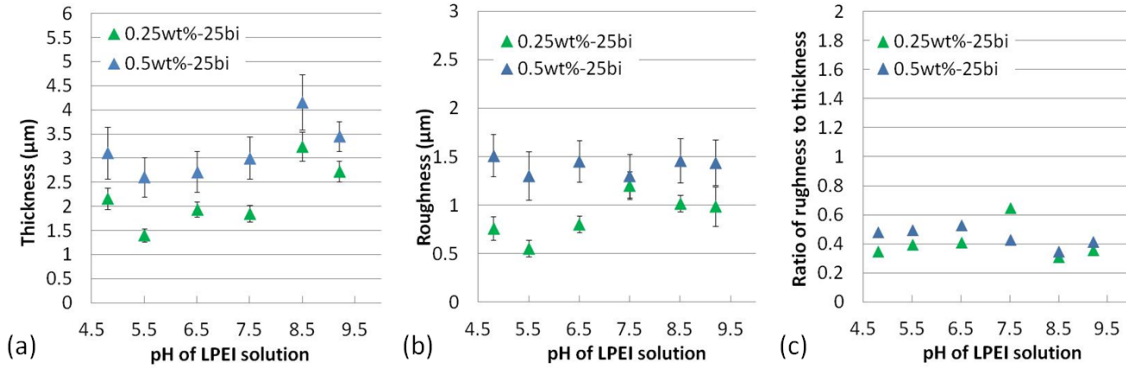


Figure 3.12: (a) Thickness and (b) roughness of $(\text{LPEI}_{0.01M}/\text{EMAA}_{0.25wt\%})_{25}$ and $(\text{LPEI}_{0.01M}/\text{EMAA}_{0.5wt\%})_{25}$ LbL films at various pH values.

the chains become flexible and are capable of interpenetrating into layers with the help of intermolecular interactions. The coiled-like conformation makes more polyelectrolytes deposition and then increase the thickness; it is also why some LbL films exhibit exponential growth.

Due to the migration of proton from LPEI to EMAA at low pH values or from EMAA to LPEI at high pH values, the LPEI chain conformation changes and is not just as a function of solution pH, like pK_a has been changes after assembly. So, it complicates the prediction of thickness. Furthermore, low content of ion pairs in EMAA tend to congregate; they share the counterions and form nano-scale spherical aggregations, and literatures show the morphology of Na-EMAA ionomers is more complex than other ionomers [100, 163]. The incorporation of LPEI, therefore, has to break through the ionic aggregations first and form complex with EMAA by charge compensation. The competition between the persistence of ionic aggregations and attraction between polymers may also affect the thickness. So, they complicate the prediction of film thickness. What we can suggest is that after the proton migration, LPEI chains at high pH values have more obvious conformation arrangement to

create high population of loops, trains, and tails (a loopy conformation), and it is possible that after assembling more ionic aggregations still exist with larger mobility-restricted region resulting in hard interpenetration. Both eventually cause thicker layers with the increment of deposition pH value.

The roughness in Figure 3.12(b) is root mean square (RMS) roughness, it is a roughness calculation method widely used. Roughness in LPEI/EMAA LbL system always keeps high. It does not be affected a lot when using low concentration of EMMA THF solution, shown in Figure 3.12(c). There are many reasons able to affect the roughness; EMMA colloidal dispersion, bilayer number, rinsing solution, chemical nature, and manufacture processing all involve this issue. In Figure 3.13(a), at the

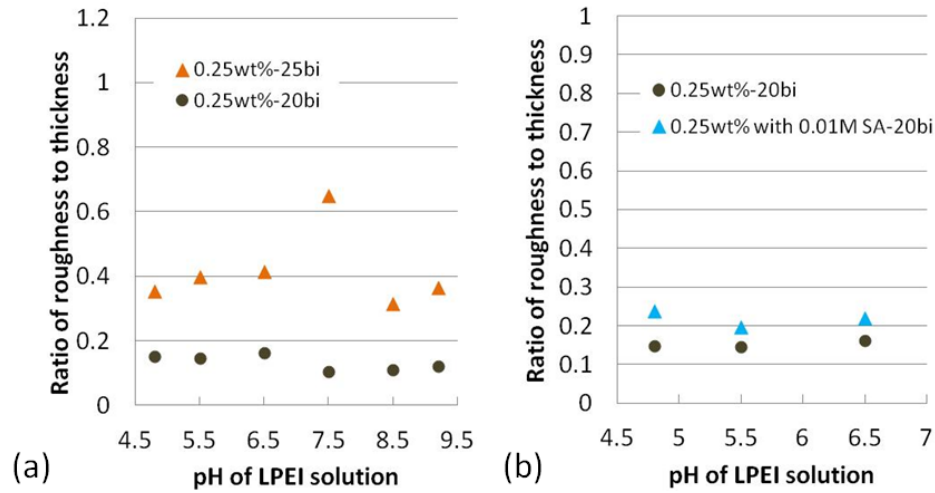


Figure 3.13: Ratio of roughness to thickness of (a)(LPEI_{0.01M}/EMAA_{0.25wt%}) LbL films with 20 and 25 bilayers (b)(LPEI_{0.01M}/EMAA_{0.25wt%})₂₀ LbL film and (LPEI_{0.01M}/EMAA_{0.25wt%} adding 0.01 M sebacic acid)₂₀ LbL film, as a function of LPEI pH value

same EMMA concentration, LbL films with lower bilayer number show smoother surface. Decreasing bilayer number probably is helpful, but in this case, in addition to

layer number, there was a difference for the two samples with respect to manufacture processing; that is the number of substrates which were taken into LbL assembly for making the 20-bilayer and 25-bilayer films are 1 and 17, respectively. In Figure 3.13(b), the addition of sebacic acid (SA), a plasticizer, into the EMAA THF solution also affects the roughness. But in this study, we found heating is the best way to smooth the surface.

3.5 Surface morphology

The roughness change by temperature is verified by profilometer and atomic force microscopy (AFM). Figure 3.14 displays the images with photography treatment by profilometer 3D scanning of different film surfaces. The figure compares the texture of LbL film and heated films at different temperatures and duration, and the cross as a reference is the substrate without coating. It is sand paper-like texture for the

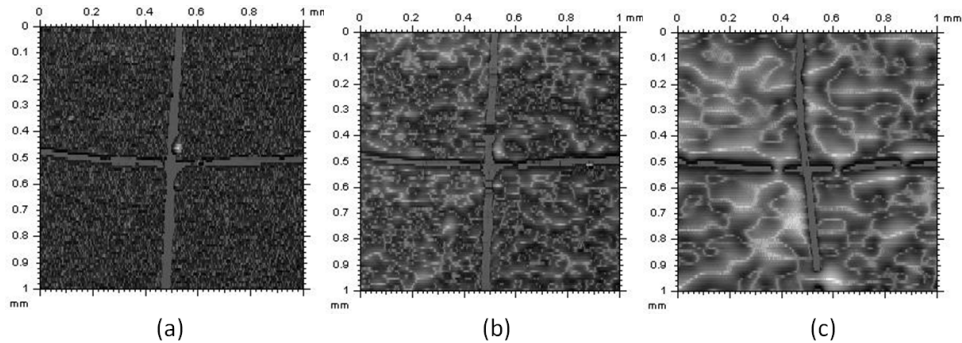


Figure 3.14: Surface images of films of $(\text{LPEI}_{7.5}/\text{EMAA}_{0.25\text{wt}\%})_{25}$ (a) as deposited (LbL film), (b) heated at 120 °C 15 min, and (c) heated at 100 °C 18 hours, scanned by profilometer

LbL film while after heating, the surface materials look melting, mix together, and smooth the surface. The ratio of maximum height of LbL film to heated films are 2.9

and 9 for the samples heated at 120 °C 15 min and at 100 °C 18 hours, respectively. The ratio indicates heating affects the roughness profoundly. Additionally, since both temperatures are above the melting point of EMAA ionomers, the materials interrupt the cross, found especially at 100 °C 18 hours, evidence the flow of polymers.

Figure 3.15 displays the AFM images of LbL film taken by a Bruker Dimension Icon AFM. The surface of LbL multilayers is very rough. In Figure 3.15(a), it can

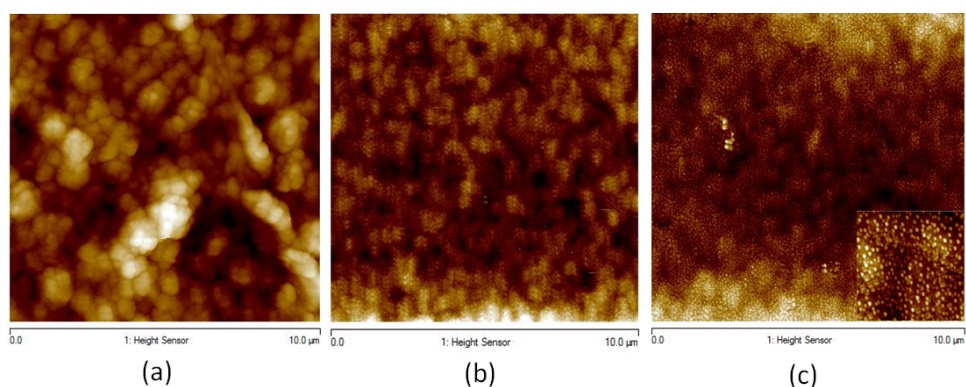


Figure 3.15: Surface images of films of $(\text{LPEI}_{7.5}/\text{EMAA}_{0.25\text{wt}\%})_{25}$ (a) as deposited (LbL film), (b) heated at 120 °C 15 min, and (c) peeled off the substrate (free-standing film), taken by AFM

be found that there are some cavities (the darker portion) and the hills seem to be formed by the accumulation of many aggregations. The phenomenon indicates that the colloidal size of EMAA ionomers in THF probably does not change or even become larger after incorporating into LbL assembly. Also, solvent effect exists and absorbed EMAA dispersion hardly move once the electrostatic interactions occur with LPEI chains so that the opportunity of making a film with uniform thickness diminishes naturally. That not all of the EMAA ionomer which physically deposit on the outmost layer are rinsed away makes in part contribution to the high roughness.

Compared to the LbL film, AFM image of heated film is more smooth and the roughness measured by AFM decreases $\sim 97\%$. The aggregations in Figure 3.15(a) all disappear even though there are still some darker cavities. Smoothing the surface is due to the melt of PE crystalline and the flow of polymer chains upon thermal energy. Another benefit of heating is the difficulty of scratching a heated film dramatically increases; otherwise, it is easy to scratch LbL films by a tweezers. Figure 3.15(c) shows the surface image of a free-standing film. The surface is still very smooth, but different from heated film, many ellipsoids with major and minor axis being 62 and 31 nm, respectively, condense and uniformly disperse on the surface. The exact origin of the ellipsoids is not fully understood. But since they do not appear in heated film, the deprotonation of materials due to base immersion should involve the creation of the ellipsoids.

3.6 Solvent effect

In order to investigate solvent effect in LbL fabrication, this study added DI water directly into 0.25 wt% of EMAA THF dispersion as the polyanion solution. Before making LbL films, we made 0.002 wt% of EMAA dispersion containing different weight percent of water in vials and stored them in the ambient environment to detect the uniformity condition of the dispersions. The change with stored time is shown in Figure 3.16. The weight percent of water in the dispersions are 0, 10, 20, 30, 40, 50, 60, 70, 80, and 90. According to Figure 3.16, EMAA particles in dispersion would aggregate in the water containing solvents. Water is not a good solvent for EMAA ionomers and the two solvents (THF and water) are only partially miscibility; therefore, EMAA ionomers tend to aggregate based on the hydrophobic interactions and obvious phase separations are shown. The EMAA clusters were created, especially in the cases that the ratio of THF and water are 60/30 to 30/60.

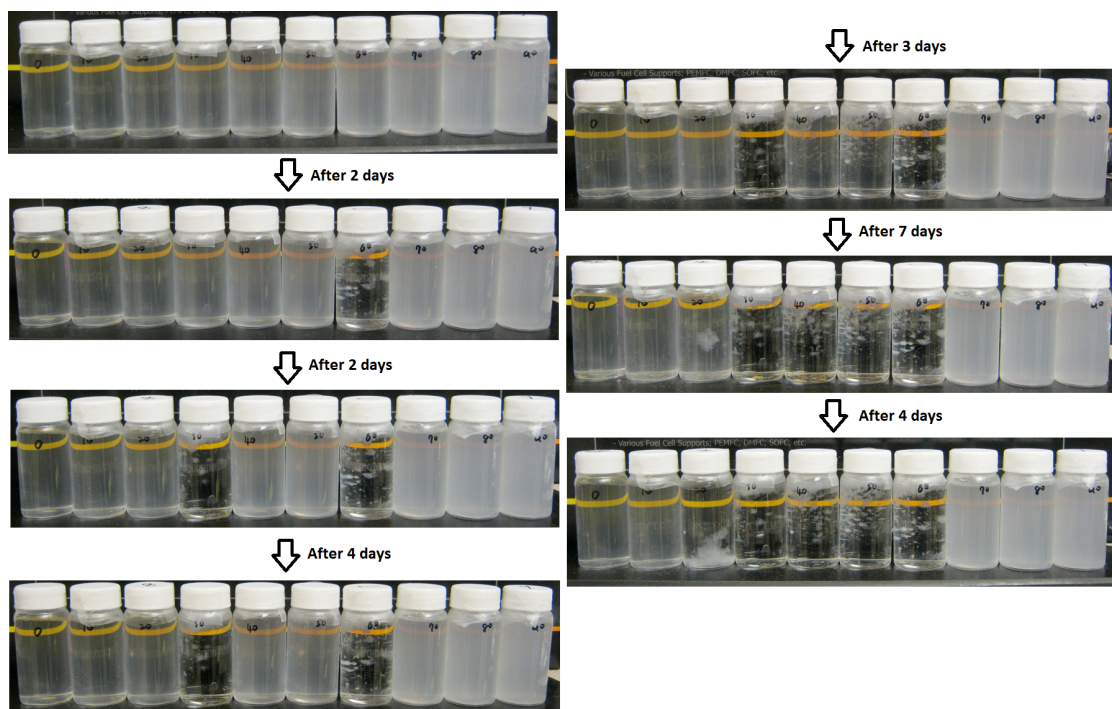


Figure 3.16: Stored EMAA dispersion containing water for different time duration. The weight percent of water from left to right vials are 0, 10, 20, 30, 40, 50, 60, 70, 80, and 90 wt%.

Oppositely, at high water or THF content, EMAA particles dispersed well. It is because the solvent with low content is miscible in the main solvent.

Figure 3.17 shows the LbL films made by hand dipping with 15 bilayers and the polyanion is the water containing EMAA dispersion. The dipping time is 4 minutes for both polyion solutions followed by 1 minute total water rinsing, and finally the fabricated films were dried in the ambient environment. The concentration of LPEI solution is 0.01M, and the concentration of EMAA dispersion containing 10-50 wt% and 60-90 wt% of water are 0.25 wt% and 0.05 wt%, respectively. The surface morphology of these LbL films under the microscope, and the film thickness and surface roughness are shown in Figure 3.18(a) and 3.18(b), respectively. The changes in terms of surface morphology and film thickness with water content indicate the

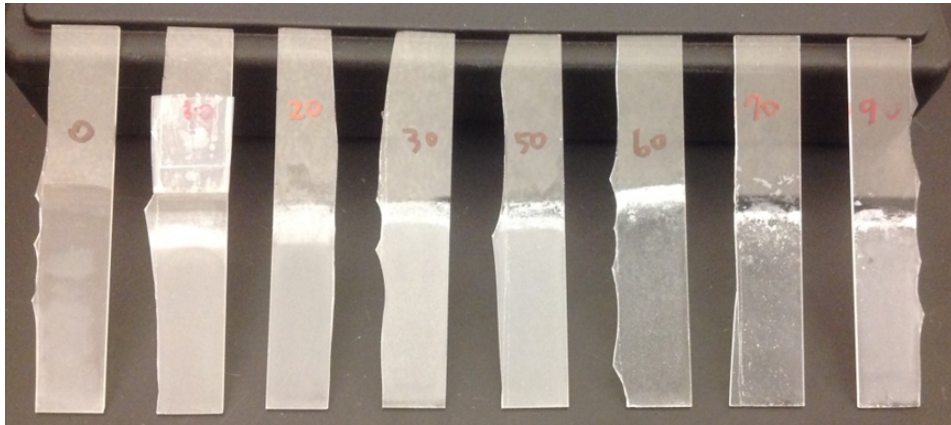


Figure 3.17: The LbL films of (LPEI/EMAA with water)₁₅. From left to right, the water weight percent in EMAA dispersion are 0, 10, 20, 30, 50, 60, 70, and 90.

solvent effect in the LbL fabrication. Adding water affects the film surface quality and increases the surface roughness, resulting some of the film surfaces are under poor quality and probably get phase separation. Further measurements, such as elemental analysis and film growth curve, are needed to verify the LPEI content in these water-containing LbL films.

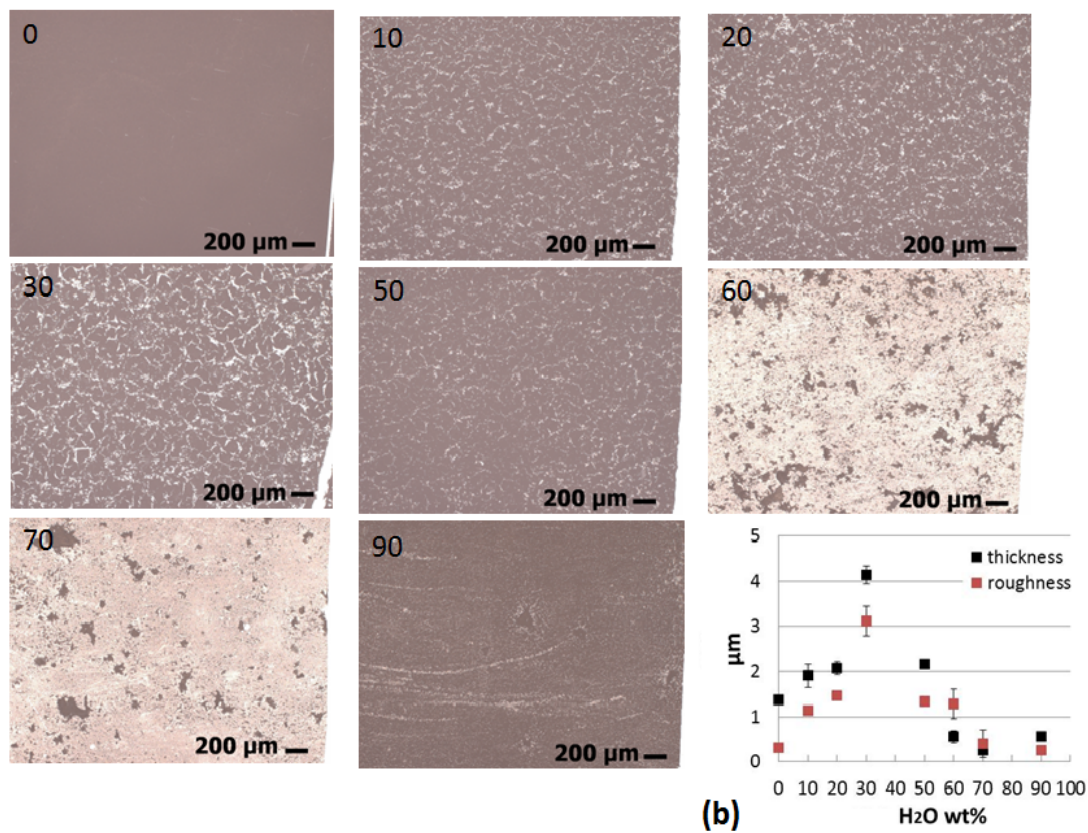


Figure 3.18: (a) Surface morphology and (b) film thickness and roughness of LbL films of (LPEI/EMAA with water)₁₅. In (a), the number on the left top of each microscopic image is the weight percent of water in the EMAA dispersion.

4. EXPERIMENTAL SECTION: THERMAL PROPERTIES

In section 2, we discussed a lot about thermal properties of EMAA ionomers, especially focus on the endotherms in differential scanning calorimetry (DSC) thermogram. There are two major explanation for the low-temperature peak that is shown during 1st heating, disappears at an immediate 2nd heating, but recovers after a long relaxation time [120, 161, 111, 93, 91]. One of them assigned the origin of the DSC peak to the melting of secondary polyethylene crystals distributing in amorphous matrix, and the thin crystals are also the bridges of ionic aggregations and major PE crystalline. The other group assumed the thermal transition is an order-disorder transition of ionic aggregations; below the peak temperature, ion pairs in the aggregate have strong association or in an order state while above the temperature, the association becomes weak even though ionic aggregations still persist. So far, there is no direct evidence to prove which explanation is correct. The investigation of thermal property in this study did not attempt to evaluate either explanation right or wrong; what we focused is to determine and analyse the effect of incorporation of LPEI into EMAA ionomers using LbL technique.

In the study, thermal characteristics of the fabricated films were conducted via traditional DSC and modulated DSC (Q20 and Q200, respectively, TA instruments), and all DSC thermogram are plotted by endotherm down. DSC is a powerful tool to monitor the relationship between heat effects and phase transitions, such as melting, and some chemical reactions. Basically, DSC heats two materials together by two heaters; one material is as reference and the other is the unknown sample. Supposed they are different materials, they will absorb different amount of heat to change their temperatures but their temperatures are increased at a constant rate. So, DSC

record the difference of heat flow as a function of temperature. In this study, the typical temperatures, like melting point and crystallization temperature, were read by the maximum point of peaks, and the enthalpy changes were calculated by the area under peaks.

In a traditional DSC, the study used $10\text{ }^{\circ}\text{C}/\text{min}^{-1}$ for both heating and cooling rates and each sample was at least 8 mg. The sample was initially cooled down to -50°C , followed by heating to 130°C , and then provided a 5 min isothermal treatment, and cooled back to -50°C , and finally heated to 130°C . In a MDSC, a similar thermal cycle was provided, but the average heating and cooling rates were lower, $3\text{ }^{\circ}\text{C}/\text{min}^{-1}$ was used, and during the measurement cycles, the temperature-modulated amplitude was 0.64°C with a period of 40 s.

The biggest difference between DSC and MDSC is that MDSC applies a superimposed sinusoidal oscillation on heating rate. In other words, although the temperature still keeps increasing or decreasing with time, at every point, heating rate changes by a sinusoidal function resulting in a modulated temperature. Like a dynamic analysis, the response of a material to the heating rate can be distinguish into in-phase and out-of-phase response. MDSC detects how a material responds to the changing heating rate and measures the heat flow; usually, only heat capacity and melting respond to the change.

A formula, $dH/dt=C_p \times dT/dt + f(T, t)$, describe that how MDSC separate total heat flow (dH/dt) into two parts. The first term indicates the part as a function of changing heating rate; C_p is heat capacity and dT/dt is heating rate. Change in C_p results from a transition in material structure, such as molecular motion which consume energy during heating process, so larger mobility of polymer chains will need more energy to increase material temperature during heating. The second term indicates the part not affected by heating rate but affected by an absolute

temperature (T) with time (t). So, the second term is related to kinetic process. MDSC uses signals of reversible heat flow and nonreversible heat flow to display the C_p component and kinetic component in total heat flow, respectively, and the sum is total heat flow. A traditional DSC only monitors total heat flow. Signal of reversible heat flow usually involves glass transition and most melting process. In contrast, signal of nonreversible heat flow involves polymer crystallization, thermoset curing, evaporation, enthalpy recovery, decomposition, and certain thermal events. Based on our data, the DSC and MDSC thermogram of a material in total heat flow signal are almost the same except a little bit temperature shift for peaks, and all DSC and MDSC thermograms are plotted with endotherm down.

4.1 Study of glass transition by DSC

DSC is widely used to find out the glass transition temperature (T_g) of a new material. Glass transition is not a phase transition and the temperature is highly dependent on thermal history, so T_g can be different for a material. Since glass transition is germane to considerable molecular motions, motion of 10-50 backbone atoms [30], which absorb much energy, during heating heat capacity is present as a abrupt step when glass transition occurs. There is no latent energy of fusion for glass transition. T_g of many materials cannot be found out from the thermogram by using a traditional DSC. It is because that DSC cannot provide heat capacity baseline so that some thermal events such as enthalpic recovery occurring at the same time with T_g will overlap and mess up the signal only representing T_g. In general, these thermal events do not be affected by changing heating rate; therefore, their contribution in heat flow can be separated if using MDSC to measure T_g. So, MDSC is a better tool to determine T_g of complexes.

No literatures discussed in section 2 about thermal property of EMAA ionomers

detected and recorded Tg using DSC. In the study, we also attempted to find out Tg by using MDSC for both surlyn 8940 and LPEI/EMAA films fabricated by LbL assembly method; however, Tg did not be detected even trying many different testing conditions. But their Tg has been defined by using dynamic mechanical analysis (DMA) successfully and it is discussed in the next section. Tg of LPEI is $\sim -23^{\circ}\text{C}$ [189, 185, 96].

4.2 DSC thermogram of pure surlyn 8940 and pure LPEI

Figure 4.1 and 4.2 are the MDSC thermogram including non-reversible heat flow, reversible heat flow, and total heat flow of pure LPEI and pure surlyn 8940, respectively. Based on Figure 4.1, LPEI did not crystallized in the first cooling process

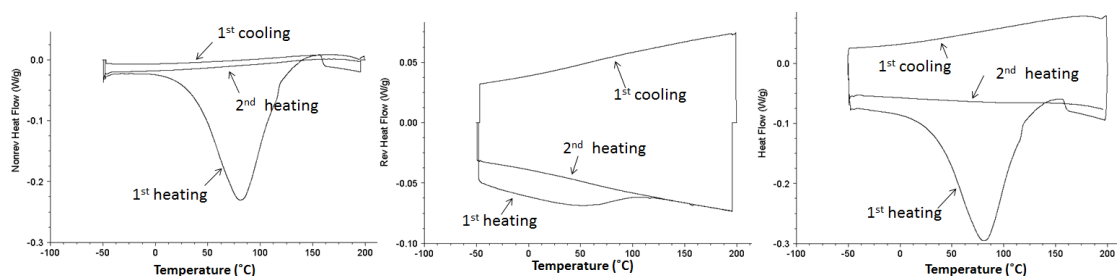


Figure 4.1: Modulated DSC thermogram of pure LPEI.

and its Tg was not analysed out under this experimental condition. The melting point of LPEI is $\sim 60^{\circ}\text{C}$ [56], so the broad endothermic peak is also attributed to the presence of water in pure LPEI under ambient conditions. As mentioned before, high crystalline hinders the Tg determination of surlyn 8940 even by MDSC. Figure 4.2 is the DSC thermogram of surlyn 8940 under the experimental condition of $3^{\circ}\text{C}/\text{min}^{-1}$ of heating/cooling rate with 0.64°C amplitude and 40 s period. Except glass transition, another 3 important thermal transitions were monitored and shown in Figure

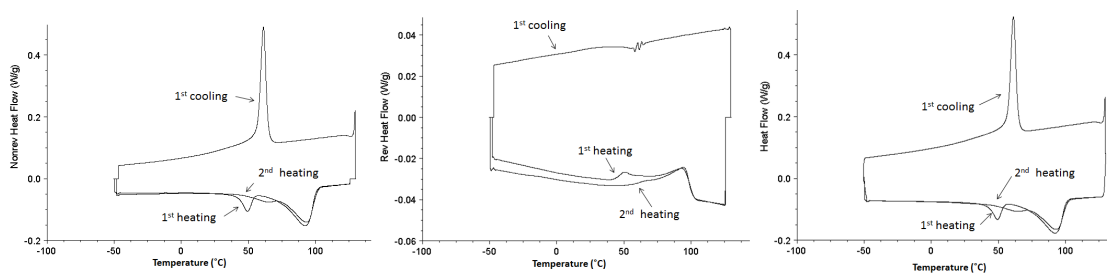


Figure 4.2: Modulated DSC thermogram of pure surlyn 8940.

3.17. The exothermic peak is from PE crystallization and usually shown in the non-reversible heat flow signal. The high temperature endothermic peak ($\sim 92.5^{\circ}\text{C}$) is assigned as melting of major PE crystalline and the temperature is denoted as T_m . Melting is an endothermic process; absorbed heat is consumed in increasing both heat capacity and latent energy of fusion, and both have respective response to the sinusoidal heat input. Latent energy is the energy needed for a phase transition. So, not like glass transition, we cannot only consider melting as heat capacity component of total heat flow ($C_p \times dT/dt$). The fact that different experimental conditions (temperature amplitude, heating rate, and period) can cause different nonreversible and reversible heat flow signals, and the phenomenon really happened in our MDSC results.

In Figure 4.2, it is clear that the LT peak ($\sim 49^{\circ}\text{C}$) is present in the 1st heating and then disappears in the immediate 2nd heating, consistent with the literature consequences. Also, similar to melting, it is a thermal transition involving latent heat.

Actually, Dupont produces a series of EMAA resin; In addition to surlyn 8940, surlyn 8920 in which there is 5.4 mol % of MAA groups and 60 % of MAA groups are also neutralized by sodium and nucrel 925 which is EMAA copolymers with 5.4 mol % of MAA groups are all their main EMAA products. Here, we compared

the DSC curves of these EMAA, shown in Figure 4.3. In the first heating, two

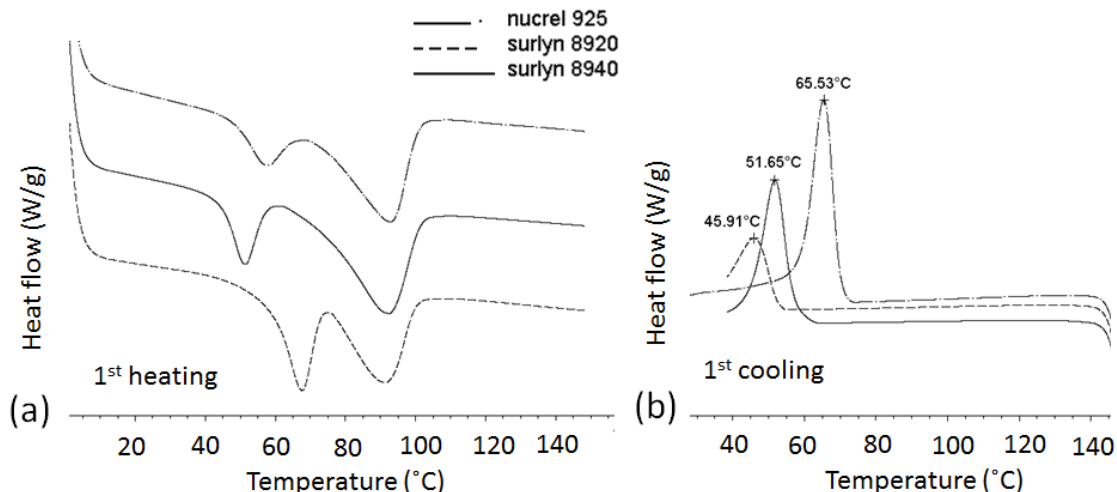


Figure 4.3: DSC thermogram of surlyn 8920, surlyn 8940, and nucrel 925.

endothermic peaks are found in all materials. Melting points are very close while the LT peaks shift and the peak area, indicating enthalpy change or latent energy, are also different; a higher peak temperature does not definitely correspond to a higher enthalpy change. Since there are two explanations for the low-temperature transition, just based on the curves, it is hard to provide a correct interpretation. But if the peak is attributed to order-disorder transition, the nucrel 925 curve indicates in EMAA copolymer, COOH groups also form ionic aggregations. In the first cooling, the crystallization temperatures and enthalpy change shift to lower value with the increase in neutralization degree of MAA groups.

Figure 4.4 presents the recover of LT peak for surlyn 8940 with storage time after a heating process. The samples after 1st heating were stored in the ambient environment at RT; after different storage duration (2 hours to 95 days), they were heated again by DSC and the thermograms were recorded. Identical to the literatures, the

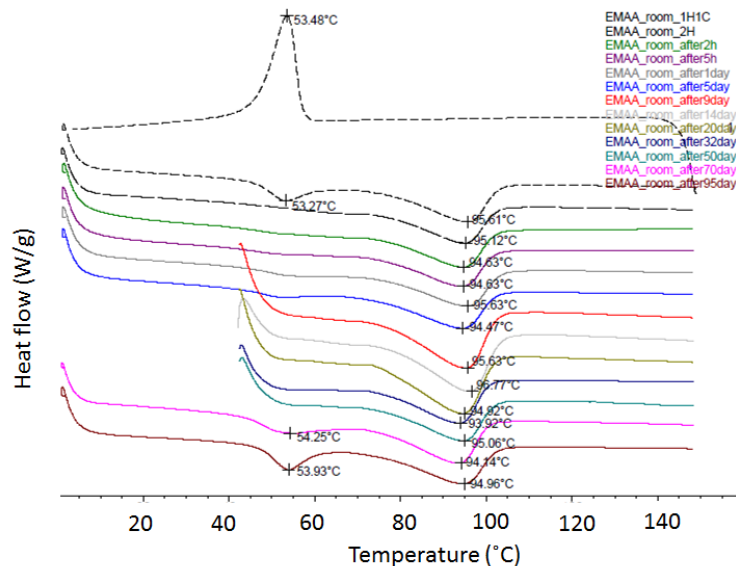


Figure 4.4: DSC thermograms of surlyn 8940; after 1st heating, surlyn was heated at an immediate 2nd heating, and heated after the storage at RT of 2 hr, 5 hr, 1 day, 5 day, 9 day, 14 day, 20 day, 32 day, 50 day, 70 day, and 95 day.

LT peak of surlyn 8940 is absent in the immediate 2nd heating process, but with the storage time, the LT peak appears again and the recovery temperature does not have a great change.

Figure 4.5 shows the effect of high-temperature (180°C) annealing on the LT peak of surlyn 8940 as a function of time. Annealing temperature, 180°C, is higher than the melting point of surlyn 8940. After annealing, high temperature endothermic peaks still exist but T_m shift to lower temperature which indicates the crystalline structure becomes weaker as annealing time is longer. There is no cold crystallization showing in the heating process. Thus, during annealing, PE major crystalline perhaps melt and re-formed, or in a shorter annealing duration, PE crystalline did not melt completely. LT peaks, like un-annealed material, were absent in the immediate 2nd heating, but after an apparent depression after 1 hr annealing other peaks almost keep in an equilibrium. There are two major explanation for the LT peak

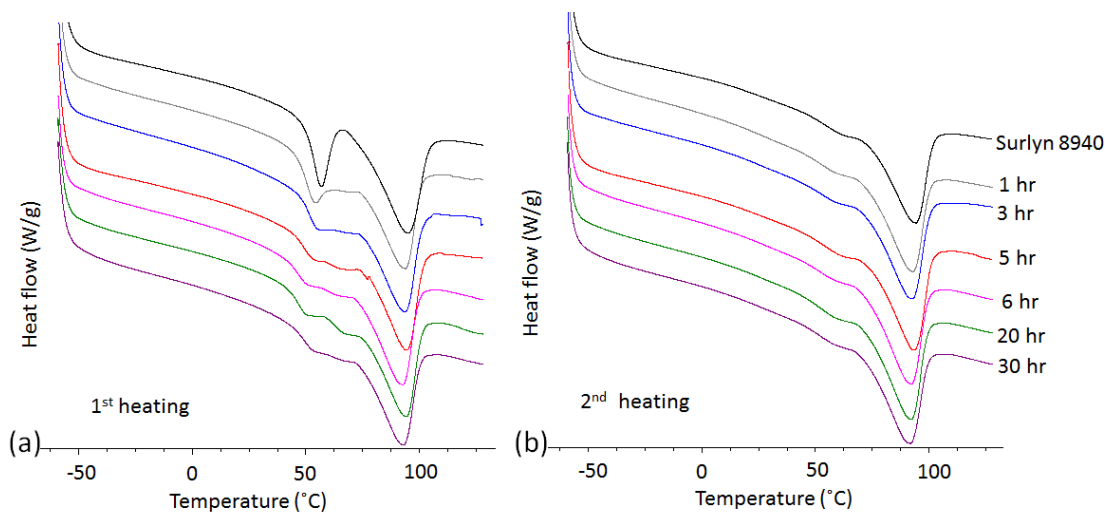


Figure 4.5: DSC thermogram of surlyn 8940; before testing, surlyn was stored at 180°C for 0, 1, 3, 5, 6, 20, and 30 hr.

from literatures. If standing on the assumption of order-disorder transition, after 180°C annealing ion pairs in ionic aggregations normally should be all in an disorder state, like the case after 1st heating. The existence of LT peak when annealing time increases, therefore, seems more unreasonable, unless the origin of the peak is not purely from the order-disorder transition. If standing on the assumption of secondary PE crystalline, the presence of melting point in all annealing time indicates primary PE crystalline can form during annealing so that the opportunity of formation of thin PE crystals in the amorphous phase is likely to happen, and probably since annealing temperature is high, less secondary crystals causes the weaker LT peak.

4.3 DSC thermogram of LPEI/EMAA complex and LbL assembly

The thermal properties of our LPEI/EMAA blends were also characterized by DSC or MDSC. In Figure 4.6, the total heat flow of (LPEI_{8.5}/EMAA_{0.5wt%}) (1:1) complexes and (LPEI_{4.8}/EMAA_{0.25wt%}) LbL film are separated into nonreversible and reversible heat flow. Like pure surlyn 8940, T_g of complex and LbL assemblies did not

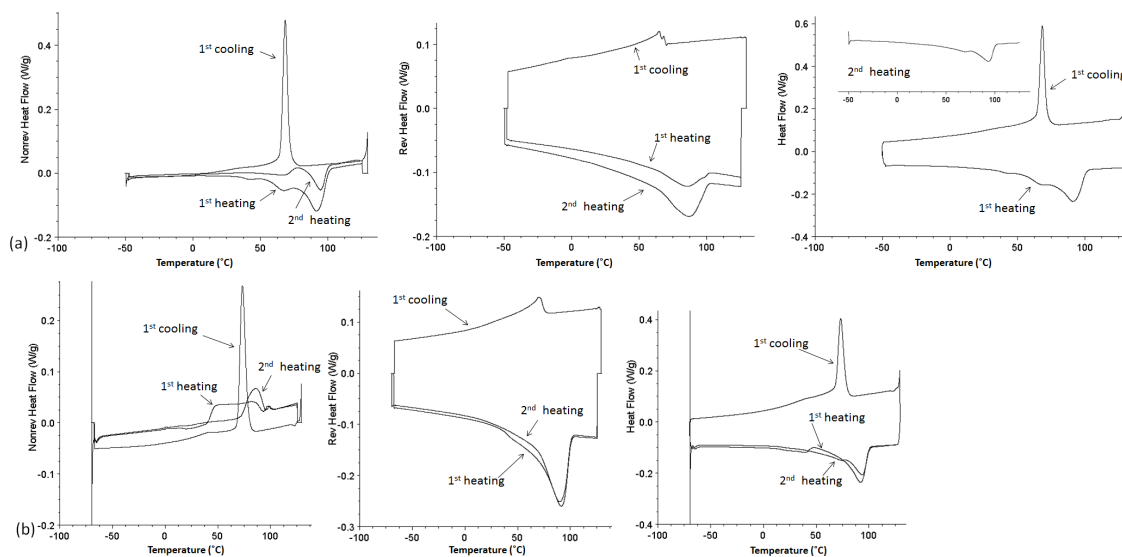


Figure 4.6: Modulated DSC thermogram of (a)(LPEI_{8.5}/EMAA_{0.5wt%}) (1:1) complexes, (b)(LPEI_{4.8}/EMAA_{0.25wt%})₂₅ LbL film.

found in the thermogram, and obviously, the exothermic peak of PE crystallization is still shown in the nonreversible signal. Compared to MDSC thermogram of surlyn 8940, it is found that the signals of endothermic peaks are changed from nonreversible to reversible curve on the same experimental conditions. Figure 4.7 demonstrates the MDSC thermogram of (LPEI_{0.01M}/EMAA_{0.25wt%})₂₅ LbL films as a function of LPEI solution pH. Basically, the thermograms of LbL assemblies are very similar to that of EMAA ionomers. T_m , PE crystallization degree, and the corresponding enthalpy changes are close, shown in the tables on pages 61 and 62.

In this study, we made free-standing film by heating at 120 or 180°C for 15 min and subsequently doing base treatment. In section 3, we found that heating can not only drastically increase the degree of neutralization of COOH groups but also deprotonate the secondary amine groups of both LPEI. Additionally, the NaOH immersion did not decompose the films. Because of the change in charge density, followed changes in chain conformation and arrangement, interactions between poly-

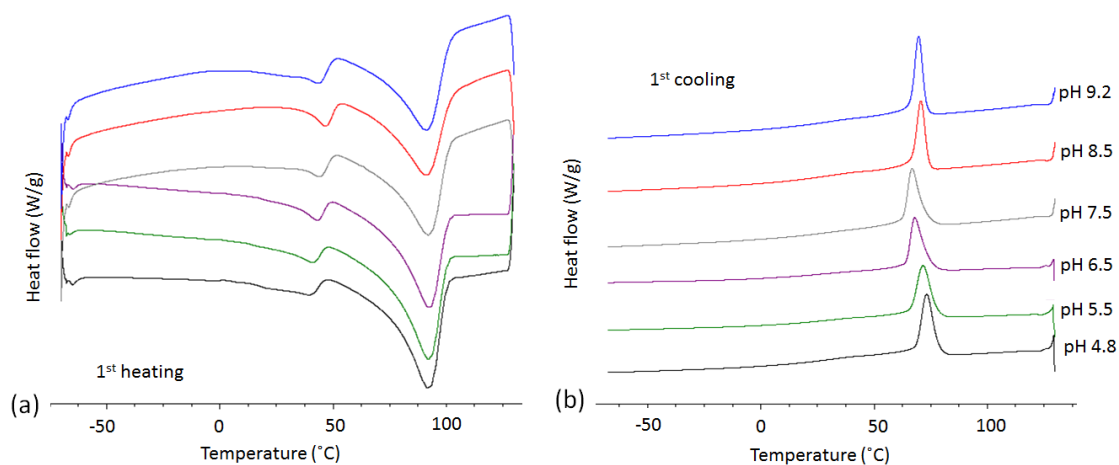


Figure 4.7: Total heat flow of MDSC thermogram of $(\text{LPEI}_{0.01M}/\text{EMAA}_{0.25\text{wt}\%})_{25}$ LbL films at various pH values.

mers, and ionic interactions in ion-rich domains will affect the material structure and properties. The MDSC thermogram of free-standing film made at LPEI pH8.5 and 0.5 wt % of EMMA is illustrated by Figure 4.8. Different from surlyn 8940 and LbL

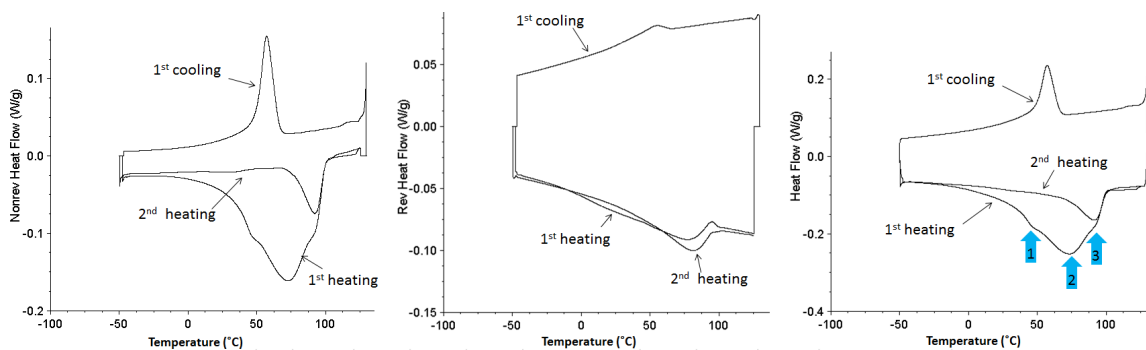


Figure 4.8: Non-reversible (Nonrev), reversible (Rev), and total heat flow of MDSC thermogram of isolated $(\text{LPEI}_{8.5}/\text{EMAA}_{0.5\text{wt}\%})_{25}$ films.

films, in the first heating, there is a very broad endothermic peak in free-standing film. The broad peak is formed by overlapping of three endotherms (marked by ar-

rows 1, 2, and 3); arrow 1 and 3 correspond to the low-temperature peak and melting point, respectively, previously observed for pure surlyn 8940. The peak denoted by arrow 2 is a new peak, which was created after post-treating the LbL films.

The fact that peak 1 and 2 disappear in the 2nd heating implies that the initial structure or certain bonding in the polymers are not able to reform during the cooling cycle, unlike major PE crystalline. According to our experiments, the peak 1 is reversible after a long ageing; however, the new peak is still absent even though after stored in the ambient environment for 3 month. We provided couple assumptions for the origin of the new peak. First, since the new peak temperature (T_n) is close to that of LPEI broad weak, as shown in Figure 4.1, pure LPEI may contribute to the peak. But, LPEI broad peak is mainly due to water evaporation and LPEI content is less than 10 wt% in the films so that pure LPEI cannot fully interpret the size of the peak. In addition, the new endotherm is still present for the dried free-standing films in a vacuum oven. Solvent effect, thus, can be excluded. Eventually, it is believed that the new peak perhaps derives from a new association between LPEI and EMAA after post-treatment. The post treatment including heating and NaOH immersion changed charge density of both materials; the new association, therefore, was achieved by chain rearrangement for adapting the adjusted interactions between polymers as well as chain conformation to maintain a lowest-energy equilibrium.

The assumption based on changing ionization degree for both materials was also used to explain the cases in Figure 4.9(a) and (c). In Figure 4.9(a), the intermediate peak grows up with the increase in pH value. According to FTIR results, the intensity of absorbance peaks of carboxylate and free amine groups become stronger when LbL and free-standing films are at higher pH value. So, only when functional groups of materials are highly deprotonated, the presence of the new peak exists and becomes obvious. Furthermore, we did not see the new peak shown in LbL films (Figure 4.7),

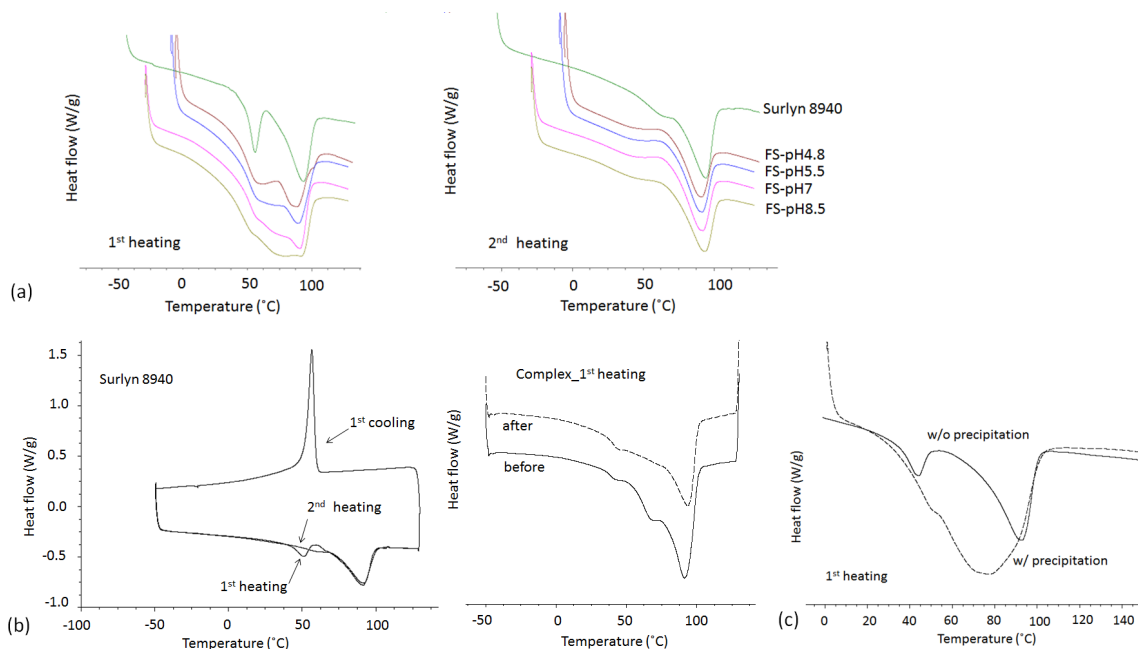


Figure 4.9: DSC thermogram of (a) free-standing film of $(\text{LPEI}_{0.01M}/\text{EMAA}_{0.5wt\%})_{25}$ at a function of pH value, (b) surlyn 8940 and LPEI/EMAA complexes after the same post-treatment, (c) LbL film of $\text{LPEI}_{0.02M}/\text{EMAA}_{0.5wt\%}$ at pH12 with crystalline hydrates (dash line) or not (solid line).

except the pH of LPEI dipping solution is at 12 and the created precipitation is still remained in the solution. Once the precipitation is filtered out, in other words, LbL films are fabricated in the LPEI solution without precipitation, the new peak is absent, as shown in Figure 4.6(c). At very high pH, the great majority of amine groups are uncharged, resulting in water insolubility and the precipitation. FTIR results in Figure 3.8(b) illustrate the phenomena by peaks at ~ 3280 and $\sim 1120 \text{ cm}^{-1}$ and the strong intensity of the carboxylate peak at pH12 also confirms the migration of hydrogen ions. The condition of pH12 is very similar to the NaOH treatment for making free-standing film. So, deprotonation process indeed plays a key role in the origin of the new peak. The incorporation of LPEI and LbL assembly method are also required. It is because that in Figure 4.9(b), the new peak is not found in surly

Table 4.1: Comparison of data collected from the thermogram in Figure 4.2 and 4.6-4.8 for different sample types. In type, S8940 means Surlyn8940. The third column (EMAA) indicates the concentration of EMAA ionomer solution and the unit is wt%. T_m and T_c are the peak temperatures of melting point and crystallization during first cooling, respectively, and their units and the unit of T_n are $^{\circ}\text{C}$. ΔH_t , ΔH_n , ΔH_m , and ΔH_c are enthalpy changes of the new peak, melting peak, and crystallization peak during first cooling, respectively, and their units are J/g.

Type	pH	EMAA	LT	ΔH_t	T_n	ΔH_n	T_m	ΔH_m	T_c	ΔH_c
LbL	4.8	0.25	39.6	8.3	—	—	91.8	56.5	73.2	61
LbL	5.5	0.25	41.2	7.4	—	—	91.9	52.6	71.6	59.5
LbL	6.5	0.25	43.2	7.0	—	—	92.4	47.6	68	51.8
LbL	7.5	0.25	44.3	9.3	—	—	92.1	51.4	66.8	53.5
LbL	8.5	0.25	46.8	5.8	—	—	91.4	45.8	70.7	50.5
LbL	9.2	0.25	43.5	12.2	—	—	91.4	51.4	69.7	51.9
FS	8.5	0.5	46.6	179.2	73.4	101.2	92.1	84.6	57.2	35.6
complex	8.5	0.5	42.1	25.6	67.7	65.3	91.5	14.1	68.4	52
S8940	—	—	49.4	8.8	—	—	92.5	41	61.2	50.4

8940 which is treated by the same procedures of making free-standing film, and the broad peak was also not observed in LPEI/EMAA complexes, which are made by directly mixing LPEI and EMAA solutions, after the deprotonation treatment.

The temperatures of LT peak, new peak, melting point, and crystallization peak and the corresponding enthalpy changes of these peaks in Figure 4.2 and Figure 4.6 to 4.8 were measured and calculated. The data were concluded in Table 4.1. Besides, polyethylene crystallization of the samples in Figure 4.2 and Figure 4.6 to 4.8 were also calculated and recorded in Table 4.2. We found the temperature of T_m all are close, but LT peak temperature of LPEI/EMAA assemblies are lower than that of pure 8940. Eisenberg and Simmons ever discussed the effect of different wt% poly(ethyleneimine) (PEI) blended into lithium salts of EMAA copolymers [150]. Our observation was consistent with their result that the low-temperature endotherm in their system was depressed when inserting PEI into the ionic aggregations

Table 4.2: Comparison of the degree of polyethylene (PE) crystallization collected from the thermogram in Figure 4.2 and 4.6-4.8 for different sample types. The degree is the ratio of the enthalpy change of crystallization peak during first cooling (ΔH_c , in Table 4.1) to 290. The unit is %. 290 is the enthalpy change (J/g) of pure PE crystalline.

Type	PE crystallization degree
LbL	21
LbL	20.5
LbL	17.9
LbL	18.4
LbL	17.4
LbL	17.9
FS	12.3
complex	17.9
S8940	17.4

of EMAA ionomers. It also implies Eisenberg et al. supported the relationship between the LT peak and ionic aggregations. Incorporating LPEI into EMAA ionomer, especially after post treatment, changes the initial properties of EMAA ionomers in terms of PE crystallization degree. PE crystallization degree is drastically depressed in the free-standing films while at a low pH value of LPEI solution, the crystallization degree increases. PE crystalline is destroyed less at lower LPEI content and perhaps it is affected by LPEI chain conformation. Free-standing films, due to the broad endothermic peak, drastically increases absorbed latent energy. The increased energy before melting by utilizing phase transitions or breaking bonding between polymers is believed to benefit dissipation of mechanical energy as well as heat, and the improvement of damage-resistant ability.

4.4 Water effect on DSC thermogram

Water sorption is able to affect properties of EMAA ionomers since it works like a plasticizer to soften the interactions in ionic aggregations. The affected properties

include thermal properties. In Figure 4.10, the response of surlyn 8940 soaked in water to heating were monitored by MDSC. The depression of the LT peak and

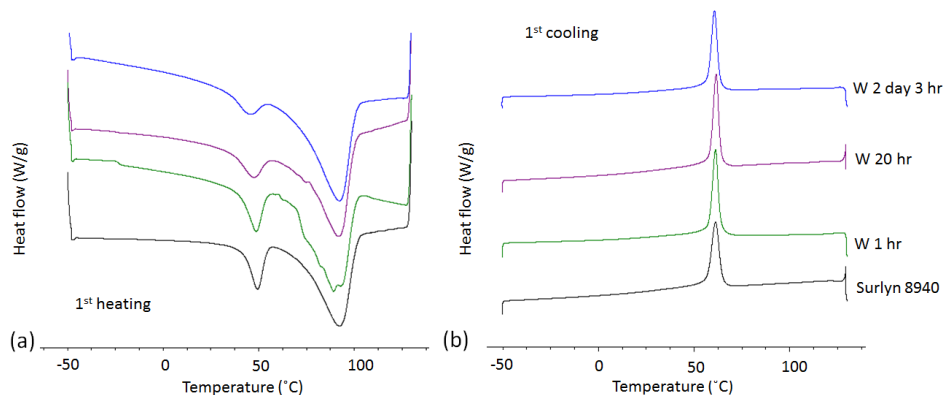


Figure 4.10: MDSC thermogram of surlyn 8940 soaked in water for different duration

temperature shift are seen clearly. The explanation that the LT peak is the order-disorder transition in ionic aggregations can be used to interpret the observation. The DSC thermogram for free-standing films shows a different way in Figure 4.11. With the increase of immersion time, the intermediate peak depresses and finally disappears, and the LT peak still exists but depresses first and then increases with temperature shift back to initial temperature. If the LT peak is assigned to the order-disorder transition in ionic aggregation, the result indicates sorbed water chooses to affect the new association of LPEI and EMAA formed after deprotonation process first, even destroys it eventually. A highly possible reason is that water dilutes the deprotonation effect so that the COO^- concentration decreases and charged amine groups increase, which has been proved by FTIR. The release of Na^+ was also confirmed by conductivity measurement by a conductivity meter. The conductivity increased with the soaking time of free-standing film in DI water, implying the ionic

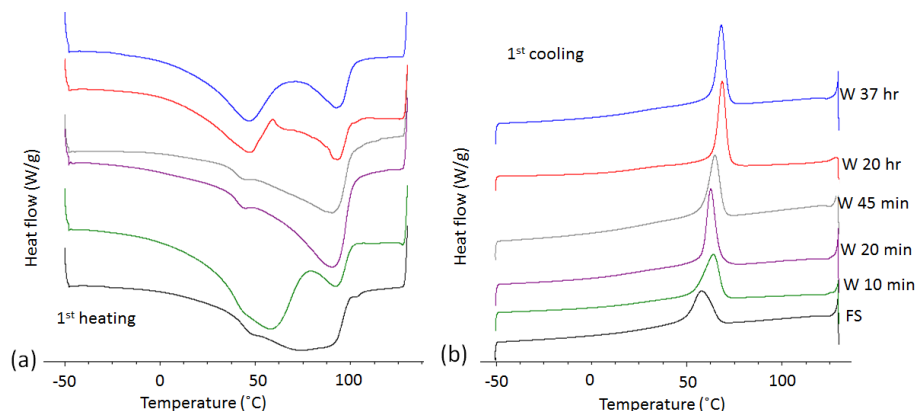


Figure 4.11: MDSC thermogram of free-standing films of $(\text{LPEI}_{0.01M}/\text{EMAA}_{0.5wt\%})_{40}$ soaked in water for different duration; the 40-bilayer LPEI/EMAA LbL film was made using a shorter dipping time.

strength or salt concentration increases, shown in Figure 4.12. On the other hand, according to Figure 4.13, the LT peak after water immersion recovers back as that in the LbL film.

In order to confirm the effect of NaOH immersion, we immersed the free-standing film of $(\text{LPEI}_{0.01M}/\text{EMAA}_{0.5wt\%})_{40}$ soaked in water 20 hours into 0.1 M NaOH. From Figure 4.14, the recover of the new peak was found with the increase in NaOH immersion duration. The broad peak was shown again, and it is the overlapping of the LT peak, new peak, and the melting point. In addition, the degree of PE crystallization also depresses. As a result, based on these testing we believed that ionic interactions in ionic aggregations in free-standing films are protected against water plasticization in the tested range of immersion time, and the origin of intermediate peak between LT peak and melting point is a new association between polymers after deprotonation process. The deprotonation process and the change in chain conformation also inhibit the crystallization of polyethylene chains. It represents the charge density of polymers has a profound influence on the material structure and morphology of LbL

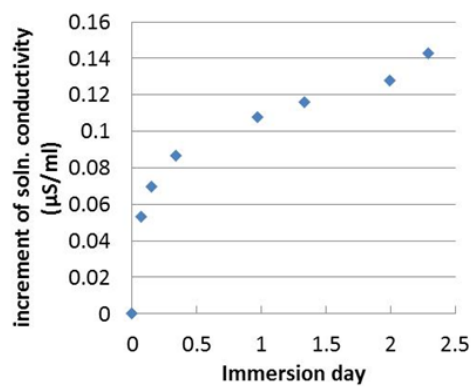


Figure 4.12: The increment of conductivity of $(\text{LPEI}_{0.01M}/\text{EMAA}_{0.25wt\%})_{25}$ free-standing film as a function of time.

assemblies, and they will control the thermal properties of the new materials.

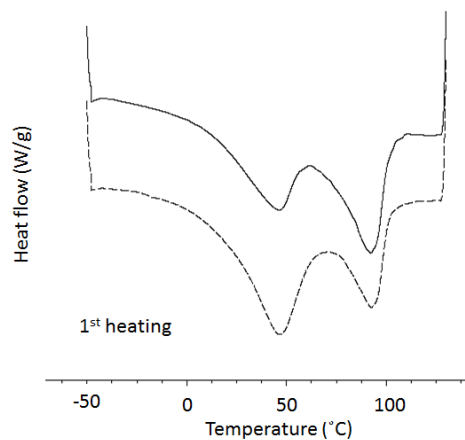


Figure 4.13: Modulated DSC thermogram of $(\text{LPEI}_{0.01\text{M}}/\text{EMAA}_{0.5\text{wt}\%})_{40}$ LbL film (solid line) and free-standing film (dash line) which is soaked in water for 37 hours.

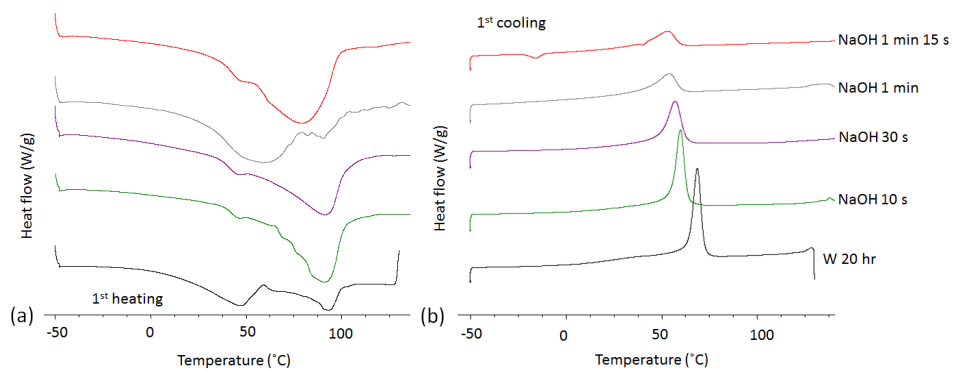


Figure 4.14: Modulated DSC thermogram of $(\text{LPEI}_{0.01\text{M}}/\text{EMAA}_{0.5\text{wt}\%})_{40}$ free-standing film that first soaked in water for 20 hours and then soaked in 0.1 M NaOH for different time.

5. EXPERIMENTAL SECTION: SURFACE WETTABILITY

Surface wettability is an important field of research due to the many practical applications it relates to, such as painting, contact lenses, superhydrophobic or superhydrophilic coatings, microfluidic systems, and liquid transportation. Contact angle (CA, θ) measurement is the most common way to determine quantitatively the wetting of a solid surface by a liquid. CA includes static CA and dynamic CA. The former method is to measure the angle when a water droplet sits on a surface, and a high CA indicates that the surface is hydrophobic. The latter method is to measure the advancing and receding angles when the substrate is tilted; the difference between advancing and receding angles is called contact angle hysteresis. Water droplets in air tend to become a sphere to get the smallest ratio of surface area to volume because the cohesive force between water molecules are strong and spherical shape can decrease the needed energy for creating a surface. However, when water droplets are on a surface, there are three interfaces and the surface tension between solid-liquid (γ_{ls}), solid-air (γ_{sa}), and liquid-air (γ_{la}) are all necessary to consider so that wetting is a complicated behavior. Young's equation is used to describe the relationship of these three interfacial tension with CA, $\gamma_{sa}-\gamma_{ls}=\gamma_{la}\cos\theta$. But since in practice the solid surface is not perfectly flat, the CA calculated from Young's equation cannot represent the real contact angle. The fundamental effect of surface roughness was taken into account by Wenzel [187, 188]. The Wenzel's equation is $r\times(\gamma_{sa}-\gamma_{ls})=\gamma_{la}\cos\theta_w$, where r is a Wenzel's roughness factor and $\cos\theta_w=r\times\cos\theta$. In this equation, the surface is supposed to be homogeneous. Cassie and Baxter in 1944 proposed an equation for a solid/air composite surface, and the relationship with Young's CA is $\cos\theta_c=\varphi_s(1+\cos\theta)-1$, where φ_s is the solid fraction of the surface [19].

Inspired by natural materials, more and more development in the aspect of biomimetic techniques and novel materials have been reported in the literature recently. Superhydrophobic and non-sticky surfaces by mimicking lotus leaves are a well-known examples. Upon Cassie's non-wet contact mode, the superhydrophobic surface is rough and the solid-liquid contact area is pretty small. The trapped air in the surface structures of the relatively reduced contact area would disturb the stability of three-phase contact lines, which result in the strong water repellency and low contact angle hysteresis. So, the water droplets on the lotus mimetic surface can roll off easily; it means the surface has a small sliding angle. The functionalized surface with a larger than 150°C contact angle (superhydrophobic) with lotus effect has been broadly investigated for microfluidic devices and self-cleaning application [3, 11]. More recently, the opposite wetting behavior to lotus leaves in the nature has also attracted considerable interests. Rose petals to pin water droplets while the surface is turned upside down is the case. This phenomenon is called rose petal effect and a low contact angle hysteresis is required. Allium leaves and the surface of gecko's feet show the same effect [47, 7, 22]. This effect benefits various potential applications, like no-loss transfer of liquid microdroplets and antidrip function for agricultural greenhouse and aviation industry.

Rose petal effect is categorized into Cassie pinning wetting state. It is a phenomenon between the homogeneous wetting regime (Wenzel) and composite wetting regime (Cassie) [47, 7]. The surface is still rough to maintain a low surface tension, but partially wetted for sticky on water droplets. Many literatures carried out a conclusion that surface morphology governs the significant solid-liquid adhesion by duplicating rose petals [47] and making biomimetic surfaces artificially [7, 74, 194, 130, 94, 53]. The microscale features distributing over the surface show a larger pitch value so that water can partially penetrate into the micrometric nubs and

their subsidiary fine grooves [7, 130, 65, 108, 206, 164]. The increased solid-liquid interactions efficient limit air packet formation and continue three-phase contact line. The forces contain van der Waal's force, capillary force, and capillarity-induced negative pressure when the cavities are sealed [7, 74, 94, 53, 62]. The increased surface tension forces and energy barrier overcome the gravitational pull-force of water droplets at an inclined surface. Surface chemical composition was also taken into consideration on the effect of pinning water droplets since the addition of hydrophilic domains on a surface can increase the adhesive force between the substrate and liquid. But the hydrophilic domains may lower contact angle. Introducing hydrophilic metal microdomes [65] and clustered copper nanorods [21], depositing water affinity molecules [95], and using phase separation of polymer blending [213] were studied to achieve petal effect.

5.1 Wettability of polyelectrolyte multilayers

It has been proved that LbL assembly method is important for making thin films with a very hydrophobic surface [151, 208, 212, 68, 75, 64, 180, 182, 205, 109, 60, 181]. Polyelectrolytes, since they in generally have functional groups and water soluble, are hydrophilic. So, these superhydrophobic films usually took several layers of polyelectrolyte multilayers as base, such as PAA/PAH and SPS/PDAC and then deposit hydrophobic layers [151, 208, 64, 182]; otherwise, it is necessary to use hydrophobic materials, like fluorinated polymers [75]. Roughness is a requirement for hydrophobic surfaces. In order to develop hierarchical micro- and nano-structures, different assembled building blocks besides polyelectrolytes, rough substrates, and multiple assembly steps or postassembly treatments become necessary. The work done by Soeno et al. was the first one to use LbL assembly technique to make a superhydrophobic and water-repellent surface [151]. They incorporated silica nanoparticles (SiO_2) in

to the multilayers by adding the nanoparticles into the dipping solutions. Then the films were treated at 650°C to get rid of the polyelectrolytes and leave a complex structures developed by SiO₂. Zhai et al. and Huang et al. used acid post-treatment to make the basic films become porous and deposited SiO₂ nanoparticles to increase surface roughness and create dual-sized structures [151, 64]. The hydrophobicity was treated after the development of surface structure by coating a layer semifluorinated silane. Hong et al. and Yoon et al. prepared colloids coated with LbL multilayers [60, 205]. Because the high roughness of the assembled particles, the surface cast by these particles had a low surface tension. Wang et al. introduced different counterions to exchange with the counterions on the outmost surface[182, 181]. Rough substrates were used to achieve the basic requirement of superhydrophobicity and then these new counterions with longer hydrophobic chain push the surface into superhydrophobic behavior. These efforts on surface modification take the advantages of LbL system. They include material versatility, independent of the substrate geometry, and the high sensitivity of materials to the surrounding environment, such as pH and ionic strength. However, it is not desired to have a complicated fabrication process in practice. Furthermore, these multilayer surfaces in general show small sliding angles or CA hysteresis (lotus effect).

5.2 Wettability of the ethylene-based ionomers containing LbL films

This study demonstrates LbL assemblies with hydrophobic surfaces and the surfaces exhibit rose petal effect. Besides, the polyelectrolyte multilayers were simply fabricated via the alternate deposition of LPEI and EMAA ionomer in a water/THF solvent mixture system without additional treatments. The surface morphology is complex; the hierarchical surface was analogous to that of raspberry-like particle deposition and contained similar nano-grooves of natural rose petals. The low di-

electric constant of ionomers material and the surface complexity were considered as the key elements of artificially producing rose-petal-like surfaces. Like the film we made for thermal characterization, the concentration of LPEI and EMAA solutions are 0.01M and 0.25 wt%, respectively, and the dipping time is 10 min for each and followed by total 2 min water rinsing. The pH values of LPEI solution were 4.8, 5.5, 6.5, 7.5, 8.5, and 9.2. We also made spin-LbL films of (LPEI/EMAA) with a spin rate of 4000 rpm. We made films of pure materials, EMAA ionomers and linear low density polyethylene (LLDPE) via spin-coating and hot pressing. LLDPE powder was dissolved in toluene at 108°C for couple days, and became a dispersion at room temperature. The concentration of LLDPE solution for spin-coating was 0.25 wt%.

5.2.1 Contact angle and 90° tilting measurements

The surface property of thin films was studied by CA and 90° tilting measurements. CA instrument is from Rame-hart Instrument Co. and for CA measurement, 2 μ L of water droplet was contacted with the examined surface by adjusting a glass syringe. Average CA was calculated by at least ten different locations for each sample surface. 90° tilting measurement was conducted with the same CA instrument. The substrate with different volumes of water droplets sitting on the measured surface were tilted from 0° to 90° at a rate of 2°/min, and the maximum volumes of water droplets pinned on the surface as tilting angle was at 90° were recorded. Then, the maximum water volumes recorded were converted into pinning force (F, μ N) by the equation, $F=mg \times \sin\theta$, where m is the mass of water droplets, g is the acceleration of gravity, and θ is the tilting angle. Because in our work, the tilting angle finally stopped at 90°, the pinning force would be equal to the weight of water droplet (F=mg).

5.2.2 Particles in EMAA THF dispersion

Ionomers are copolymers consisting of electrically neutral repeat units and a fraction of repeat units with functional groups. The repeat units with function groups are usually upto 15 mol% with negatively charged, which result in a hydrophobic behavior and aggregations of ionized species scattering over the apolar matrix. EMAA ionomers have ethylene as the primary monomers. It is not water soluble, but at room temperature it can swell in THF as shown in Figure 5.1, the weight of EMAA ionomers pellet increases with soaking time. The ionomers can dissolved in THF

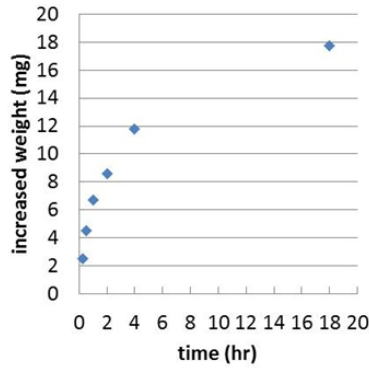


Figure 5.1: Weight change of EMAA ionomers pellet after THF immersion for different soaking time.

when heating at a temperature (65°C) close to the boiling temperature of THF. But as cooling down, the copolymers in the 65°C THF solution tend to aggregate gradually to form low surface energy of spherical particles, and finally the solution becomes a uniform colloidal dispersion at room temperature. Interestingly, the surface of the colloidal particle of EMAA ionomers in THF is covered with nano-sized features. The features were detected in both SEM and AFM images(Figure 5.2(a) and (b)) by drop-casting the particles on silicon wafer from the diluted EMAA THF

dispersion and dried in the ambient environment. In order to determine the shape of

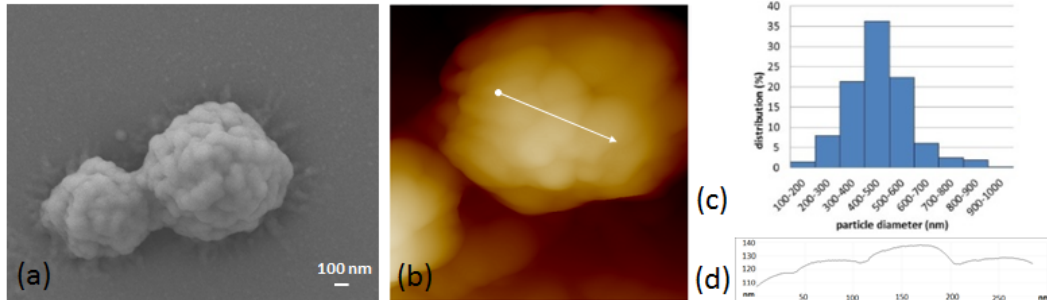


Figure 5.2: Top-view SEM images of (a) spin-coating of EMAA 0.25 wt% THF solution at room temperature, and (b) dip LbL film of (LPEI_{8.5}/EMAA)₂₅. The outmost deposited layer of LbL film is EMAA ionomers.

these nubs, we used Broker NanoScope Analysis and ImageJ to measure the height and width. Consistent results as shown in Figure 5.2(d) disclosed the features are almost under 20 nm tall and have a width in the range of 20~120 nm. The nano-scale grooves formed between two nubs randomly cross on the particle surface and the similar grooved features are also oriented on natural rose petals [47, 7, 101]. The chart in Figure 5.2(c) is the particle size distribution calculated and accounted based on the low magnification of SEM images of EMAA particles which scatter over the substrate. The diameter population of particles sits at 300~600 nm, lower than the effective diameter (~750 nm) obtained by dynamic light scattering (DLS) at 25°C. The higher diameter is because DLS measurement is more sensitive to aggregated particles than the imaging techniques.

5.2.3 Surface morphology of films

The assembly of particles with dual-scale roughness have demonstrated a superhydrophobic surface [205, 60, 124, 197, 165, 145]. Ming et al. reported a 165° CA on the

films deposited over raspberry-like particles and capped by poly(dimethylsiloxane) (PDMS) [124]. The particles with raspberry shape were formed by covalently grafting the small particles (~ 70 nm) onto the large ones (~ 700 nm). They found that two conditions would raise surface energy; one was to replace the raspberry-like particles with only small or large SiO₂ particles, and the other was when PDMS was absent (22°). It indicated both the hierarchical micron- and nanostructures and material hydrophobic property simultaneously affect the surface wettability. EMAA ionomers in this work comprise more than 90 mol% of ethylene monomers. Hemispherical water droplets or a high CA tend to form on a surface lacking polar groups [31]. So, it is reasonable to expect the intrinsically hydrophobic matrix and the EMAA submicron particles combined with the nanometric features should lead EMAA ionomers as a highly potential material with low solid/air interfacial tensions (γ_{sa}). Figure 5.3(a) and (b) are the surface morphology of hot-pressed films of EMAA ionomers and LDPE, respectively, and Figure 5.3(c) and (d) are the surface morphology of spin-coating of EMAA ionomers and LDPE, respectively. Obviously, the surface morphology of the films fabricated by different methods are different. There is almost featureless for hot-pressed films. Surface structure and roughness of hot-pressed films are highly governed by templates which contact with the materials during compression in order to peel off the film easily. The common templates for hot-pressing are kapton films and teflon sheet; in this study, we used both, and the films are much rougher when the used template is teflon. Surface morphology of spin-coated EMAA and LDPE is distinct. We can see LDPE dispersed particles are clay-like. The size is much larger than EMAA particles so that the surface structure is on the micro-scale and roughness is higher than that of EMAA spin-coating. The fine surface features on EMAA particles apparently became submerged, which caused a 0.07 ± 0.01 μm roughness, although there were still some independent particles sit-

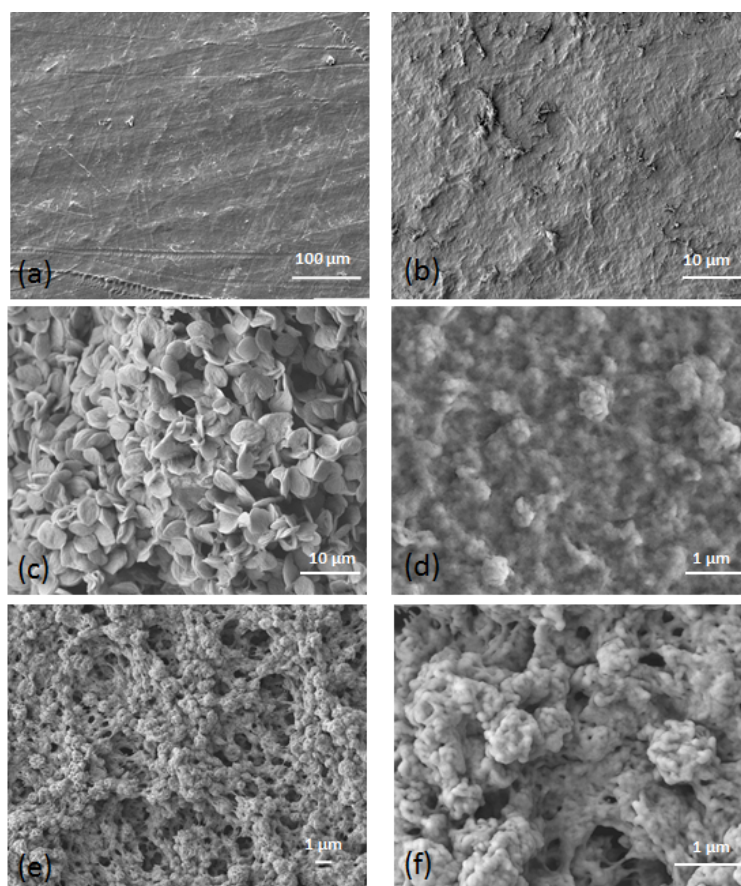


Figure 5.3: Top-view SEM images of (a) hot-pressed film of EMAA ionomers, (b) hot-pressed film of LDPE, (c) spin-coated film of EMAA ionomers, (d) spin-coated film of LDPE, (e) and (f) dipped LbL film of $(\text{LPEI}_{8.5}/\text{EMAA})_{25}$ with different magnifications.

ting on the surface. The surface structure and roughness dramatically changed while LPEI was incorporated into EMAA ionomers using dipping LbL assembly technique. The surfaces in Figure 5.3(e) and (f) have high a roughness ($0.9 \pm 0.1 \mu\text{m}$) and exhibits textured structures. Pores with various sizes and the nano-height nubs as well as grooves are obvious. This geometry of surface was not present in spin-coated LbL film of $(\text{LPEI}/\text{EMAA})$. It is possible to get different morphologies by using different fabrication methods even though the same materials are blended. In addition,

dipping process perhaps provides sufficient time for polymer chains to react and arrange one another and occurs under no externally applied force. The films with a similar hierarchical dual roughness were proposed by Telford et al. [165] and Shang et al. [145] recently. They made the structures by depositing composite particles with raspberry shape on substrates, and the raspberry-like colloidal films not only led to a superhydrophobic behavior but also showed high water adhesion.

5.2.4 The effect of surface roughness of hot-pressed films on surface property

Polyethylene (PE) is the main repeat unit for EMAA ionomers, and different from PE, EMAA ionomers contain 5.4 mol% of methacrylic acid. In order to compare their surface property, this study took LDPE films as the control sample. As mentioned above, we made LDPE spin-coating and hot-pressed films. The hot-press temperatures for LDPE are 120, 150, and 200°C, and for EMAA ionomers are 100 and 200°C. Figure 5.4 shows their CA and the ability of pinning water are dependent on the surface roughness. The result of CA increasing with the surface roughness is consistent with many reports and both surfaces are very hydrophobic at high roughness (around 120°). Interestingly, in terms of rose petal effect, EMAA ionomers exhibit an opposite performance to LDPE. The pinning force of LDPE decreases when the surfaces become rough but the surfaces of EMAA ionomers exhibit rose petal effect. The pinning force of natural rose petal is 63.8 μN with a $\sim 152^\circ$ contact angle [47, 101]. Surface chemical components and surface structure have always thought as two critical points for surface wettability. At low surface roughness, pinning forces of EMAA ionomers and LDPE are close, but at high surface roughness, pinning force of EMAA ionomers increases. It maybe because the more surface area allows carboxylic acid groups to expose on the interfacial to adhere to water droplets. Since LDPE is electrically neutral, the increased surface roughness may just raise the trapped

air in the surface structures, resulting in the water-repellence. For the spin-coating

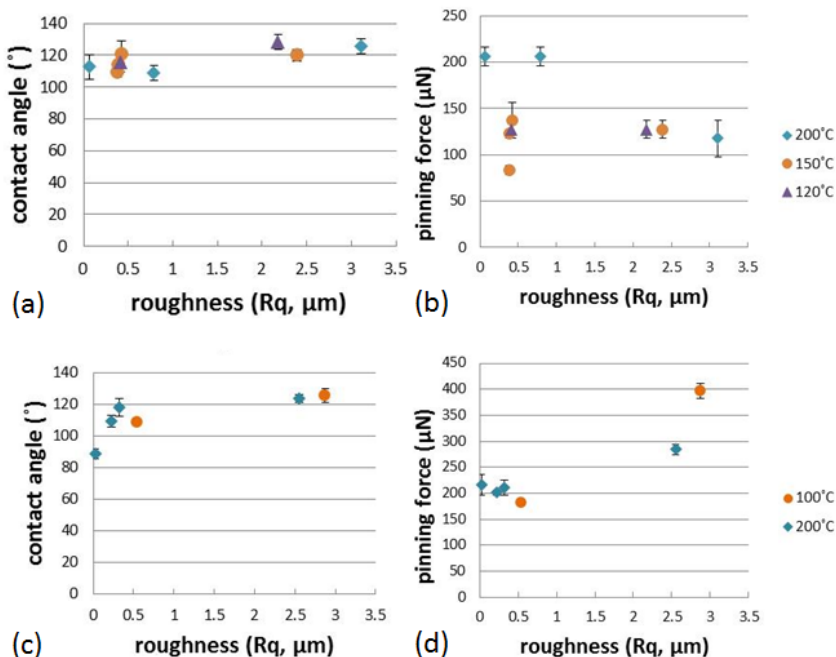


Figure 5.4: (a)Contact angle and (b)pinning force of hot-pressed LDPE films as a function of surface roughness, (c)contact angle and (d)pinning force of hot-pressed EMAA ionomers films as a function of surface roughness.

of EMAA ionomers and LDPE, the surface of LDPE is superhydrophobic; however, the pinning force is very low, $< 30\mu\text{N}$. The results are related to the micrometric surface structures of LDPE films. The CA for EMAA spin-coating is $108\pm 1^\circ$ and the range of pinning force is $290\sim 330\mu\text{N}$. So, compared to the rough hot-pressed EMAA ionomers, roughness indeed affects not only contact angle but also water adhesion.

5.2.5 The surface performance of LbL films

SEM images in Figure 5.3(e) and (f) have demonstrated the different surface morphology of LbL films from pure materials. Figure 5.5 shows the surface roughness,

contact angle, and pinning force for the LbL films made at different pH values of LPEI solutions. The surface roughness of all LbL films in Figure 5.5(a) are higher

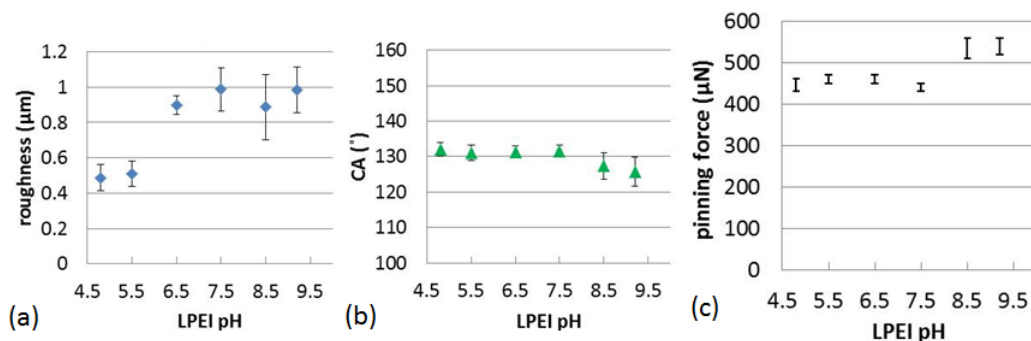


Figure 5.5: (a)Surface roughness, (b)contact angle, and (c)the range of pinning force of dipped LbL films of (LPEI/EMAA)₂₅ as a function of pH value of LPEI solutions.

than that of EMAA spin-coating. Besides, both the contact angle and pinning force of LbL films are better than the pure ionomers. The EMAA ionomers containing PEMs demonstrate high CA although they are not superhydrophobic ($> 150^\circ$), no extra treatments or building blocks were needed after alternate deposition of LPEI/EMAA solutions, which would considerably shorten fabrication time and diminish process complexity. In order to verify the influence of surface chemical components on wettability in our system, we did chemical deposition (CVD) of 1H, 1H, 2H, 2H-Perfluorooctyltriethoxysilane (POTs) onto the LbL film surface of LPEI pH6.5, and the CA increased to $144 \pm 2^\circ$. The CVD of POTs at the same time also decreased surface adhesive force for water droplets. The pinning force decreased to $350 \sim 390 \mu\text{N}$. Different from many polyelectrolyte multilayers with a superhydrophobic property, our LbL films containing ethylene-co-methacrylic ionomers exhibit the rose petal effect by pinning a large volume of water droplets. The surfaces can keep

45~55 μL water droplets in place no matter when the substrates were rotated to 90° or 180° . The range of the maximum pinned force for the films at different LPEI pH values slightly increased with the dipping solution pH. The adhesive forces are much larger than the pinning force of natural rose petals, and competitive with the forces, 680~690 μN , with a $70\sim 115^\circ$ static contact angles reported in a recent work [101]. We believe LPEI has certain effect on pinning water since it has been proved that surface or hydrophilic defects can improve contact angle hysteresis [98, 183]. But LPEI content in the PEMs of (LPEI/EMAA) is low [63], the outstanding water adhesion behavior (rose petal effect) in this work should be mainly attributed to the hierarchical surface morphology developing by simply mixing LPEI and EMMAA ionomers in a LbL system. The micrometric pores allow water to partially penetrate into so that solid-liquid contact area increases [101]. The grooved fine features on the nanoscale similar to those on rose petals are also able to absorb water which involves different intermolecular bonding [164]. The adhesion energy gain exchanges with the dynamic work done by hemispherical water droplets moving into a tear-like shape due to the gravity and capillarity. In the period of droplet deforming as tilting, the strong adhesion, on the one side, allows water expanding but prevents the motion of water front to get a maximum advancing angle; on the other part, water are held back when contracting to approach a minimum receding angle [207]. A high contact angle hysteresis therefore generates. Besides, continuous pinning sites stabilize the sited water droplets. So, adequate adhesive force is necessary to maintain the location of water droplets and highly relies on surface heterogeneity and proper surface geometry. A recent work created a surface possessing rose petal effect as well and it was a deposited film by polystyrene (PS) particles decorated with poly(paraffluorosyrene) (P1FS) corona particles [165]. The PS and P1FS particle sizes are 850 and 108 nm, respectively, very close to the dimensions of our EMMAA ionomers particles and the

surface features (nubs). The raspberry-like surface can pin a 30 μL of water droplet (pinning force $\sim 295 \mu\text{N}$). Consequently, it is possible that there is an optimum range of surface structure dimension for designing a rose-petal-like surface. We furthermore examined the effect of surface morphology and roughness on CA and water-pinning ability by annealing the LbL films at 100°C for different time durations. Figure 5.6(a) and (b) show the surfaces appreciably became flatten and smooth with annealing time at 100°C , which consistent with the roughness measurement (Figure 5.6(d)). Heating above the melting point of $(\text{LPEI}_{8.5}/\text{EMAA})_{25}$ LbL films ($\sim 90^\circ$) [63] improves chain diffusion, decreases free volume, and finally compacts the film; subsequently, film thickness decreased as shown in Figure 5.6(c). The fade-out textured structures altered the contact mode with water, resulting in a drop on both CA and pinning forces in Figure 5.6(e) and (f). The results confirm the roughness and surface complexity are the requirements for a very hydrophobic and sticky surface.

5.2.6 *LbL films fabricated by water-contained EMAA THF dispersion*

So far, the ionomers are dispersed in 100% THF. It is known that solvents can affect the polymer chain conformation in a solution and therefore, further affect the interactions between materials and the morphology of the produced mixtures. In section 3, we have presented the LbL films assembled by LPEI and water containing EMAA dispersion; here, we furthermore used dynamic light scattering (DLS) to determine the size of EMAA particles in these solutions. The results are plotted in Figure 5.7. The effective diameters change with water content. We used SEM to image these particles (Figure 5.8) and found they have similar particle sizes. So, the larger diameters got from DLS is perhaps because of the aggregated particles. After mixing these particles in EMAA $\text{H}_2\text{O}/\text{THF}$ dispersion with LPEI to form the LbL films, we measured the CA and pinning force as shown in Figure 5.9. Based

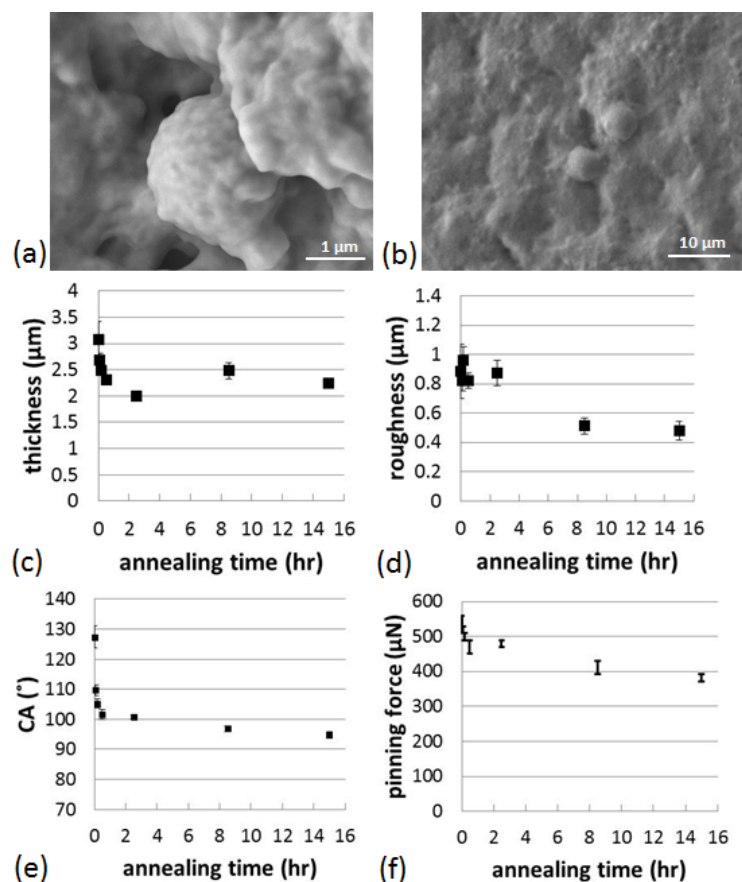


Figure 5.6: (a) and (b) are the SEM images of the LbL films of $(\text{LPEI}_{8.5}/\text{EMAA})_{25}$ annealed at 100°C for 5 min and 30 min, respectively. (c) to (f) are the film thickness, surface roughness, contact angle, and water pinning force for the same LbL films after annealing with time.

on the results, solvent effect by adding water is not obvious in the aspect of surface property. The contact angle and pinning force only change slightly for different water percentages. But, Figure 3.18 in section 3 demonstrates poor surface quality was found in some LbL films. This may also affects the measurements although the fact that the particle surface morphology does not have obvious changes in the mixing solvents probably is the main reason why these LbL films have similar surface properties.

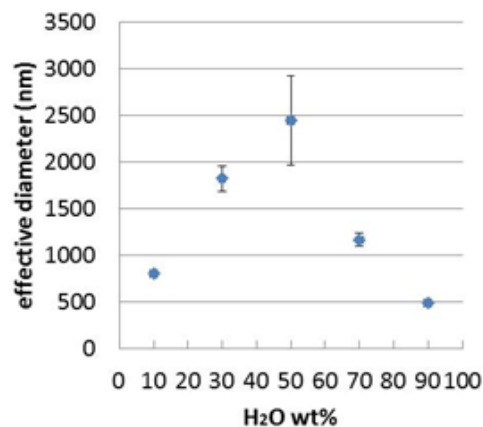


Figure 5.7: Effective diameters of EMAA particles in water-containing THF solution as a function of different weight percentage of water.

5.2.7 Water separation from immiscible organic solvents

The ionomers containing LbL films exhibit a very hydrophobic surface for water droplets and can pin a large volume of water droplets. However, for organic solvents, our films are superoleophilic. When the droplets of organic solvents, such as THF, ethanol, acetone, toluene, chloroform, and decane, are placed on the LbL film surface, they spread and wet the surface right away; by other words, contact angle is zero. We used this opposite phenomenon to separate water out of the mixture of water and other liquid, especially for immiscible solvents. We mixed decane (dyed by sudan, red color) and water (dyed by methylene blue, blue color) in a vial and shaken the vial, then put the emulsion on the film surface. The mixture is 50/50 volume percentage of H₂O/decane. Figure 5.10(a) and (b) are the pictures of separated water droplets. It is obvious that the surfaces of LbL films absorb decane and repel water droplets, and the static contact angle of repelled water droplets is $\sim 90^\circ$, read by the inset in Figure 5.10(b). The interesting phenomenon appears in the mixture of water with decane, cooking oil, silicon oil, toluene, and chloroform. These mentioned solvents

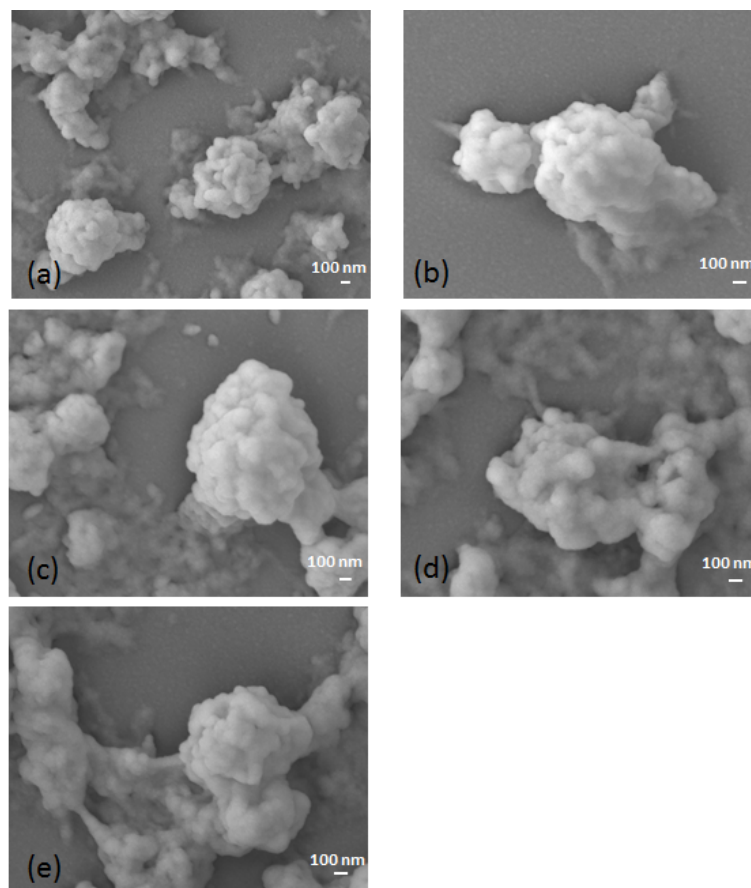


Figure 5.8: SEM images for EMAA water-containing THF dispersion; (a)90 wt%, (b)70 wt%, (c)50 wt%, (d)30 wt%, and (e)10 wt% of water.

are almost immiscible with water. No matter the density of the solvents is higher or lower than that of water, when the mixing solvents pour on the LbL multilayers surface, water is always as a droplet and float above the organic solvents. But definitely, there is a volume limitation that the surface absorb the organic solvents. Therefore, when there is too much decane, it will oil the surface and a low contact angle appears. But, as long as the solvents are dried, the surface shows the same behavior again. The film is very robust and repeatable. In order to determine how much water can be repelled in a fix volume of the H₂O/decane mixed solvent, we

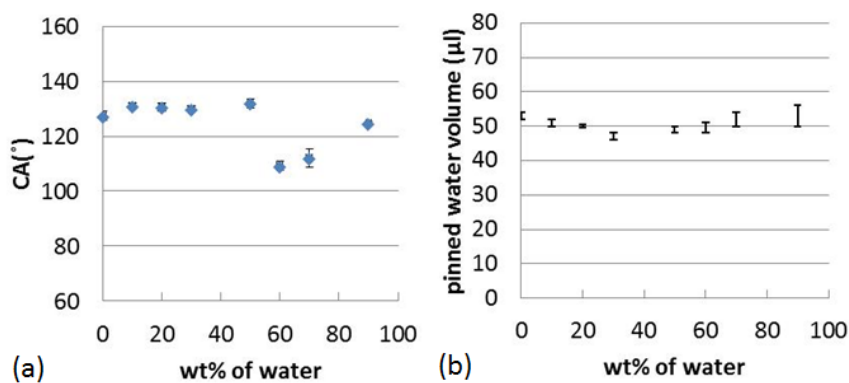


Figure 5.9: (a) Contact angle and (b) pinning force of the dipped LbL films made by EMAA H₂O/THF dispersions and LPEI.

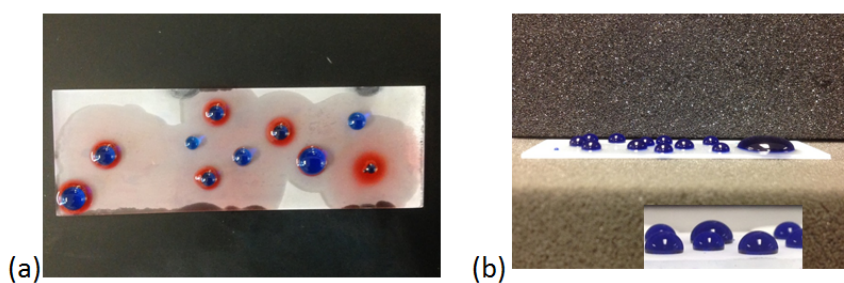


Figure 5.10: (a) Top-view and (b) side-view of the separated water droplet dyed by methylene blue from decane on the surface LbL films. The inset in (b) is on larger magnification.

recorded the initial and flow-down water weight, and the results show the ratio is around 96.5%. Although we still can see some decane floating on the top of water and few mixture residue in the vial, the high value indicates the surface has a great ability in terms of water separation in a mixture. This behavior can be used in the applications about purification of water and oil-spilling treatment in the sea.

5.2.8 Silica nanoparticles and polystyrene latex in LbL films

Silica nanoparticles (SiO_2) and polystyrene (PS) latex were used a lot in superhydrophobic surfaces in order to increase surface roughness and develop a textured surface [151, 208, 64, 165]. Although the surfaces of LbL films containing ethylene-based ionomers are rough and have dual-sized structures, it is interesting to insert these nanoparticles into the multilayers because this way probably can create similar structures to lotus leaves. We used two methods to assemble SiO_2 nanoparticles and PS latex into LbL films. The first method (method 1) is to deposit couple LbL layers of LPEI/ SiO_2 on the top of LbL films of $(\text{LPEI}_{8.5}/\text{EMAA})_{25}$ which are in a dry state. The other method (method 2) is to mix these particles into dipping solutions for LbL film fabrication. For both method, the pH value and concentration of LPEI solutions keep at 8.5 and 0.01 M, respectively. In this work, the diameters of used SiO_2 nanoparticles include 4 and 14 nm, and PS latex has 92 nm of particle size. The concentration of silica nanoparticles and PS latex in all dipping solutions are 0.05 and 0.002 wt%, respectively, and their solution pH was not adjusted. We also made a solutions with a mix of 4 and 14 nm silica nanoparticles for the LbL film fabrication; the concentration of the mix is still 0.05 wt% so the concentration of both diameters in the mixed solution is 0.025 wt% each.

Figure 5.11 are the results of all LbL films containing silica nanoparticles or PS latex . Based on the results, the incorporation of nanoparticles, no matter SiO_2 nanoparticles or PS latex, into Lbl films using method 1 and 2 did not have an obvious influence on surface wettability and water adhesion. So-far work does not conclude nanoparticles cannot change the surface properties of the $(\text{LPEI}/\text{EMAA})\text{LbL}$ films. More efforts are needed to ensure these nanoparticles are really in the LbL films or not, and the effect of these nanoparticles on the surface morphology. After more other

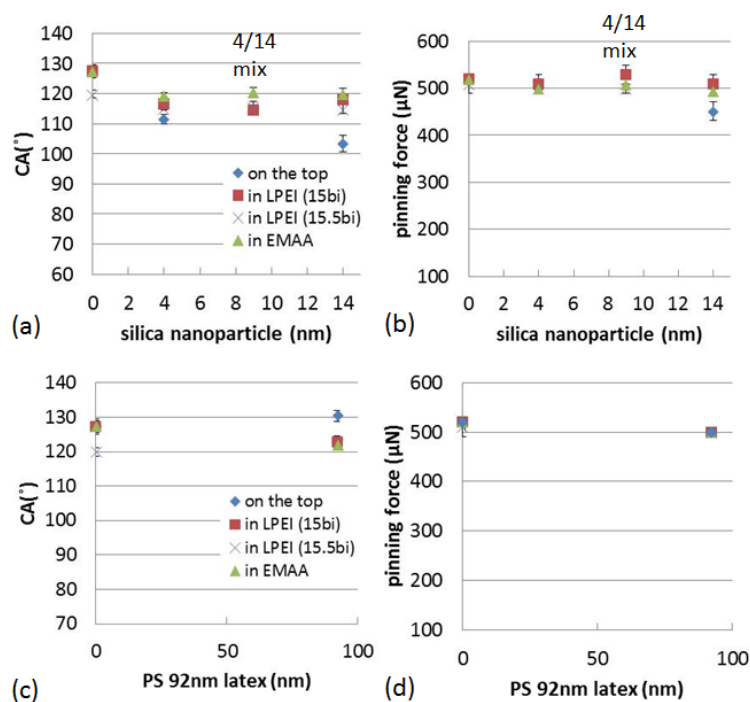


Figure 5.11: (a) Contact angle and (b) pinning force of the LPEI/EMAA LbL film containing silica nanoparticles. (c) Contact angle and (d) pinning force of the LPEI/EMAA LbL films containing PS latex. Blue diamond denotes the samples fabricated by method 1. Red square and cross denote the samples for method 2 that nanoparticles was in LPEI solutions and the films have 15 and 15.5 bilayers, respectively. Green triangle denotes the samples for method 2 that nanoparticles was in EMAA THF dispersion and the films have 15 bilayers.)

characterization, such as imaging surface by SEM, it is possible to create a biomimetic surface and improve surface properties using the incorporation of nanoparticles into the ethylene-based ionomers containing polyelectrolyte multilayers.

6. CONCLUSIONS AND RECOMMENDATIONS

6.1 Conclusions

Poly(ethylene-co-methacrylic acid) EMAA ionomers are commercially widely-used polymeric materials. In the work, we blended this material and linear polyethylenimine (LPEI) using LbL technique, a powerful method of making thin films, in order to modify the properties of EMAA ionomers and explore a novel material. Via electrostatic forces, LPEI was successfully incorporated into EMAA ionomers. LPEI content in the assemblies was not high (lower than 10 wt%) but still affected the morphology and properties of the fabricated LbL multilayers. Since this research was the first work of demonstrating the use of EMAA ionomers as a material in the LbL system, basic physical performance of the thin films, such as thickness and roughness, and the effect of LPEI solution pH were studied for a start. We found the micro-thick films had a rough surface no matter what pH is for the LPEI solutions. Annealing at the temperature above the melting point of EMAA ionomers can improve the diffusion of polymer chains, resulting in the decrease of roughness as well as compact films. The thermal properties and surface wettability were mainly characterized by differential scanning calorimetry (DSC), fourier transform infrared spectroscopy (FTIR), contact angle, and scanning electron microscope (SEM). DSC results showed polyethylene crystallinity of LbL films was suppressed compared to bulk EMAA ionomers. Three peaks overlapped to form a huge endothermic peak shown in DSC thermogram and the center bridge peak was attributed to the association of EMAA ionomers and LPEI. Therefore, the amount of energy required to disrupting the interactions between the two materials and the order-to-disorder transition of the association between the ionic groups of the ionomers was increased. In

terms of surface properties, the multilayers containing EMAA ionomers had surfaces with an around 130° of contact angle. The very hydrophobic surfaces additionally can pin water droplet with a high volume ($\sim 50\mu\text{L}$). The phenomenon is called rose petal effect and significant in the application of micro-liquid transfer. On the other hand, droplets of many organic solvents, such as decan, toluene, THF, and ethanol, spread on the surfaces with a nearly zero contact angle. The surfaces were superoleophilic. Due to the coexistence of hydrophobicity and superoleophilicity, water can be separated out of oil-water emulsion by dropping the emulsion on the surface of (LPEI/EMAA) films, and the films were quite robust for repeating the process of solvent separation. The results indicated LbL assembly method was a good method to mix materials to combine different properties into a novel material, and the new mixture of LPEI and EMAA ionomers in this investigation providing the interesting surface properties and high absorbed latent energy during heating definitely can be the highlight in future coating applications.

6.2 Recommendations

It is well-known that EMAA ionomers have outstanding mechanical behaviors compared to polyethylene because ionic aggregations and formed ionic clusters act as chemical and physical cross-links inside the ionomers. They improve the strength of EMAA ionomers, so commercial EMAA ionomers are broadly used in high strength and abrasion-resistant products, such as packaging and golf ball cover. Actually, biological world exists many materials that use breaking sacrificial bonds and opening hidden length to protect their body against forces. Spider silk is the best example. The reason that the materials break these bonds is to dissipating mechanical energy and diminish fracture. Because EMAA ionomers possess ion-rich domains and physical cross-links, it may be a potential material to mimic the biomaterials mentioned

above. Besides, we used LbL assembly technique to associate EMAA ionomers with LPEI; their interactions, such as ionic bonding as well as hydrogen bonding, perhaps benefit improve the ability of dissipating energy when the assemblies suffer from damage events. We also supposed that blending LPEI into EMAA ionomers can probably modify the mechanical behavior of pure EMAA ionomers since the incorporation of LPEI is able to change the morphology of the ionomers. So, it is interesting to understand the mechanical property of LPEI/EMAA polyelectrolyte multilayers.

Accurate measurement of mechanical properties for ultra-thin films/fibers and nanosized materials is difficult. The first reason is many artificial factors drop the quality of sample preparation for testing; for example, non-uniform samples can cause large errors between tests and final standard deviation. Equipment limitations, like machine resolution and signal-to-noise ratio, are also an issue of suppressing an operation to obtain correct experimental results. Substrates where the films are coated may affect the measurement. Thickness of LbL films are usually at a nanometric scale so that when measuring the mechanical property in a LbL system, these problems become common and increase the measurement difficulties. Here, we listed several methods for measuring mechanical properties of samples at the submicron scale. Rief et al. used AFM cantilevers to strain the modular structure of a single molecule [66, 67]. AFM cantilever also can work as a nanoindentation to investigate young's modulus (E) and hardness (H) under an elastic deformation by analysing force-displacement curves. For nanoindentation, beside E and H, other measurements include fracture toughness, creep, fatigue testing, wear resistance, and scratching testing [166, 125, 106, 105, 102, 103, 69]. Another platform to determine the mechanical properties of thin films is elastic buckling test [154, 127, 71]. The test is induced by an applied compressional strain, and then based on different stiffness

between the substrates and coated films, the mechanical property of samples can be determined by a critical wavelength which resulted from buckling instability. Bulging a membrane by applying a pressure was also used to study the elastic deflection of ultra-thin films by calculating the relative geometries [196, 70]. Damping behaviour and how a material respond to a dynamic oscillation at different temperatures or frequencies are mainly determined by dynamic mechanical analysis (DMA) [66, 67]. In this study, first we employed nanoindentation to determine the mechanical performance of the ionomers containing LbL assemblies. The main problem we had is the high surface roughness. The high roughness affects the touching area between the sample and the tip, resulting in incorrect calculation of outputs. The standard deviation is very large and the data is not reliable. Therefore, our ongoing and future work is to use tensile testing to determine young's modulus, yeild strength, and toughness of the LPEI/EMAA thin films. Tensile testing is a very common and straightforward method for measuring mechanical property of bulk materials. However, the thickness of LbL films is usually low which causes the increase in human error. As a result, raising the thickness by stacking free-standing films together and improving the film quality or uniformity are necessary work for tensile testing. In section 4, we detected the glass transition temperature of LbL films by DMA instead of DSC. So, by DMA, we also can understand the response of the films to a dynamic sinusoidal force and different frequency. Same as tensile testing, film thickness is still a key factor for dynamic mechanical analysis.

6.2.1 Mechanical properties of PEMs

There are some investigations focusing on the mechanical property of polyelectrolyte multilayers. Electrostatically assembled LbL films discussed in previous works for measuring their mechanical property include PAH/azobenzene-containing poly-

electrolyte (P-Azo) system [122], poly(sodium 4-styrenesulphonate) (SPS)/PDAC system [50], poly(*l*-lysine) (PLL)/sodium hyaluronate (HA) system [139], PAH/SPS [172] and PAH/SPS containing gold nanoparticles system [69], and PAH/PAA system [133]. These studies gave young's modulus ranging from 1 MPa to 10 GPa, and the used characterization methods included AFM, nanoindentation, bulging test, and osmotic pressure. For the common polyelectrolytes, the young's modulus of SPS/PDAC obtained by osmotic pressure method was 136 MPa [50]; PAH/SPS films had 100 MPa measured by swelling microcapsules [172], and when containing gold nanoparticles, the elastic modulus range was improved to 3-11 GPa dependent on gold content measured by bulging test [69]; PAH/PAA films in air had \sim 11 GPa but in water dropped to 0.07 GPa measured by nanoindentation [133]. Hydrogen-bonded free-standing films of poly(ethylene oxide) (PEO)/PAA was also discussed by Lutkenhaus et al. in 2005 [112]. They made 100-bilayer PEO/PAA films with around 8 μ m thickness. The free-standing films acted as an elastomer; they can elongate up to around 5 times of the initial length and had a low yield strength (\sim 0.9 MPa). This study carried out electrostatically assembled multilayers are in general stiffer than the assemblies using hydrogen bonding as the driving force. In Dr. Kotove's group, they made many efforts in making ultra-strong thin films by directly incorporating inorganic materials into LbL assembly. There are two very famous studies. Mamedov et al. in 2002 used LbL technique to make a single-wall carbon nanotubes (SWNT) composite and the polymeric matrix was branched poly(ethyleneimine) (PEI) and poly(acrylic acid) (PAA) [117]. The produced composite allowed SWNT uniformly distributed in the matrix and there was only few oxidized flat graphite sheets and carbon colloids which would affect the mechanical performance. They used a custom-made tensile strength tester to measure a free-standing film with \sim 1 μ m thickness and got an ultra-high tensile strength, 220 ± 40 MPa, and young's modulus, 15.4

GPa. They also showed the strain-stress curve of the pure matrix ((BPEI/PAA) LbL film); the young's modulus and tensile strength were around 255 and 8.8 MPa, respectively. Tang et al. in 2003 demonstrate that the ordered brick-and-mortar structure of natural nacre can be reproduced by LbL deposition of anionic clays (an inorganic material) and cationic poly(diallyldimethylammonium) chloride (PDAC) [162]. A custom-made tensile testing device applied an uniaxial force on the films with different thickness at a strain rate 0.1 mm/hr. The stress-strain curve showed a typical hardening which was also observed in nacre after initial plastic deformation. Additionally, a characteristic step pattern and saw-tooth-like curves were found during hardening, which indicate a opening of polymer intra-chain loops due to the breaking ionic linkages. They disclosed the young's modulus (11 ± 2 GPa) and ultimate tensile stress (100 ± 10 MPa) in the hardening region. As a result, these works demonstrated a new way, LbL technique, to combine polymeric materials and organic fillers, the basic components for traditional composites. Due to the versatility of LbL approach and the addition of SWNT or clay, the films had very high young's modulus and tensile strength even though the corresponding elongation was scarified.

6.2.2 Nanoindentation in this study

Indentation is to apply a compressive force for an indenter to make a penetration deformation on a specimen surface. The specimen is usually mounted on a very hard substrate to avoid soft substrate deforms with the sample as applying an indentation, and in general, penetration depth should be less than 10 % of the sample thickness in order to neglect the influence from the substrate. There are two kinds of commercial indentation equipments dependent on the indentation size; one is microindentation and the other is nanoindentation. The indentation made by a microindentation is able to be detected by naked eyes and the projected area of the indentation is mea-

sured by imaging the penetration directly. In contrast, the indentation made by a nanoindentation is on a nano-scale so that the projected depth has to be determined by the equipment itself. This is why nanoindentation has another name called depth sensing indentation. The measurement of displacement is very important since projected contact area and mechanical properties, E and H , all are calculated based on the measured displacement. Different indenters, such as spherical and conical indenters and Berkovich indenter, make different shape of an impression so that each indenter has corresponding formula dependent on its geometry to calculate contact area, E , and H .

The nanoindentation used in the study is Hysitron TriboIndenter with an open-loop load control and precise displacement of tests is determined through the use of three-plate capacitive displacement transducer. Figure 6.1 demonstrates the applied force function and main output of load-displacement curve. The force is loaded and

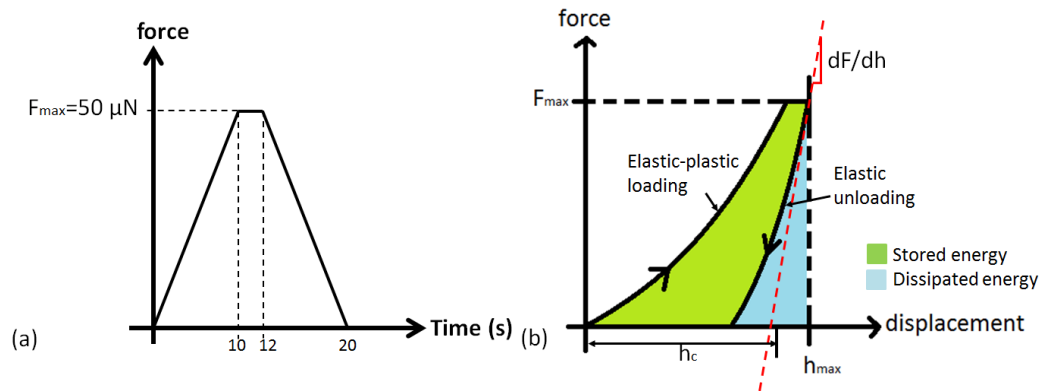


Figure 6.1: Nanoindentation experiment: (a) Force vs. time plot in this study, (b) a typical load-displacement curve.

unloaded at the same and linear rate, $5 \mu\text{N}$ per second, and between loading and

unloading a pause of 2 seconds is added on the peak force, 50 μN . The force was decided based on the pre-testing results in terms of penetration depth of samples; the depth under an applied force has to be above 50 nm and less than 10 % of the sample thickness, otherwise, the substrate effect and higher E and H will take place and decrease data reliability. In a nanoindentation experiment, because of the creation of an impression it is not surprised that the sample is deformed elastically and plastically. The typical load-displacement curve in Figure 6.1(b), as a result, clearly shows after unloading the material does not recover completely and there is a residual impression depth, h_c . According to Oliver and Pharr method, when using Berkovich indenter, the depth is given by $h_c = h_{max} - \varepsilon \times F_{max}/(dF/dh)$, and the young's modulus and hardness are given by $E = (dF/dh) \times (\pi/4A)^{1/2}$ and $H = F_{max}/A$, respectively [48, 129]. Here, for Berkovich geometry, ε is 0.75, and contact area, A, is equal to 24.56 times of square of penetration depth (h_c). Berkovich indenter with three-side sharp geometry is the most popular choice for nanoindentation testing. This study used a Berkovich indenter with a ~ 150 nm radius of curvature and followed Oliver and Pharr method to calculate elastic modulus and hardness. Figure 6.1(b) also shows there are two closed area respectively indicating stored energy (W_e) and dissipated energy (W_p) during an indentation. Stored energy is elastic energy which is able to be released after applied force is completely unloaded by recovering material shape while dissipated energy is attributed to the plastic deformation and change in material structure. Therefore, with the help of nanoindentation testing we can not only get the mechanical properties of LPEI/EMAA thin films but also analysis the internal response and ability of materials to a force.

Figure 6.2 shows the young's modulus (E) and hardness (H) of pure EMMA ionomers and various LPEI/EMAA assemblies. The film of pure surlyn 8940 was hot-pressed at 200°C for total 40 minutes, and all samples were stored in a desicca-

tor before testing. It is obvious that the standard deviation of LbL films assembled

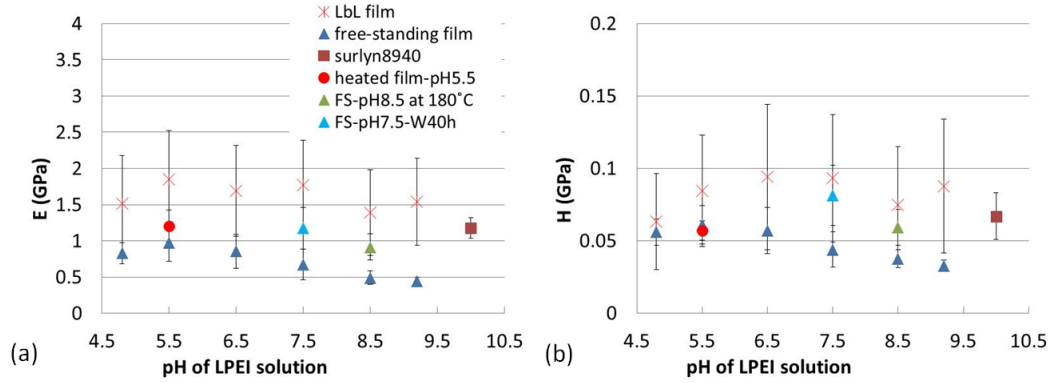


Figure 6.2: (a)The young's modulus and (b)hardness of pure surlyn 8940, LbL films and free-standing films of $(\text{LPEI}_{4.8,5.5,6.5,7.5,8.5,9.2}/\text{EMAA}_{0.5\text{wt}\%})_{25}$, heated film of $(\text{LPEI}_{5.5}/\text{EMAA}_{0.5\text{wt}\%})_{25}$ at 120°C , free-standing film of $(\text{LPEI}_{8.5}/\text{EMAA}_{0.5\text{wt}\%})_{25}$ heated at 180°C before base treatment, and free-standing film of $(\text{LPEI}_{7.5}/\text{EMAA}_{0.5\text{wt}\%})_{25}$ soaked in water for 40 hours.

by different pH values of LPEI solutions no matter in E or H performance is much larger than that of other samples. High surface roughness is the key reason of scattering the data. Some literatures have pointed out surface morphology has a significant influence on the results from nanoindentation tests, which were considered by experimental measurements and numerical simulations [14, 36, 176, 73]. It is because that in nanoindentation experiment, the impressed area is calculated from the penetration depth and the indenter geometry instead of measured directly. This implies the mechanical properties outputted from nanoindentation tests are based on the assumption that the sample surface is completely smooth and the indentation contact is continuous. Therefore, chosen indenter should be reasonable and penetration depth should be much larger than the surface roughness in order to get an accurate and reliable measurement. According to the information provided by Hysitron com-

pany, the ratio of indentation depth to the characteristic size of surface roughness should be greater than 10.

Refer to our surface roughness and film thickness data in Figure 3.12 and 3.13, the study definitely suffered the problems about surface morphology and substrate effect unless drastically smoothing the contact surface. Post-treating LbL thin films, including heating and base immersion, are the efficient methods to decrease the roughness. The disadvantage is the post-treatment may change the initial material properties. From Figure 5.10, pure material and free-standing films have much lower standard deviation and the trend of hardness is almost consistent with the elastic modulus. For the samples with high roughness, the number of indented points were over 100 in more than 3 sample specimens so that here we still have a discussion and make comparisons of E and H between the LbL assemblies and other samples.

It can be seen that the differences between all LPEI/EMAA LbL films are small so pH value of LPEI solution does not have a great influence on the mechanical performance of contact surface in indentation tests. But, compared to pure EMMA, LPEI/EMAA LbL films in all pH range have higher average of E and H. It indicates the incorporation of LPEI into Na-neutralized EMMA ionomers by LbL technique may affect the mechanical properties of pure EMMA; since the LPEI content in LbL assemblies are less than 10 wt%, the influence according to Figure 6.2 is not very apparent. In contrast, the pure surlyn 8940 is stiffer than free-standing films, especially for films assembled at high pH values. Besides, the free-standing film heated at 180°C before NaOH immersion is stiffer than that heated at 120 °C with the same heating time. Water sorption also affect the mechanical properties of free-standing films.

Involved energy in the indentation process for these films are plotted in Figure 6.3. Total energy per volume, W_{total} , is the sum of stored energy (W_e) and dissipated

energy (W_p), and these energy are calculated by the values of closed area, as shown in Figure 6.1, divided by the volume of residue impressions. Like E and H, the standard

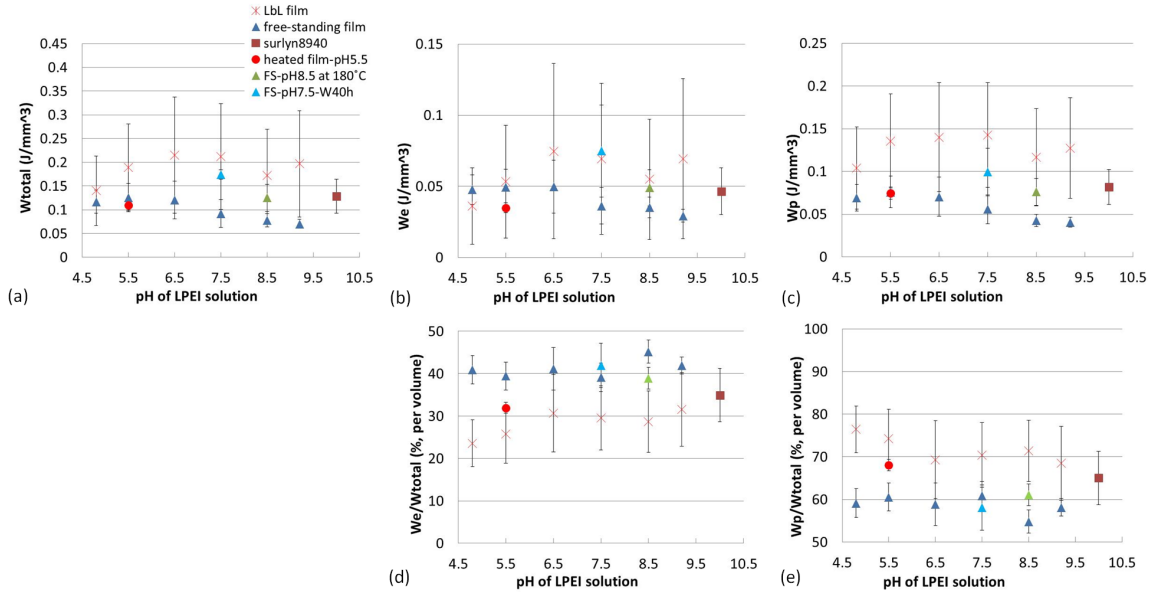


Figure 6.3: (a)The total energy per volume, (b)the stored energy per volume, (c)the dissipated energy per volume, (d)the fraction of stored energy, (e)the fraction of dissipated energy of pure surlyn 8940, LbL film and free-standing film of(LPEI_{4,8,5.5,6.5,7.5,8.5,9.2}/EMAA_{0.5wt%})₂₅, 120°C-heated film of (LPEI_{5.5}/EMAA_{0.5wt%})₂₅, the 180°C-heated free-standing film of (LPEI_{8.5}/EMAA_{0.5wt%})₂₅, and the free-standing film of (LPEI_{7.5}/EMAA_{0.5wt%})₂₅ soaked in water for 40 hours.

deviation of W_{total} , W_e , and W_p for LbL assemblies are large. But, the average data show total energy absorbed by LbL assemblies during elastic-plastic loading is higher than free-standing films, especially in terms of dissipated energy (shown in Figure 6.3(c)and 6.3(e)). According to the discussion in section 4 about thermal properties, the biggest difference between LbL and free-standing films is polymer chains rearrange to form a new association between LPEI and EMAA because of deprotonation of NaOH immersion. So, the new association in a unit volume, supposing samples

are uniform, has greater ability to absorb and then yield energy to recover its original shape as releasing the applied force, and at the same time, it probably softens the free-standing films, a lower young's modulus in Figure 6.2(a).

On the other hand, when free-standing films containing thermal cross-links, tertiary amide groups, the fraction of dissipated energy increases, as shown in Figure 6.3(e). The formation of amide groups consumes the charged carboxylic acid groups so that the new association between LPEI and EMAA should be less than the usual free-standing films heated at 120°C. The increased covalent bonds may depress the fraction of elastic energy absorbed by materials. The free-standing film soaked in water shows better performance than its original film although the functional groups are protonated again after water immersion. However, as a whole, all samples, including the pure material, the fraction of dissipated energy is higher than the fraction of stored energy. The phenomenon implies these materials tend to digest input energy from indentation by changing material structure, such as chain movement and breakage of bonds, and this kind of deformation in order to dissipate energy is permanent and irreversible.

6.2.3 Tensile testing in this study

Tensile testing is the most popular and straightforward method of determining mechanical properties of a new material. Unlike some methods, a stress-strain curve can tell us many mechanical properties; young's modulus (E), yield stress (σ_y), necking, elongation, fracture toughness and so on, all can be examined. This study uses tensile testing model in DMA Q800 of TA instrument. The sample feature is rectangle instead of a dog bone shape and the speed of stretching a sample is 200 μm per minute.

In this study, due to the problems of film thickness, film uniformity, and without a

custom-made tensile device it is a challenge to get very consistent stress-strain curves. In section 3, we have already discussed about the fabrication of free-standing films. Our first experiment condition was to take the made free-standing films mentioned in section 3 directly as the sample pieces for tensile testing. We also soaked the 120°C-heated free-standing films into water for 2 days as one of testing samples. The thickness of these free-standing films was 3~4 μm and static force created between the films and people hands was strong, resulting in the increased difficulties in handling the films. The control sample, pure EMAA ionomers, was made by a compressor at 200°C and under a 9 tons force with total 40 min of pressing time; however, the thickness of EMAA hot-pressed film was ~ 10 times thicker than that of free-standing films. It is known that for tensile testing, size can affect the final results so in general there is a standard sample size. As a result, our second experiment condition was to increase the thickness of free-standing films and control the sample diameter for all testing pieces.

In this condition, the heating time for 120°C did not change, still for 15 min, but the heating time for 180°C increased from 15 min to 20 min in order to let the films more uniform. The water immersion time was also changed to 64 hours due to the increased thickness. In addition, the process we did for increasing the thickness was that first, 8 pieces of free-standing films were stacked and then the 8-times thick free-standing films were cut into small pieces with a size close to the final sample. These small pieces were hot-pressed one by one by a compressor under ~ 500 psi for 30 min. The hot-press temperatures for 120°C- and 180°C-heated free-standing films were 85 and 100°C. After hot-pressing, these films were stored in desiccator at room temperature around one week before examining for stress relaxation. EMAA ionomers films were still fabricated by hot-pressing; the temperature kept at 200°C, but the pressure increased to 3500 psi and total time was 3.5 hours. The film thickness

was measured by a point-measured micrometer and the thickness range was 17~21 μm . On the other hand, strain rate used in this study is far lower than the standard tensile testing for bulk materials. The literatures doing tensile testing for EMAA ionomers used a high strain rate, such as 5.3 cm/min, and it maybe the reason of why their mechanical performance, especially in terms of elastic modulus (E) and yield strength (σ_y), was more competitive than our results [153, 58, 143].

Figure 6.4 shows the mechanical property of EMAA ionomers and free-standing films in the first and second experiment conditions. In terms of E and σ_y results, the average values for the thin and thick films are close except the case of 120°C-heated free-standing films in water. But the tendency is slightly different; for the first experiment condition (thinner film), 180°C-heated free-standing films had the best mechanical performance, but 120°C-heated free-standing films in the second condition had higher E than 180°C-heated free-standing films and had higher σ_y than EMAA hot-pressed films. The different results may attribute to the different sample preparation and size effect. The films after water immersion had very distinct mechanical behavior in the first and second conditions. We are still looking for the main cause, but based on so-far data, it is necessary to extend the soaking time since the film thickness in the second condition is much larger than in the first condition. The free-standing films, no matter heat-treated at 120 or 180°C, are stiffer and stronger than EMAA ionomers. Also, compared to the many polyelectrolyte multilayers, such as PAH/SPS, PEO/PAA, and BPEI/PAA, the E (~ 200 MPa) and σ_y (5.5~8 MPa) are high. The main contributor is EMAA ionomers. PEO/PAA LbL assemblies has been approved they worked like elastomer with ultra-high elongation due to hydrogen-bonding. From Figure 6.4(c), the elongation of 180°C-heated free-standing films is $\sim 200\%$ which means the final length is ~ 3 times of the initial length. Although smaller than the elongation of PEO/PAA free-standing films, our

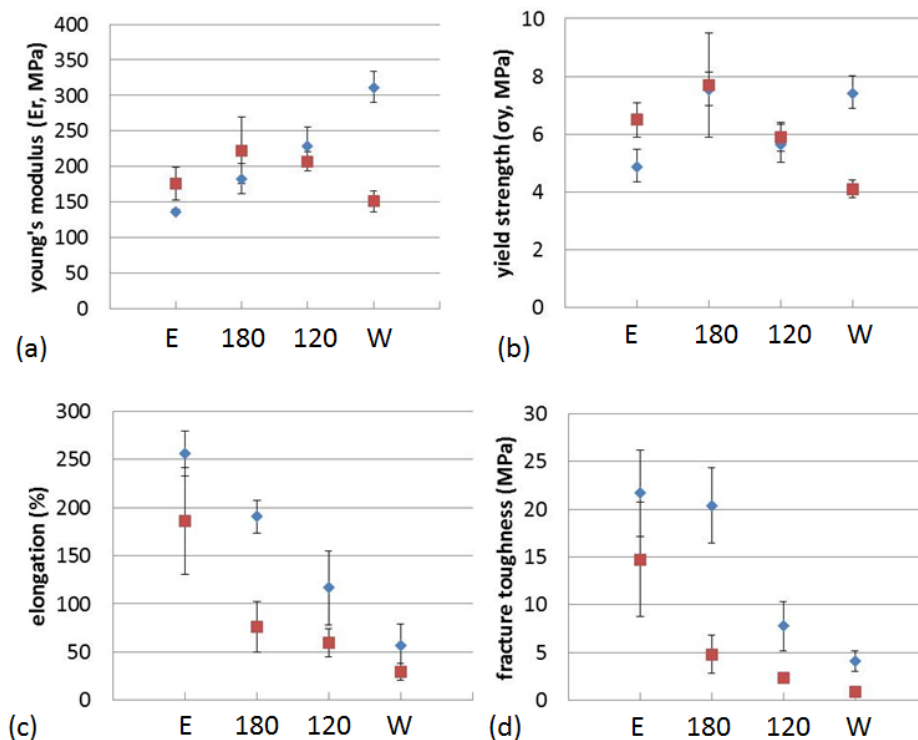


Figure 6.4: The tensile testing results: (a)Young’s modulus, (b)yield strength, (c)elongation, and (d)fracture energy of EMAA hot-pressed films, 120°C- and 180°C-heated free-standing films. Red-color square and blue-color diamond denote the results from the first and second experiment conditions, respectively. E, 180, 120, and W denote EMAA hot-pressed films, 180°C-heated free-standing films, 120°C-heated free-standing films, and 120°C-heated free-standing films soaked in water, respectively.

LPEI/EMAA free-standing films are also tough. The fracture toughness of 180°C-heated free-standing films is close to that of pure EMAA ionomers. We can see actually the E and σ_y of films made by LbL technique do not have a obvious improvement compared to EMAA ionomers. The elongation and fracture toughness of free-standing films are lower than those of EMAA ionomers. It is because LPEI content in LbL films, less than 10%, only has a limited effect in terms of E and σ_y . But, it is believed that the ionic cross-links between LPEI and EMAA ionomers

should affect the mechanical property, such as toughness.

Figure 6.5 are the stress-strain curves of EMAA hot-pressed film and 180°C-heated free-standing film got in the second experiment condition. Compared to low thick-

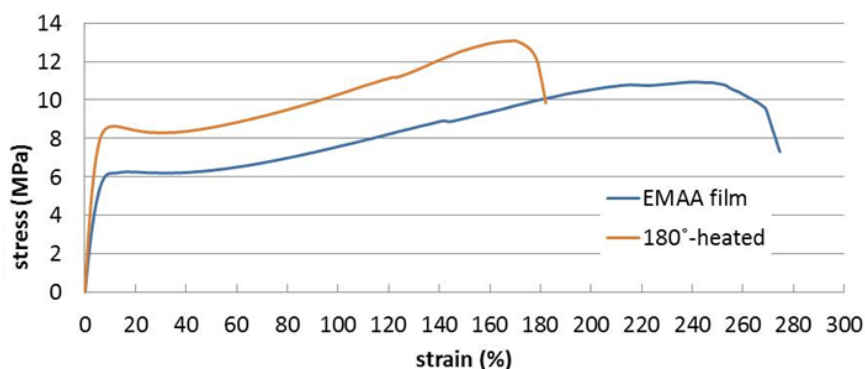


Figure 6.5: Stress-strain curves of EMAA hot-pressed film and 180°C-heated free-standing film.

ness in the first condition, the consistence of stress-strain curves of EMAA and 180°C-heated films from different pieces in the second condition (same thickness) was improved. It is because the samples are more uniform and "strong" to handle. It is worthy to mention that at 120~140 elongation both curves have a small drop in stress. This drop is attributed to the initiation of a crack on the sample edge; the force required to deform the sample at that time drastically decrease until achieving next equilibrium Like many polymers, crack initiation and propagation finally cause the rupture of the examined samples in this study. We observed crazing in a macroscopic scale during plastic deformation. Crazing is a well-known mechanisms for the plastic deformation of polymeric materials. The fissures spanned top to bottom by fibrils absorb mechanical energy and grow to form new surfaces with elongation. Because of the fibrils which hold the material together, the sample still can be elongated

until the crack goes across the sample and input mechanical energy cannot be dissipated any more. Interestingly, there are observed plenty of micro- even nano-scale crazing on the surfaces of both strained EMAA and 180°C-heated free-standing films. The SEM images are shown in Figure 6.3. In Figure 6.6(a) and (b), the applied force directions is vertical (y direction) to the images. In Figure 6.6(c), (d), and (e), the applied force direction is horizontal (x direction) to the images. It is possible that

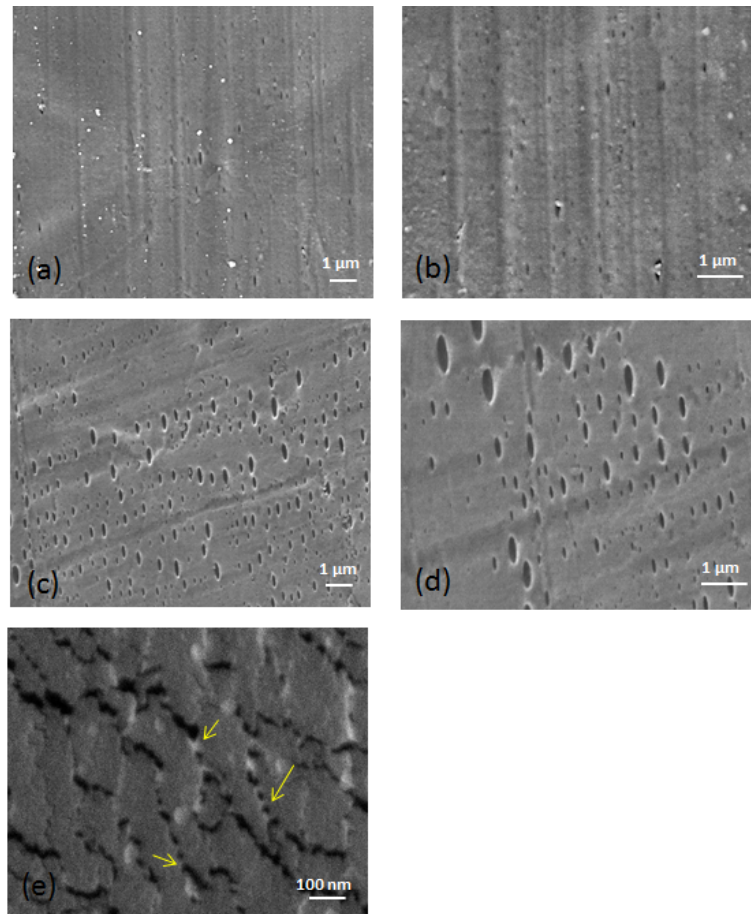


Figure 6.6: Top-view SEM images of surfaces of strained EMAA hot-pressed film (a, b) and 180°C-heated free-standing film (c, d) in the second experiment condition with different magnifications. (e) is SEM image of surface of strained 180°C-heated free-standing film in the first experiment condition.

these tiny crazing finally connect and assemble to become macro-scale crazing with stretching. The formation of these crazing is a form to dissipate energy. So, probably these crazing plays a critical role in the high fracture toughness of EMAA hot-pressed film and 180°C-heated free-standing films. The crazing shape in both films is ellipse. The major axis, for EMAA films, is along the applied force, but for 180°C-heated films, is perpendicular to the applied force. The reason is still unknown. Besides, the SEM image for 180°C-heated films in the first experiment condition (shown in Figure 6.5(e)) is different from Figure 6.6(c) and (d). The film in Figure 6.6(e) is much thinner than that in Figure 6.6(c) and (d). The features show fish-scale architectures and many nano-sized fissures (the yellow arrows) spanned top to bottom by fibres. It is possible that after hot-pressing, the increased chain diffusion allows the material to rearrange and change the morphology, resulting in different fracture mechanism.

6.2.4 *Future work in mechanical properties*

It is important to understand mechanical property of a new material for further design. In this section, many methods of measuring mechanical behavior for thin films are listed, and we have already chose nanoindentation and tensile testing as the start. We also got some systematic results from nanoindentation. However, the issue of high surface roughness causes some of young's modulus and hardness unreliable, especially for LbL assemblies without any post-treatments. In tensile testing, we tried different thickness of free-standing films by stacking free-standing films layer by layer and as a bulk material using hot-pressing, and compared with the results of single free-standing films heated at different temperatures. The controlled thickness in the second experiment condition diminished size effect on tensile testing. So-far work showed the strain-stress curves of EMAA hot-pressed films and 180°C-heated free-

standing films are reproducible and much consistent than the curves in the testing of single free-standing films. Therefore, our future work is to improve the uniformity of other free-standing films. The key factors of making a good sample for tensile testing in this study are the fabrication of LPEI/EMAA LbL films and the hot-pressing process, such as temperature and pressure control. Once we can produce uniform, thick, and large-size free-standing films stably, many measurements only suitable for bulk materials can be used. For example, we can use custom-made uni-axial stretcher to measure birefringence, true stress, and true strain. The technique involves the real-time study on the process of structural reorganization during deformation. It is interesting to explore the effect of incorporated LPEI on the re-crystallization and chain movements of EMMA ionomers because there exist different cross-links when changing the fabrication conditions during LbL assembly process. we also can use x-ray scattering to detect how or will ionic clusters of EMMA ionomers affect after blending with different materials and after plastic deformation.

Tensile testing is a measurement to determine the response of a material to one-direction force or strain, and the applied deformation is stable and constant. Dynamic mechanical analysis (DMA), oppositely, is to detect the response of a material to an oscillation, a sinusoidal force or strain. Rheology is always a hot issue for the development of a new material because polymers exhibit viscoelastic properties. Solid-like (spring) or liquid-like (dashpot) behaviour of a polymer is highly dependent on the temperature and time. So, it combines DMA to determine the viscoelastic properties of a new polymeric material. In our future work, we will focus on stress relaxation of the LbL films and the modulus change with oscillation frequency in order to investigate the mobility of polymer chains under different temperatures and frequencies.

Figure 6.7 is the curves of storage modulus (E'), loss modulus (E''), and $\tan\delta$

of a hot-pressed EMAA ionomers film. The DMA used in the study is Q800 of TA instrument, and measured sample was hot-pressed by the same condition for the first experiment condition of tensile testing and was cut into a rectangle. The film

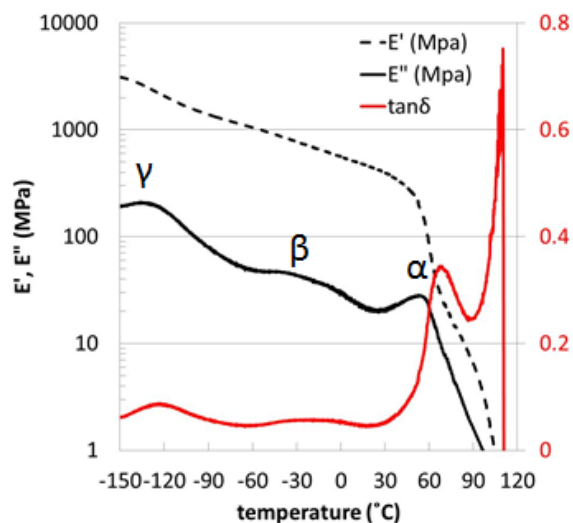


Figure 6.7: Temperature dependence of dynamic storage modulus (E'), loss modulus (E''), and $\tan\delta$ at 1Hz for hot-pressed surlyn 8940 films.

was deformed dynamically by a sinusoidal strain with an amplitude of $30 \mu\text{m}$ and at a frequency of 1 Hz and heated from -150 to 120°C at a rate of $2^\circ\text{C}/\text{min}$. The amplitude value, $30 \mu\text{m}$, was determined by strain sweep tests before stress relaxation tests in order to make certain the material is deformed in a linear viscoelastic region. When a material is in the linear viscoelastic region, the modulus is a constant and the sample maintains a linear stress-strain relationship; in other words, when applying a sinusoidal force on a sample, the sample will deform sinusoidally and it is reproducible. E'' and $\tan\delta$ curves show three typical stress relaxations in EMAA ionomers; from high to low temperature, they are α , β , and γ relaxation peaks, respectively [159]. Based on the E'' curve, γ relaxation peak at $\sim -134^\circ\text{C}$

is attributed to a micro-Brownian motion and vibration of some short segments in the amorphous phase. β relaxation peak is broad and indicates the glass transition of EMAA ionomers so that the relaxation is attributed to a large-scale motion of long segments in the amorphous phase and the Tg of surlyn 8940 is at ~ -15 °C. The pendant COOH and COO⁻ groups which are included in these movable atoms are not incorporated in ionic aggregations. α relaxation occurs just before polymer melting and causes a very steep drop in the E' curve at ~ 56 °C. The peak is the second glass transition for EMAA ionomer since the stress relaxation is due to the glass-rubber transition of ionic clusters.

It is known that E'' represents the viscous performance of a material to respond a sinusoidal oscillation and the corresponding stress is out-of-phase of the applied strain. Based on the viscous property deriving from the liquid component (dashpot) of the polymer, E'' can characterize the ability of losing energy as heat via internal molecular motion and created frictions. On contrast, E' represents the elastic performance of a material and characterizes the ability of a material to return the stored energy. So, the damping behaviour is determined by $\tan\delta$ or called loss factor, the ratio of E'' to E'. The dynamic response of EMAA ionomers clearly shows that ionic aggregations inhibiting the mobility of surrounding polyethylene chains and increasing the local viscosity improve the energy dissipation in a defined temperature range. This study will then look into the effect of LPEI incorporation in the dynamic mechanical properties. With the help of temperature sweep, we can figure out Tg and understand what kind of stress relaxations will display for the LPEI/EMAA assemblies and further discuss their damping properties. Furthermore, we will start from pure EMAA ionomers to see its response for the frequency sweep at a constant strain and temperature, then finally put the LbL system into this measurement.

REFERENCES

- [1] H. Akimoto, T. Kanazawa, M. Yamada, S. Matsuda, G. O. Shonaike, and A. Murakami. Impact fracture behavior of ethylene ionomer and structural change after stretching. *Journal of Applied Polymer Science*, 81(7):1712–1720, 2001.
- [2] J. N. Ashcraft, A. A. Argun, and P. T. Hammond. Structure-property studies of highly conductive layer-by-layer assembled membranes for fuel cell PEM applications. *Journal of Materials Chemistry*, 20(30):6250–6257, 2010.
- [3] W. Barthlott and C. Neinhuis. Purity of the sacred lotus, or escape from contamination in biological surfaces. *Planta*, 202(1):1–8, 1997.
- [4] N. M. Benetatos, B. W. Smith, P. A. Heiney, and K. I. Winey. Toward reconciling STEM and SAXS data from ionomers by investigating gold nanoparticles. *Macromolecules*, 38(22):9251–9257, 2005.
- [5] N. M. Benetatos and K. I. Winey. Ionic aggregates in Zn-and Na-neutralized poly(ethylene-ran-methacrylic acid) blown films. *Journal of Polymer Science Part B: Polymer Physics*, 43(24):3549–3554, 2005.
- [6] N. M. Benetatos and K. I. Winey. Nanoscale morphology of poly(styrene-ran-methacrylic acid) ionomers: The role of preparation method, thermal treatment, and acid copolymer structure. *Macromolecules*, 40(9):3223–3228, 2007.
- [7] B. Bhushan and E. K. Her. Fabrication of superhydrophobic surfaces with high and low adhesion inspired from rose petal. *Langmuir*, 26(11):8207–8217, 2010.
- [8] H. J. Bixler and A. S. Michaels. Polyelectrolyte complexes. *Encyclopedia of Polymer Science and Technology*, 10:765–780, 1969.

- [9] K. B. Blodgett. Monomolecular films of fatty acids on glass. *Journal of the American Chemical Society*, 56(2):495–495, 1934.
- [10] K. B. Blodgett and I. Langmuir. Built-up films of barium stearate and their optical properties. *Physical Review*, 51(11):964, 1937.
- [11] R. Blossey. Self-cleaning surfaces: virtual realities. *Nature Materials*, 2(5):301–306, 2003.
- [12] S. Bonotto and E. F. Bonner. Effect of ion valency on the bulk physical properties of salts of ethylene-acrylic acid copolymers. *Macromolecules*, 1(6):510–515, 1968.
- [13] T. N. Borodina, D. O. Grigoriev, D. V. Andreeva, H. Mohwald, and D. G. Shchukin. Polyelectrolyte multilayered nanofilms as a novel approach for the protection of hydrogen storage materials. *ACS Applied Materials & Interfaces*, 1(5):996–1001, 2009.
- [14] K. D. Bouzakis, N. Michailidis, S. Hadjiyiannis, G. Skordaris, and G. Erkens. The effect of specimen roughness and indenter tip geometry on the determination accuracy of thin hard coatings stress–strain laws by nanoindentation. *Materials Characterization*, 49(2):149–156, 2002.
- [15] B. A. Brozoski, M. M. Coleman, and P. C. Painter. Local structures in ionomer multiplets. A vibrational spectroscopic analysis. *Macromolecules*, 17(2):230–234, 1984.
- [16] M. E. Buck and D. M. Lynn. Free-standing and reactive thin films fabricated by covalent layer-by-layer assembly and subsequent lift-off of azlactone-containing polymer multilayers. *Langmuir*, 26(20):16134–16140, 2010.

- [17] C. B. Bucur, Z. Sui, and J. B. Schlenoff. Ideal mixing in polyelectrolyte complexes and multilayers: entropy driven assembly. *Journal of the American Chemical Society*, 128(42):13690–13691, 2006.
- [18] F. Caruso. *Colloids and Colloid Assemblies: Synthesis, Modification, Organization and Utilization of Colloid Particles*. John Wiley & Sons, Melbourne, VIC, 2006.
- [19] A. B. D. Cassie and S. Baxter. Wettability of porous surfaces. *Transactions of the Faraday Society*, 40:546–551, 1944.
- [20] A. M. Castagna, W. Wang, K. I. Winey, and J. Runt. Structure and dynamics of zinc-neutralized sulfonated polystyrene ionomers. *Macromolecules*, 44(8):2791–2798, 2011.
- [21] I. Chakraborty, N. Singh, S. Gohil, S. Ghosh, and P. Ayyub. Clustered copper nanorod arrays: a new class of adhesive hydrophobic materials. *Soft Matter*, 9(48):11513–11520, 2013.
- [22] F. M. Chang, S. J. Hong, Y. J. Sheng, and H. K. Tsao. High contact angle hysteresis of superhydrophobic surfaces: hydrophobic defects. *Applied Physics Letters*, 95(6):064102, 2009.
- [23] W. Chen and M. Hara. Layer-by-layer ionomer films made from poly(styrene-co-styrenesulfonic acid) and poly(methyl methacrylate-co-4-vinylpyridine) in tetrahydrofuran. *Journal of Polymer Science Part B: Polymer Physics*, 50(2):101–105, 2012.
- [24] H. Cheng, X. Tuo, G. Wang, and X. Wang. A novel polyelectrolyte with branched Azo side chains: Synthesis, characterization and self-assembled

- nanostructures. *Macromolecular Chemistry and Physics*, 202(18):3530–3535, 2001.
- [25] C. Chinwanitcharoen, S. Kanoh, T. Yamada, S. Hayashi, and S. Sugano. Preparation of aqueous dispersible polyurethane: Effect of acetone on the particle size and storage stability of polyurethane emulsion. *Journal of Applied Polymer Science*, 91(6):3455–3461, 2004.
- [26] C. Cho and N. S. Zacharia. Film stability during postassembly morphological changes in polyelectrolyte multilayers due to acid and base exposure. *Langmuir*, 28(1):841–848.
- [27] K. Choi, R. Mruk, A. Moussa, A. M. Jonas, and R. Zentel. Amphotropic LC polymers and their multilayer buildup. *Macromolecules*, 38(22):9124–9134, 2005.
- [28] D. Cochin, M. Passmann, G. Wilbert, R. Zentel, E. Wischerhoff, and A. Laschewsky. Layered nanostructures with LC-polymers, polyelectrolytes, and inorganics. *Macromolecules*, 30(16):4775–4779, 1997.
- [29] M. M. Coleman, J. Y. Lee, and P. C. Painter. Acid salts and the structure of ionomers. *Macromolecules*, 23(8):2339–2345, 1990.
- [30] R. D. Corsaro and L. H. Sperling. *Sound and Vibration Damping with Polymers*. American Chemical Society, Washington, DC, 1990.
- [31] P. G. De Gennes. Wetting: statics and dynamics. *Reviews of Modern Physics*, 57(3):827, 1985.
- [32] G. Decher. Fuzzy nanoassemblies: toward layered polymeric multicomposites. *Science*, 277(5330):1232–1237, 1997.

- [33] G. Decher and J. B. Schlenoff. *Multilayer Thin Films: Sequential Assembly of Nanocomposite Materials*. Wiley VCH, Weinheim, BW, 2003.
- [34] B. W. Delf and W. J. MacKnight. Low angle X-ray scattering from ethylene-methacrylic acid copolymers and their salts. *Macromolecules*, 2(3):309–310, 1969.
- [35] D. M. DeLongchamp and P. T. Hammond. Fast ion conduction in layer-by-layer polymer films. *Chemistry of Materials*, 15(5):1165–1173, 2003.
- [36] E. Donnelly, S. P. Baker, A. L. Boskey, and M. C. van der Meulen. Effects of surface roughness and maximum load on the mechanical properties of cancellous bone measured by nanoindentation. *Journal of Biomedical Materials Research Part A*, 77(2):426–435, 2006.
- [37] S. T. Dubas and J. B. Schlenoff. Factors controlling the growth of polyelectrolyte multilayers. *Macromolecules*, 32(24):8153–8160, 1999.
- [38] S. T. Dubas and J. B. Schlenoff. Polyelectrolyte multilayers containing a weak polyacid: construction and deconstruction. *Macromolecules*, 34(11):3736–3740, 2001.
- [39] S. T. Dubas and J. B. Schlenoff. Swelling and smoothing of polyelectrolyte multilayers by salt. *Langmuir*, 17(25):7725–7727, 2001.
- [40] T. R. Earnest and W. J. MacKnight. Infrared studies of hydrogen bonding in ethylene-methacrylic acid copolymers and ionomers. *Macromolecules*, 13(4):844–849, 1980.
- [41] A. Eisenberg. Clustering of ions in organic polymers. A theoretical approach. *Macromolecules*, 3(2):147–154, 1970.

- [42] A. Eisenberg, B. Hird, and R. B. Moore. A new multiplet-cluster model for the morphology of random ionomers. *Macromolecules*, 23(18):4098–4107, 1990.
- [43] A. Eisenberg, J. S. Kim, and M. Ratner. Introduction to ionomers. *Physics Today*, 52:68, 1999.
- [44] G. E. Fantner, T. Hassenkam, J. H. Kindt, J. C. Weaver, H. Birkedal, L. Pechenik, J. A. Cutroni, G. A. Cidade, G. D. Stucky, D. E. Morse, et al. Sacrificial bonds and hidden length dissipate energy as mineralized fibrils separate during bone fracture. *Nature Materials*, 4(8):612–616, 2005.
- [45] G. E. Fantner, E. Oroudjev, G. Schitter, L. S. Golde, P. Thurner, M. M. Finch, P. Turner, T. Gutsman, D. E. Morse, H. Hansma, et al. Sacrificial bonds and hidden length: unraveling molecular mesostructures in tough materials. *Biophysical Journal*, 90(4):1411–1418, 2006.
- [46] T. R. Farhat and P. T. Hammond. Fabrication of a soft membrane electrode assembly using layer-by-layer technology. *Advanced Functional Materials*, 16(3):433–444, 2006.
- [47] L. Feng, Y. Zhang, J. Xi, Y. Zhu, N. Wang, F. Xia, and L. Jiang. Petal effect: a superhydrophobic state with high adhesive force. *Langmuir*, 24(8):4114–4119, 2008.
- [48] A. fC. Fischer-Cripps. *The IBIS Handbook of Nanoindentation*. Fischer-Cripps Laboratories, Killarney Heights, NSW, 2005.
- [49] R. M. Fuoss and H. Sadek. Mutual interaction of polyelectrolytes. *Science*, 110(2865):552–554, 1949.
- [50] C. Gao, S. Leporatti, S. Moya, E. Donath, and H. Möhwald. Stability and mechanical properties of polyelectrolyte capsules obtained by stepwise assem-

- bly of poly(styrenesulfonate sodium salt) and poly(diallyldimethyl ammonium) chloride onto melamine resin particles. *Langmuir*, 17(11):3491–3495, 2001.
- [51] R. J. Goddard, B. P. Grady, and S. L. Cooper. The room temperature annealing peak in ionomers: ionic crystallites or water absorption? *Macromolecules*, 27(7):1710–1719, 1994.
- [52] Z. Gui, J. Qian, B. Du, M. Yin, and Q. An. Fabrication of free-standing polyelectrolyte multilayer films: a method using polysulfobetaine-containing films as sacrificial layers. *Journal of Colloid and Interface Science*, 340(1):35–41, 2009.
- [53] Z. G. Guo and W. M. Liu. Sticky superhydrophobic surface. *Applied Physics Letters*, 90(22):223111, 2007.
- [54] K. Han and H. L. Williams. Ionomers: two formation mechanisms and models. *Journal of Applied Polymer Science*, 42(7):1845–1859, 1991.
- [55] D. L. Handlin, W. J. MacKnight, and E. L. Thomas. Critical evaluation of electron microscopy of ionomers. *Macromolecules*, 14(3):795–801, 1981.
- [56] K. Hatada, T. Kitayama, and O. Vogl. *Macromolecular Design of Polymeric Materials*. CRC Press, New York, NY, 1997.
- [57] E. Hirasawa, Y. Yamamoto, K. Tadano, and S. Yano. Formation of ionic crystallites and its effect on the modulus of ethylene ionomers. *Macromolecules*, 22(6):2776–2780, 1989.
- [58] E. Hirasawa, Y. Yamamoto, K. Tadano, and S. Yano. Effect of metal cation type on the structure and properties of ethylene ionomers. *Journal of Applied Polymer Science*, 42(2):351–362, 1991.

- [59] H. W. Holden. A differential thermal analysis study of the effects of thermal history on polyethylene. In *Journal of Polymer Science Part C: Polymer Symposia*, volume 6, pages 53–64. Wiley Online Library, 1964.
- [60] J. Hong, W. K. Bae, H. Lee, S. Oh, K. Char, F. Caruso, and J. Cho. Tunable superhydrophobic and optical properties of colloidal films coated with block-copolymer-micelles/micelle-multilayers. *Advanced Materials*, 19(24):4364–4369, 2007.
- [61] J. D. Hong, B. D. Jung, C. H. Kim, and K. Kim. Effects of spacer chain lengths on layered nanostructures assembled with main-chain azobenzene ionenes and polyelectrolytes. *Macromolecules*, 33(21):7905–7911, 2000.
- [62] X. Hong, X. Gao, and L. Jiang. Application of superhydrophobic surface with high adhesive force in no lost transport of superparamagnetic microdroplet. *Journal of the American Chemical Society*, 129(6):1478–1479, 2007.
- [63] H. C. Huang and N. S. Zacharia. Polyelectrolyte multilayers and complexes to modify secondary interactions in ethylene-co-methacrylic acid ionomers. *ACS Macro Letters*, 1(1):209–212, 2011.
- [64] X. Huang, J. D. Chrisman, and N. S. Zacharia. Omniphobic slippery coatings based on lubricant-infused porous polyelectrolyte multilayers. *ACS Macro Letters*, 2(9):826–829, 2013.
- [65] D. Ishii, H. Yabu, and M. Shimomura. Novel biomimetic surface based on a self-organized metal- polymer hybrid structure. *Chemistry of Materials*, 21(9):1799–1801, 2009.
- [66] J. A. Jaber and J. B. Schlenoff. Dynamic viscoelasticity in polyelectrolyte multilayers: Nanodamping. *Chemistry of Materials*, 18(24):5768–5773, 2006.

- [67] J. A. Jaber and J. B. Schlenoff. Mechanical properties of reversibly cross-linked ultrathin polyelectrolyte complexes. *Journal of the American Chemical Society*, 128(9):2940–2947, 2006.
- [68] J. Ji, J. Fu, and J. Shen. Fabrication of a superhydrophobic surface from the amplified exponential growth of a multilayer. *Advanced Materials*, 18(11):1441–1444, 2006.
- [69] C. Jiang, S. Markutsya, Y. Pikus, and V. V. Tsukruk. Freely suspended nanocomposite membranes as highly sensitive sensors. *Nature Materials*, 3(10):721–728, 2004.
- [70] C. Jiang, S. Markutsya, and V. V. Tsukruk. Compliant, robust, and truly nanoscale free-standing multilayer films fabricated using spin-assisted layer-by-layer assembly. *Advanced Materials*, 16(2):157–161, 2004.
- [71] C. Jiang, S. Singamaneni, E. Merrick, and V. V. Tsukruk. Complex buckling instability patterns of nanomembranes with encapsulated gold nanoparticle arrays. *Nano Letters*, 6(10):2254–2259, 2006.
- [72] S. P. Jiang and H. Tang. Methanol crossover reduction by Nafion modification via layer-by-layer self-assembly techniques. *Colloids and Surfaces A: Physicochemical and Engineering Aspects*, 407:49–57, 2012.
- [73] W. G. Jiang, J. J Su, and X. Q. Feng. Effect of surface roughness on nanoindentation test of thin films. *Engineering Fracture Mechanics*, 75(17):4965–4972, 2008.
- [74] M. Jin, X. Feng, L. Feng, T. Sun, J. Zhai, T. Li, and L. Jiang. Superhydrophobic aligned polystyrene nanotube films with high adhesive force. *Advanced Materials*, 17(16):1977–1981, 2005.

- [75] R. M. Jisr, H. H. Rmaile, and J. B. Schlenoff. Hydrophobic and ultrahydrophobic multilayer thin films from perfluorinated polyelectrolytes. *Angewandte Chemie International Edition*, 44(5):782–785, 2005.
- [76] R.l John Varley and S. van der Zwaag. Development of a quasi-static test method to investigate the origin of self-healing in ionomers under ballistic conditions. *Polymer Testing*, 27(1):11–19, 2008.
- [77] S. J. Kalista and T. C. Ward. Thermal characteristics of the self-healing response in poly(ethylene-co-methacrylic acid) copolymers. *Journal of the Royal Society Interface*, 4(13):405–411, 2007.
- [78] S. J. Kalista Jr, T. C. Ward, and Z. Oyetunji. Self-healing of poly(ethylene-co-methacrylic acid) copolymers following projectile puncture. *Mechanics of Advanced Materials and Structures*, 14(5):391–397, 2007.
- [79] V. K. Kamineni, Y. M. Lvov, and T. A. Dobbins. Layer-by-layer nanoassembly of polyelectrolytes using formamide as the working medium. *Langmuir*, 23(14):7423–7427, 2007.
- [80] Y. P. Khanna, E. A. Turi, T. J. Taylor, V. V. Vickroy, and R. F. Abbott. Dynamic mechanical relaxations in polyethylene. *Macromolecules*, 18(6):1302–1309, 1985.
- [81] E. Kharlampieva and S. A. Sukhishvili. Hydrogen-bonded layer-by-layer polymer films. *Journal of Macromolecular Science, Part C: Polymer Reviews*, 46(4):377–395, 2006.
- [82] B. S. Kim, S. W. Park, and P. T. Hammond. Hydrogen-bonding layer-by-layer-assembled biodegradable polymeric micelles as drug delivery vehicles from surfaces. *ACS Nano*, 2(2):386–392, 2008.

- [83] D. J. Kinning and E. L. Thomas. Hard-sphere interactions between spherical domains in diblock copolymers. *Macromolecules*, 17(9):1712–1718, 1984.
- [84] B. P. Kirkmeyer, R. C. Puetter, A. Yahil, and K. I. Winey. Deconvolution of scanning transmission electron microscopy images of ionomers. *Journal of Polymer Science Part B: Polymer Physics*, 41(4):319–326, 2003.
- [85] B. P. Kirkmeyer, A. Taubert, J. S. Kim, and K. I. Winey. Vesicular ionic aggregates in poly(styrene-ran-methacrylic acid) ionomers neutralized with Cs. *Macromolecules*, 35(7):2648–2653, 2002.
- [86] B. P. Kirkmeyer, R. A. Weiss, and K. I. Winey. Spherical and vesicular ionic aggregates in Zn-neutralized sulfonated polystyrene ionomers. *Journal of Polymer Science Part B: Polymer Physics*, 39(5):477–483, 2001.
- [87] N. A. Kotov. Layer-by-layer self-assembly: the contribution of hydrophobic interactions. *Nanostructured Materials*, 12(5):789–796, 1999.
- [88] R. H. Krämer, M. A. Raza, and U. W. Gedde. Degradation of poly(ethylene-co-methacrylic acid)-calcium carbonate nanocomposites. *Polymer Degradation and Stability*, 92(10):1795–1802, 2007.
- [89] S. Kutsumizu, Y. Hashimoto, S. Yano, and E. Hirasawa. Conductivity anomaly in the zinc (II) complex salts of ethylene-methacrylic acid copolymer with 1, 3-bis(aminomethyl)cyclohexane. *Macromolecules*, 24(9):2629–2631, 1991.
- [90] S. Kutsumizu, N. Nagao, K. Tadano, H. Tachino, E. Hirasawa, and S. Yano. Effects of water sorption on the structure and properties of ethylene ionomers. *Macromolecules*, 25(25):6829–6835, 1992.
- [91] S. Kutsumizu, K. Tadano, Y. Matsuda, M. Goto, H. Tachino, H. Hara, E. Hirasawa, H. Tagawa, Y. Muroga, and S. Yano. Investigation of microphase

- separation and thermal properties of noncrystalline ethylene ionomers. 2. IR, DSC, and dielectric characterization. *Macromolecules*, 33(24):9044–9053, 2000.
- [92] S. Kutsumizu, H. Tagawa, Y. Muroga, and S. Yano. Small-angle X-ray scattering investigation of noncrystalline poly(ethylene-co-methacrylic acid) ionomers. *Macromolecules*, 33(10):3818–3827, 2000.
- [93] K. Kuwabara and F. Horii. Solid-state NMR analyses of the crystalline–noncrystalline structure and its thermal changes for ethylene ionomers. *Journal of Polymer Science Part B: Polymer Physics*, 40(11):1142–1153, 2002.
- [94] Y. Lai, X. Gao, H. Zhuang, J. Huang, C. Lin, and L. Jiang. Designing superhydrophobic porous nanostructures with tunable water adhesion. *Advanced Materials*, 21(37):3799–3803, 2009.
- [95] Y. Lai, C. Lin, J. Huang, H. Zhuang, L. Sun, and T. Nguyen. Markedly controllable adhesion of superhydrophobic spongelike nanostructure TiO₂ films. *Langmuir*, 24(8):3867–3873, 2008.
- [96] H. M. Lambermont-Thijs, F. S. van der Woerdt, A. Baumgaertel, L. Bonami, F. E. Du Prez, U. S. Schubert, and R. Hoogenboom. Linear poly(ethylene imine)s by acidic hydrolysis of poly(2-oxazoline)s: kinetic screening, thermal properties, and temperature-induced solubility transitions. *Macromolecules*, 43(2):927–933, 2009.
- [97] I. Langmuir. The constitution and fundamental properties of solids and liquids. II. liquids. *Journal of the American Chemical Society*, 39(9):1848–1906, 1917.
- [98] A. Laschewsky, E. Wischerhoff, M. Kauranen, and A. Persoons. Polyelectrolyte multilayer assemblies containing nonlinear optical dyes. *Macromolecules*, 30(26):8304–8309, 1997.

- [99] M. E. Launey and R. O. Ritchie. On the fracture toughness of advanced materials. *Advanced Materials*, 21(20):2103–2110, 2009.
- [100] J. H. Laurer and K. I. Winey. Direct imaging of ionic aggregates in Zn-neutralized poly(ethylene-co-methacrylic acid) copolymers. *Macromolecules*, 31:9106–9108, 1998.
- [101] J. B. Law, A. M. Ng, A. Y. He, and H. Y. Low. Bioinspired ultra-high water pinning nanostructures. *Langmuir*, 30(1):325–331, 2014.
- [102] J. H. Lee, J. P. Singer, and E. L. Thomas. Micro-/nanostructured mechanical metamaterials. *Advanced Materials*, 24(36):4782–4810, 2012.
- [103] J. H. Lee, L. Wang, S. Kooi, M. C. Boyce, and E. L. Thomas. Enhanced energy dissipation in periodic epoxy nanoframes. *Nano Letters*, 10(7):2592–2597, 2010.
- [104] S. W. Lee, B. S. Kim, S. Chen, Y. Shao-Horn, and P. T. Hammond. Layer-by-layer assembly of all carbon nanotube ultrathin films for electrochemical applications. *Journal of the American Chemical Society*, 131(2):671–679, 2008.
- [105] A. M. Lehaf, H. H. Hariri, and J. B. Schlenoff. Homogeneity, modulus, and viscoelasticity of polyelectrolyte multilayers by nanoindentation: refining the buildup mechanism. *Langmuir*, 28(15):6348–6355, 2012.
- [106] A. M. Lehaf, M. D. Moussallem, and J. B. Schlenoff. Correlating the compliance and permeability of photo-cross-linked polyelectrolyte multilayers. *Langmuir*, 27(8):4756–4763, 2011.
- [107] C. Li, R. A. Register, and S. L. Cooper. Direct observation of ionic aggregates in sulphonated polystyrene ionomers. *Polymer*, 30(7):1227–1233, 1989.

- [108] J. Li, X. Liu, Y. Ye, H. Zhou, and J. Chen. Gecko-inspired synthesis of superhydrophobic ZnO surfaces with high water adhesion. *Colloids and Surfaces A: Physicochemical and Engineering Aspects*, 384(1):109–114, 2011.
- [109] Y. Li, F. Liu, and J. Sun. A facile layer-by-layer deposition process for the fabrication of highly transparent superhydrophobic coatings. *Chemical Communications*, (19):2730–2732, 2009.
- [110] R Longworth and D. J. Vaughan. Physical structure of ionomers. *Nature*, 218:85–87, 1968.
- [111] Y. L. Loo, K. Wakabayashi, Y. E. Huang, R. A. Register, and B. S. Hsiao. Thin crystal melting produces the low-temperature endotherm in ethylene/methacrylic acid ionomers. *Polymer*, 46(14):5118–5124, 2005.
- [112] J. L. Lutkenhaus, K. D. Hrabak, K. McEnnis, and P. T. Hammond. Elastomeric flexible free-standing hydrogen-bonded nanoscale assemblies. *Journal of the American Chemical Society*, 127(49):17228–17234, 2005.
- [113] J. L. Lutkenhaus, K. McEnnis, and P. T. Hammond. Nano- and microporous layer-by-layer assemblies containing linear poly(ethylenimine) and poly(acrylic acid). *Macromolecules*, 41(16):6047–6054, 2008.
- [114] W. J. MacKnight and T. R. Earnest Jr. The structure and properties of ionomers. *Journal of Polymer Science: Macromolecular Reviews*, 16(1):41–122, 1981.
- [115] W. J. MacKnight, L. W. McKenna, and B. E. Read. Properties of ethylene-methacrylic acid copolymers and their sodium salts: mechanical relaxations. *Journal of Applied Physics*, 38(11):4208–4212, 1967.

- [116] W. J. MacKnight, W. P. Taggart, and R. S. Stein. A model for the structure of ionomers. In *Journal of Polymer Science: Polymer Symposia*, volume 45, pages 113–128. Wiley Online Library, 1974.
- [117] A. A. Mamedov, N. A. Kotov, M. Prato, D. M. Guldi, J. P. Wicksted, and A. Hirsch. Molecular design of strong single-wall carbon nanotube/polyelectrolyte multilayer composites. *Nature Materials*, 1(3):190–194, 2002.
- [118] C. L. Marx, D. F. Caulfield, and S. L. Cooper. Morphology of ionomers. *Macromolecules*, 6(3):344–353, 1973.
- [119] C. L. Marx and S. L. Cooper. Polyethylene ionomers. The effect of annealing. *Die Makromolekulare Chemie*, 168(1):339–344, 1973.
- [120] C. L. Marx and S. L. Cooper. The crystallinity of ionomers. *Journal of Macromolecular Science, Part B: Physics*, 9(1):19–33, 1974.
- [121] I. C. McNeill and M. Barbour. Degradation of synthetic polymers: application of some pyrolysis methods in an investigation of the degradation behaviour of ionomers containing methacrylate salt units. *Journal of Analytical and Applied Pyrolysis*, 11:163–179, 1987.
- [122] O. Mermut, J. Lefebvre, D. G. Gray, and C. J. Barrett. Structural and mechanical properties of polyelectrolyte multilayer films studied by AFM. *Macromolecules*, 36(23):8819–8824, 2003.
- [123] M. Michel, A. Taylor, R. Sekol, P. Podsiadlo, P. Ho, N. Kotov, and L. Thompson. High-performance nanostructured membrane electrode assemblies for fuel cells made by layer-by-layer assembly of carbon nanocolloids. *Advanced Materials*, 19(22):3859–3864, 2007.

- [124] W. Ming, D. Wu, R. van Benthem, and G. De With. Superhydrophobic films from raspberry-like particles. *Nano Letters*, 5(11):2298–2301, 2005.
- [125] M. D. Moussallem, S. G. Olenych, S. L. Scott, T. C. Keller III, and J. B. Schlenoff. Smooth muscle cell phenotype modulation and contraction on native and cross-linked polyelectrolyte multilayers. *Biomacromolecules*, 10(11):3062–3068, 2009.
- [126] R. Mruk, S. Prehl, and R. Zentel. Amphotropic ionomers by attachment of secondary amines to a reactive ester polymer. *Macromolecular Chemistry and Physics*, 205(16):2169–2174, 2004.
- [127] A. J. Nolte, M. F. Rubner, and R. E. Cohen. Determining the young’s modulus of polyelectrolyte multilayer films via stress-induced mechanical buckling instabilities. *Macromolecules*, 38(13):5367–5370, 2005.
- [128] M. Ohta, T. Ono, and K. Sada. Layer-by-layer deposition of ionomers with lipophilic ion-pairs dissociated in less-polar media. *Chemistry Letters*, 40(6):648–650, 2011.
- [129] W. C. Oliver and G. M. Pharr. Improved technique for determining hardness and elastic modulus using load and displacement sensing indentation experiments. *Journal of Materials Research*, 7(6):1564–1583, 1992.
- [130] D. Öner and T. J. McCarthy. Ultrahydrophobic surfaces. Effects of topography length scales on wettability. *Langmuir*, 16(20):7777–7782, 2000.
- [131] P. C. Painter, B. A. Brozoski, and M. M. Coleman. FTIR studies of calcium and sodium ionomers derived from an ethylene–methacrylic acid copolymer. *Journal of Polymer Science: Polymer Physics Edition*, 20(6):1069–1080, 1982.

- [132] M. Paßmann and R. Zentel. LC ionomers with phosphonate groups and their multilayer build-up. *Macromolecular Chemistry and Physics*, 203(2):363–374, 2002.
- [133] P. V. Pavor, A. Bellare, A. Strom, D. Yang, and R. E. Cohen. Mechanical characterization of polyelectrolyte multilayers using quasi-static nanoindentation. *Macromolecules*, 37(13):4865–4871, 2004.
- [134] A. Peacock. *Handbook of Polyethylene: Structures, Properties, and Applications*. CRC Press, New York, NY, 2000.
- [135] P. J. Phillips and W. J. MacKnight. Dielectric relaxation in ethylene–methacrylic acid copolymers and their salts. *Journal of Polymer Science Part A-2: Polymer Physics*, 8(5):727–738, 1970.
- [136] E. Poptoshev, B. Schoeler, and F. Caruso. Influence of solvent quality on the growth of polyelectrolyte multilayers. *Langmuir*, 20(3):829–834, 2004.
- [137] P. Rajagopalan, A.T. Tsatsas, and W. M. Risen Jr. Synthesis and near infrared properties of rare earth ionomers. *Journal of Polymer Science Part B: Polymer Physics*, 34(1):151–161, 1996.
- [138] R. W. Rees and D. J. Vaughan. Physical structure of ionomers. *Polymer preprints. American Chemical Society. Division of Polymer Chemistry*, 6:287, 1965.
- [139] L. Richert, A. J. Engler, D. E. Discher, and C. Picart. Elasticity of native and cross-linked polyelectrolyte multilayer films. *Biomacromolecules*, 5(5):1908–1916, 2004.
- [140] B. B. Sauer and R. S. McLean. AFM and X-ray studies of crystal and ionic domain morphology in poly(ethylene-co-methacrylic acid) ionomers. *Macro-*

- molecules*, 33(21):7939–7949, 2000.
- [141] S. Schlick. *Ionomers: Characterization, Theory, and Applications*. Taylor & Francis, Detroit, MI, 1996.
- [142] R. C. Scogna and R. A. Register. Rate-dependence of yielding in ethylene–methacrylic acid copolymers. *Polymer*, 49(4):992–998, 2008.
- [143] R. C. Scogna and R. A. Register. Yielding in ethylene/methacrylic acid ionomers. *Polymer*, 50(2):585–590, 2009.
- [144] M. E. Seitz, C. D. Chan, K. L. Opper, T. W. Baughman, K. B. Wagener, and K. I. Winey. Nanoscale morphology in precisely sequenced poly(ethylene-co-acrylic acid) zinc ionomers. *Journal of the American Chemical Society*, 132(23):8165–8174, 2010.
- [145] Q. Shang, M. Wang, H. Liu, L. Gao, and G. Xiao. Facile fabrication of superhydrophobic raspberry-like SiO₂/polystyrene composite particles. *Polymer Composites*, 34(1):51–57, 2013.
- [146] L. Shen, J. Fu, K. Fu, C. Picart, and J. Ji. Humidity responsive asymmetric free-standing multilayered film. *Langmuir*, 26(22):16634–16637, 2010.
- [147] Y. Shimazaki, M. Mitsuishi, S. Ito, and M. Yamamoto. Preparation of the layer-by-layer deposited ultrathin film based on the charge-transfer interaction. *Langmuir*, 13(6):1385–1387, 1997.
- [148] Y. Shimazaki, M. Mitsuishi, S. Ito, and M. Yamamoto. Alternate adsorption of polymers on a gold surface through the charge-transfer interaction. *Macromolecules*, 32:8220–8223, 1999.

- [149] S. S. Shiratori and M. F. Rubner. pH-dependent thickness behavior of sequentially adsorbed layers of weak polyelectrolytes. *Macromolecules*, 33(11):4213–4219, 2000.
- [150] A. Simmons and A. Eisenberg. Miscibility enhancement in ionomeric blends with poly(ethyleneimine). In *Meeting of the Division of Polymer Chemistry, American Chemical Society*, pages 341–342, 1986.
- [151] T. Soeno, K. Inokuchi, and S. Shiratori. Ultra-water-repellent surface: fabrication of complicated structure of SiO₂ nanoparticles by electrostatic self-assembled films. *Applied Surface Science*, 237(1):539–543, 2004.
- [152] J. G. Speight and S. K. Oelker. *Lange’s Handbook of Chemistry*. McGraw-Hill Companies, New York, NY, 2005.
- [153] M. W. Spencer, M. D. Wetzell, C. Troeltzsch, and D. R. Paul. Effects of acid neutralization on the properties of K⁺ and Na⁺ poly(ethylene-co-methacrylic acid) ionomers. *Polymer*, 53(2):569–580, 2012.
- [154] C. M. Stafford, C. Harrison, K. L. Beers, A. Karim, E. J. Amis, M. R. Vanlandingham, H. C. Kim, W. Volksen, R. D. Miller, and E. E. Simonyi. A buckling-based metrology for measuring the elastic moduli of polymeric thin films. *Nature Materials*, 3(8):545–550, 2004.
- [155] R. Steitz, W. Jaeger, and R. Klitzing. Influence of charge density and ionic strength on the multilayer formation of strong polyelectrolytes. *Langmuir*, 17(15):4471–4474, 2001.
- [156] W. B. Stockton and M. F. Rubner. Molecular-level processing of conjugated polymers. 4. Layer-by-layer manipulation of polyaniline via hydrogen-bonding interactions. *Macromolecules*, 30(9):2717–2725, 1997.

- [157] G. B. Sukhorukov, E. Donath, H. Lichtenfeld, E. Knippel, M. Knippel, A. Budde, and H. Möhwald. Layer-by-layer self assembly of polyelectrolytes on colloidal particles. *Colloids and Surfaces A: Physicochemical and Engineering Aspects*, 137(1):253–266, 1998.
- [158] J. Y. Sun, X. Zhao, W. R. Illeperuma, O. Chaudhuri, K. H. Oh, D. J. Mooney, J. J. Vlassak, and Z. Suo. Highly stretchable and tough hydrogels. *Nature*, 489(7414):133–136, 2012.
- [159] H. Tachino, H. Hara, E. Hirasawa, S. Kutsumizu, K. Tadano, and S. Yano. Dynamic mechanical relaxations of ethylene ionomers. *Macromolecules*, 26(4):752–757, 1993.
- [160] H. Tachino, H. Hara, E. Hirasawa, S. Kutsumizu, and S. Yano. Water absorption effects on the thermal transition and stiffness of ethylene ionomers. *Journal of Applied Polymer Science*, 55(1):131–138, 1995.
- [161] K. Tadano, E. Hirasawa, H. Yamamoto, and S. Yano. Order-disorder transition of ionic clusters in ionomers. *Macromolecules*, 22(1):226–233, 1989.
- [162] Z. Tang, N. A. Kotov, S. Magonov, and B. Ozturk. Nanostructured artificial nacre. *Nature Materials*, 2(6):413–418, 2003.
- [163] A. Taubert and K. I. Winey. Imaging and X-ray microanalysis of a poly(ethylene-ran-methacrylic acid) ionomer melt neutralized with sodium. *Macromolecules*, 35(19):7419–7426, 2002.
- [164] H. Teisala, M. Tuominen, and J. Kuusipalo. Adhesion mechanism of water droplets on hierarchically rough superhydrophobic rose petal surface. *Journal of Nanomaterials*, 2011:33–39, 2011.

- [165] A. M. Telford, B. S. Hawkett, C. Such, and C. Neto. Mimicking the wettability of the rose petal using self-assembly of waterborne polymer particles. *Chemistry of Materials*, 25(17):3472–3479, 2013.
- [166] M. T. Thompson, M. C. Berg, I. S. Tobias, M. F. Rubner, and K. J. Van Vliet. Tuning compliance of nanoscale polyelectrolyte multilayers to modulate cell adhesion. *Biomaterials*, 26(34):6836–6845, 2005.
- [167] Y. Tsujita, K. Shibayama, A. Takizawa, T. Kinoshita, and I. Uematsu. Thermal properties of ethylene ionomers. *Journal of Applied Polymer Science*, 33(4):1307–1314, 1987.
- [168] X. Tuo, D. Chen, H. Cheng, and X. Wang. Fabricating water-insoluble polyelectrolyte into multilayers with layer-by-layer self-assembly. *Polymer Bulletin*, 54(6):427–433, 2005.
- [169] P. Vanhoorne and A. Richard. Low-shear melt rheology of partially-neutralized ethylene-methacrylic acid ionomers. *Macromolecules*, 29(2):598–604, 1996.
- [170] R. J. Varley, S. Shen, and S. van der Zwaag. The effect of cluster plasticisation on the self healing behaviour of ionomers. *Polymer*, 51(3):679–686, 2010.
- [171] R. J. Varley and S. van der Zwaag. Towards an understanding of thermally activated self-healing of an ionomer system during ballistic penetration. *Acta Materialia*, 56(19):5737–5750, 2008.
- [172] O. I. Vinogradova, D. Andrienko, V. V. Lulevich, S. Nordschild, and G. B. Sukhorukov. Young’s modulus of polyelectrolyte multilayers from microcapsule swelling. *Macromolecules*, 37(3):1113–1117, 2004.
- [173] K. Wakabayashi and R. A. Register. Micromechanical interpretation of the modulus of ethylene-(meth)acrylic acid copolymers. *Polymer*, 46(20):8838–

8845, 2005.

- [174] K. Wakabayashi and R. A. Register. Ethylene/(meth)acrylic acid ionomers plasticized and reinforced by metal soaps. *Polymer*, 47(8):2874–2883, 2006.
- [175] K. Wakabayashi and R. A. Register. Morphological origin of the multi-step relaxation behavior in semicrystalline ethylene/methacrylic acid ionomers. *Macromolecules*, 39(3):1079–1086, 2006.
- [176] C. Walter, T. Antretter, R. Daniel, and C. Mitterer. Finite element simulation of the effect of surface roughness on nanoindentation of thin films with spherical indenters. *Surface and Coatings Technology*, 202(4):1103–1107, 2007.
- [177] R. M. Walters, K. E. Sohn, K. I. Winey, and R. J. Composto. Local acid environment in poly(ethylene-ran-methacrylic acid) ionomers. *Journal of Polymer Science Part B: Polymer Physics*, 40(24):2833–2841, 2002.
- [178] H. Wang, Y. He, X. Tuo, and X. Wang. Sequentially adsorbed electrostatic multilayers of branched side-chain polyelectrolytes bearing donor-acceptor type azo chromophores. *Macromolecules*, 37(1):135–146, 2004.
- [179] L. Wang, J. Lau, E. L. Thomas, and M. C. Boyce. Co-continuous composite materials for stiffness, strength, and energy dissipation. *Advanced Materials*, 23(13):1524–1529, 2011.
- [180] L. Wang, Y. Lin, B. Peng, and Z. Su. Tunable wettability by counterion exchange at the surface of electrostatic self-assembled multilayers. *Chemical Communications*, (45):5972–5974, 2008.
- [181] L. Wang, Y. Lin, and Z. Su. Counterion exchange at the surface of polyelectrolyte multilayer film for wettability modulation. *Soft Matter*, 5(10):2072–2078, 2009.

- [182] L. Wang, B. Peng, and Z. Su. Tunable wettability and rewritable wettability gradient from superhydrophilicity to superhydrophobicity. *Langmuir*, 26(14):12203–12208, 2010.
- [183] L. Wang, J. Wei, and Z. Su. Fabrication of surfaces with extremely high contact angle hysteresis from polyelectrolyte multilayer. *Langmuir*, 27(24):15299–15304, 2011.
- [184] W. Wang, T. T. Chan, A. J. Perkowski, S. Schlick, and K. I. Winey. Local structure and composition of the ionic aggregates in Cu(II)-neutralized poly(styrene-co-methacrylic acid) ionomers depend on acid content and neutralization level. *Polymer*, 50(5):1281–1287, 2009.
- [185] Y. Wang and E. J. Goethals. ABA block copolymers of polytetrahydrofuran and linear polyethylenimine and their complexes with copper chloride. *Macromolecules*, 33(3):808–813, 2000.
- [186] X. Wei, M. Naraghi, and H. D. Espinosa. Optimal length scales emerging from shear load transfer in natural materials: application to carbon-based nanocomposite design. *ACS Nano*, 6(3):2333–2344, 2012.
- [187] R. N. Wenzel. Resistance of solid surfaces to wetting by water. *Industrial & Engineering Chemistry*, 28(8):988–994, 1936.
- [188] R. N. Wenzel. Surface roughness and contact angle. *The Journal of Physical Chemistry*, 53(9):1466–1467, 1949.
- [189] K. F. Weyts and E. J. Goethals. New synthesis of linear polyethyleneimine. *Polymer Bulletin*, 19(1):13–19, 1988.
- [190] K. F. Weyts and E. J. Goethals. Back titration of linear polyethylenimine: decrease of pH by addition of sodium hydroxide. *Die Makromolekulare Chemie*,

- Rapid Communications*, 10(6):299–302, 1989.
- [191] S. R. Williams, W. Wang, K. I. Winey, and T. E. Long. Synthesis and morphology of segmented poly(tetramethylene oxide)-based polyurethanes containing phosphonium salts. *Macromolecules*, 41(23):9072–9079, 2008.
- [192] F. C. Wilson, R Longworth, and D. J. Vaughan. The physical structure of ionomers. III. X-ray diffraction studies. *Polymer Preprint*, 9:505, 1968.
- [193] K. I. Winey, J. H. Laurer, and B. P. Kirkmeyer. Ionic aggregates in partially Zn-neutralized poly(ethylene-ran-methacrylic acid) ionomers: shape, size, and size distribution. *Macromolecules*, 33(2):507–513, 2000.
- [194] A. Winkleman, G. Gotesman, A. Yoffe, and R. Naaman. Immobilizing a drop of water: fabricating highly hydrophobic surfaces that pin water droplets. *Nano Letters*, 8(4):1241–1245, 2008.
- [195] D. Y. Wu, S. Meure, and D. Solomon. Self-healing polymeric materials: a review of recent developments. *Progress in Polymer Science*, 33(5):479–522, 2008.
- [196] Y. Xiang, X. Chen, and J. J. Vlassak. Plane-strain bulge test for thin films. *Journal of Materials Research*, 20(9):2360–2370, 2005.
- [197] D. Xu, M. Wang, X. Ge, M. H. W. Lam, and X. Ge. Fabrication of raspberry SiO₂/polystyrene particles and superhydrophobic particulate film with high adhesive force. *Journal of Materials Chemistry*, 22(12):5784–5791, 2012.
- [198] S. Yano, K. Tadano, N. Nagao, S. Kutsumizu, H. Tachino, and E. Hirasawa. Dielectric relaxation studies on water absorption of ethylene ionomers. *Macromolecules*, 25(26):7168–7171, 1992.

- [199] D. J. Yarusso and S. L. Cooper. Microstructure of ionomers: interpretation of small-angle X-ray scattering data. *Macromolecules*, 16(12):1871–1880, 1983.
- [200] D.J. Yarusso and S. L. Cooper. Analysis of saxs data from ionomer systems. *Polymer*, 26(3):371–378, 1985.
- [201] S. Yilmaztürk, H. Deligöz, M. Yilmazoğlu, H. Damyhan, F. Öksüzömer, S. N. Koç, A. Durmuş, and M. Ali Gürkaynak. Self-assembly of highly charged polyelectrolyte complexes with superior proton conductivity and methanol barrier properties for fuel cells. *Journal of Power Sources*, 195(3):703–709, 2010.
- [202] S. Yilmaztürk, H. Deligöz, M. Yilmazoğlu, H. Damyhan, F. Öksüzömer, S. N. Koç, A. Durmuş, and M. A. Gürkaynak. A novel approach for highly proton conductive electrolyte membranes with improved methanol barrier properties: layer-by-layer assembly of salt containing polyelectrolytes. *Journal of Membrane Science*, 343(1):137–146, 2009.
- [203] S. Yilmaztürk, N. Ercan, and H. Deligöz. Influence of LbL surface modification on oxygen cross-over in self-assembled thin composite membranes. *Applied Surface Science*, 258(7):3139–3146, 2012.
- [204] D. Yoo, S. S. Shiratori, and M. F. Rubner. Controlling bilayer composition and surface wettability of sequentially adsorbed multilayers of weak polyelectrolytes. *Macromolecules*, 31(13):4309–4318, 1998.
- [205] M. Yoon, Y. Kim, and J. Cho. Multifunctional colloids with optical, magnetic, and superhydrophobic properties derived from nucleophilic substitution-induced layer-by-layer assembly in organic media. *ACS Nano*, 5(7):5417–5426, 2011.

- [206] Z. Yoshimitsu, A. Nakajima, T. Watanabe, and K. Hashimoto. Effects of surface structure on the hydrophobicity and sliding behavior of water droplets. *Langmuir*, 18(15):5818–5822, 2002.
- [207] Y. Yuan and T. R. Lee. Contact angle and wetting properties. In *Surface Science Techniques*, volume 51.
- [208] L. Zhai, F. C. Cebeci, R. E. Cohen, and M. F. Rubner. Stable superhydrophobic coatings from polyelectrolyte multilayers. *Nano Letters*, 4(7):1349–1353, 2004.
- [209] H. Zhang, D. Wang, Z. Wang, and X. Zhang. Hydrogen bonded layer-by-layer assembly of poly(2-vinylpyridine) and poly(acrylic acid): influence of molecular weight on the formation of microporous film by post-base treatment. *European Polymer Journal*, 43(7):2784–2791, 2007.
- [210] H. Zhang, Z. Wang, Y. Zhang, and X. Zhang. Hydrogen-bonding-directed layer-by-layer assembly of poly(4-vinylpyridine) and poly(4-vinylphenol): effect of solvent composition on multilayer buildup. *Langmuir*, 20(21):9366–9370, 2004.
- [211] P. Zhang, J. Qian, Q. An, B. Du, X. Liu, and Q. Zhao. Influences of solution property and charge density on the self-assembly behavior of water-insoluble polyelectrolyte sulfonated poly(sulphone) sodium salts. *Langmuir*, 24(5):2110–2117, 2008.
- [212] X. Zhang, F. Shi, X. Yu, H. Liu, Y. Fu, Z. Wang, L. Jiang, and X. Li. Polyelectrolyte multilayer as matrix for electrochemical deposition of gold clusters: toward super-hydrophobic surface. *Journal of the American Chemical Society*, 126(10):3064–3065, 2004.
- [213] N. Zhao, Q. Xie, X. Kuang, S. Wang, Y. Li, X. Lu, S. Tan, J. Shen, X. Zhang, Y. Zhang, et al. A novel ultra-hydrophobic surface: statically non-wetting but

- dynamically non-sliding. *Advanced Functional Materials*, 17(15):2739–2745, 2007.
- [214] Q. Zhao, J. Qian, Q. An, and B. Du. Speedy fabrication of free-standing layer-by-layer multilayer films by using polyelectrolyte complex particles as building blocks. *Journal of Materials Chemistry*, 19(44):8448–8455, 2009.
- [215] N. C. Zhou, C. D. Chan, and K. I. Winey. Reconciling STEM and X-ray scattering data to determine the nanoscale ionic aggregate morphology in sulfonated polystyrene ionomers. *Macromolecules*, 41(16):6134–6140, 2008.